OBSERVATIONS OF SECONDARY ORGANIC AEROSOL PRODUCTION AND SOOT AGING UNDER ATMOSPHERIC CONDITIONS USING A NOVEL ENVIRONMENTAL AEROSOL CHAMBER

A Dissertation

by

CRYSTAL CHANEA GLEN

Submitted to the Office of Graduate Studies of
Texas A&M University
in partial fulfillment of the requirements for the degree of

DOCTOR OF PHILOSOPHY

December 2010

Major Subject: Atmospheric Sciences

Observations of Secondary Organic Aerosol Production and Soot Aging under Atmospheric Conditions Using a Novel Environmental Aerosol Chamber

OBSERVATIONS OF SECONDARY ORGANIC AEROSOL PRODUCTION AND SOOT AGING UNDER ATMOSPHERIC CONDITIONS USING A NOVEL ENVIRONMENTAL AEROSOL CHAMBER

A Dissertation

by

CRYSTAL CHANEA GLEN

Submitted to the Office of Graduate Studies of
Texas A&M University
in partial fulfillment of the requirements for the degree of

DOCTOR OF PHILOSOPHY

Approved by:

Chair of Committee,	Donald R. Collins
Committee Members,	Sarah D. Brooks
	Renyi Zhang
	William H. Marlow
	Mark Ivey
	Bernard Zak
Head of Department,	Kenneth Bowman

December 2010

Major Subject: Atmospheric Sciences

ABSTRACT

Observations of Secondary Organic Aerosol Production and Soot Aging under Atmospheric Conditions Using a Novel Environmental Aerosol Chamber.

(December 2010)

Crystal Chanea Glen, B.S., Texas A&M University

Chair of Advisory Committee: Dr. Donald R. Collins

Secondary organic aerosols (SOA) comprise a substantial fraction of the total global aerosol budget. While laboratory studies involving smog chambers have advanced our understanding of the formation mechanisms responsible for SOA, our knowledge of the processes leading to SOA production under ambient gaseous and particulate concentrations as well as the impact these aerosol types have on climate is poorly understood. Although the majority of atmospheric aerosols scatter radiation either directly or indirectly by serving as cloud condensation nuclei, soot is thought to have a significant warming effect through absorption. Like inorganic salts, soot may undergo atmospheric transformation through the vapor condensation of non-volatile gaseous species which will alter both its chemical and physical properties. Typical smog chamber studies investigating the formation and growth of SOA as well as the soot aging process are temporally limited by the initial gaseous concentrations injected into the chamber environment. Furthermore, data interpretation from such experiments is generally restricted to the singular gaseous species under investigation. This dissertation discusses

the use of a new aerosol chamber designed to study the formation and growth of SOA and soot aging under atmospherically relevant conditions. The Ambient Aerosol Chamber for Evolution Studies (AACES) was deployed at three field sites where size and hygroscopic growth factor (HGF) of ammonium sulfate seed particles was monitored over time to examine the formation and growth of SOA. Similar studies investigating the soot aging process were also conducted in Houston, TX. It is shown that during the ambient growth of ammonium sulfate seed particles, as particle size increases, hygroscopic growth factors decrease considerably resulting in a significant organic mass fraction in the particle phase concluding an experiment. Observations of soot aging show an increase in measured size, HGF, mass and single scattering albedo. Ambient growth rate comparisons with chamber growth yielded similar trends verifying the use of AACES to study aerosol aging. Based on the results from this study, it is recommended that AACES be employed in future studies involving the production and growth of SOA and soot aging under ambient conditions in order to bridge the gaps in our current scientific knowledge.

ACKNOWLEDGEMENTS

First, I would like to extend my appreciation to Sandia National Laboratories and the College of Geosciences at Texas A&M University for creating the wonderful fellowship opportunity which funded my Ph.D. research, the Sandia National Laboratories/Texas A&M University Excellence in Geosciences Fellowship. In addition, I thank Bernard Zak for his continued support and encouragement. Bernie was always there to listen and give great advice as well as provide the foundation for my continued motivation over years of research. He was also a extraordinary host during my trips to Albuquerque, NM. I would also like to thank the Houston Advanced Research Center for providing additional funding.

To Don Collins, thank you for being an inspiration to me in both my undergraduate and graduate career. It wasn't until after taking Don's research course in atmospheric aerosol measurements that I found my passion in aerosol research. Since then, he has supported my Ph.D. endeavors by encouraging me to think critically and work proactively toward my research goals. I would also like to thank Renyi Zhang for serving on my Ph.D. committee and taking interest in my project providing a unique measurement opportunity in Houston, TX during the SHARP field campaign working with a small team of scientists on the impact of the atmosphere on soot aging and heterogeneous chemistry. As a part of that team, my gratitude is extended to both Jun Zheng and Alexei Khalizov for their contributions to measurements during the field study as well as their support and advice on various laboratory and research topics.

A very special thanks goes to Sarah Brooks for her guidance and advice not only in research but also in life. She taught me the keys to writing a strong proposal, had confidence in me when I doubted myself, and brought out the good ideas in me. She did not even complain much when I took over her new laboratory to build an aerosol chamber. I would also like to thank Josh Santarpia for being a valued friend and colleague. Through numerous research conversations, Josh has encouraged me to critically think about research avenues I would have not considered otherwise.

Besides those who I have worked closely with, I would like to thank the remainder of my committee: Mark Ivey, who through confidence in me, helped to facilitate a wonderful job opportunity with Sandia National Laboratories, and William Marlow, who helped me understand difficult physical concepts like particle charging and coagulation.

Let me also say 'thank you' to the following people at Texas A&M University:

- Chance Spencer: for being not only a work partner but also a friend, teaching me the ropes when I first started working under Don, constantly being there to help under any circumstance, and lending an ear when something troubled me. Chance was also available during each project at the Moody Tower at the University of Houston to help carry heavy instrumentation up the stairs, although he complained the entire time.
- Runjun Li: for aiding my research efforts through the years, discussing difficult topics with me, and helping setup numerous field projects.

- Nathan Taylor: for providing both company and support during field setup, and above all being my voice of reason when I was convinced that an idea was good even when it was not.
- Leon Rough: for making Calculus extremely interesting and encouraging me to follow my dreams.

A very special note of gratitude is extended to my friends and family:

- my parents, Cecil and Rozella Johnson, for giving me life and providing unconditional loving support, and for encouraging me to pursue my educational interests.
- My brother and sister-in-law, Roman and Michele Johnson, for always providing a loving home when I returned to Redwater, TX for a visit and supplying constant encouragement in my educational goals.
- My sister, Robyn Bal, for being there when I needed her.
- My nieces and nephews, Meleah, Colton, Garrett, and Logan Johnson for showing me that sometimes you need to cut loose and have fun to reduce stress.

Last, but certainly not least, I would like to thank my husband, Andrew Glen for providing lasting love and support in both my research efforts and in life. He was there to fly to Colorado and help me pack up the research trailer to drive back to Texas so I was not driving alone. He was there to shuttle supplies to and from Houston during the SHARP campaign, a task that truly kept the project rolling, and to help break everything down and load it back in the truck in the summer heat at the end of the project. He has

been my rock in times of despair and has been there to share my joy in times of celebration. He is the one who reassures me when I feel I have reached the end of my rope. These past few months, he has provided a shoulder to cry on when the stress of finishing my dissertation was too much to handle. Without his support, I truly would not have made it this far with confidence in myself. He is my sunshine.

TABLE OF CONTENTS

Page

LIST OF FIGURES

FIGURE Page

FIGURE Page

LIST OF TABLES

1. INTRODUCTION

Atmospheric aerosols affect climate both directly through scattering and absorption of solar radiation and indirectly by serving as cloud condensation nuclei (CCN) or ice nuclei (IN), influencing cloud longevity and reflectivity (Twomey 1991). Epidemiological studies have also reported a positive association between fine particulates and adverse health effects. Such studies have linked increased mortality rates and lung disease with exposure to outdoor air pollution (Dockery et al. 1993; Goodman et al. 2004; Hauser et al. 2001; Schwartz 2004b). Evidence also shows that air pollution is positively correlated with chronic disease and death in children (Schwartz 2004a). Understanding these impacts is challenging given that aerosol properties and concentrations are highly variable both spatially and temporally. The direct and indirect radiative impact of aerosols as well as possible health effects depends on both the emission rate of particles and precursor gases as well as the transformations they undergo in the atmosphere. Such processes that transform an aerosol include impacts from coagulation, heterogeneous surface reactions, cloud processing, and gas-to-particle partitioning through the formation of secondary organic aerosol (SOA) by organic gases (Pankow 1994). Moreover, SOA has been linked to adverse health effects as they typically contain carcinogenic materials (Dockery et al. 1993).

This dissertation follows the style of *Aerosol Science and Technology*.

SOA is primarily formed by the vapor condensation of lower volatility products through volatile organic compound (VOC) atmospheric degradation. It is estimated that organic compounds make up a significant fraction of atmospheric particulate matter accounting for roughly 20-90% of tropospheric aerosol mass concentrations (Griffin et al. 1999b; Kanakidou et al. 2005). Goldstein and Gallaby, *2007* estimated the total organic aerosol budget within a broad range between 140-910 TgC/yr, while other estimates range from 50 to 90 TgC/yr (Hallquist et al. 2009). In addition, it is estimated that as many as 100,000 organic compounds are present in the atmosphere (Goldstein and Galbally 2007). The uncertainty surrounding the atmospheric organic loading is amplified by the fact that each VOC may undergo numerous reactions involving pathways which produce a wide variety of oxidized products. Furthermore, many of the emitted VOC's are not generally thought to be significant contributors to SOA formation. Because of the large number of chemical constituents as well as a high degree of variability in sources and the possible atmospheric chemical pathways involved, predicting the SOA yield is a challenge for both experiments and models. However, certain classes of VOC's have been well established as SOA precursors, and are therefore the focus of numerous field and laboratory chamber studies in an attempt to quantify both the mechanisms responsible for organic aerosol growth as well as the resultant SOA production (Cai et al. 2008; Cocker et al. 2001; Griffin et al. 1999a; Hu and Kamens 2007; McMurry and Grosjean 1985; Ng et al. 2006; Presto et al. 2005; Saathoff et al. 2003). Such classes include cycloalkenes, aromatic hydrocarbons, and terpenes, most of which are cyclic compounds. When these compounds undergo atmospheric oxidation,

they produce first-generation products that contain one or more polar functional groups while maintaining a similar number of parent carbon atoms, a reaction pathway more likely to produce low-volatility products (Hallquist et al. 2009). One noted competitive process leading to the aging of SOA aerosols is that of oligomerization, which produces larger molecular species (Rudich et al. 2007).

Of particular importance in the determination of SOA production is understanding the contribution from biogenic VOC's (BVOC's) such as isoprene, monoterpenes, sesquiterpenes and oxygenated terpenes, because of their significant contribution to the global budget and high level of atmospheric reactivity (Kanakidou et al. 2005). In a recent study by Ng, et al., 2006, various compounds within the aforementioned groups of BVOC's were analyzed under chamber conditions for their secondary organic aerosol forming potential via ozonolysis and photooxidation. It was found that the majority of compounds reacted resulted in significant aerosol yields. Nevertheless, interpretation of overall SOA production from studies involving individual precursors is difficult given the complexity of tropospheric organic chemistry.

Models are often used as an intermediate in the quantification of SOA formation by incorporating results from chamber measurements. However, these models often predict far less SOA than is typically observed (Chen and Griffin 2005; Colville and Griffin 2004; Gouw et al. 2005; Heald et al. 2005; Jenkin 2004; Johnson et al. 2005). In a recent review by Kroll and Seinfeld it is suggested that one possible discrepancy between measured SOA production and that predicted from models may be due to the fact that many chamber studies are conducted under conditions which are not

representative of the ambient environment (Kroll and Seinfeld 2008). In particular, the majority of laboratory smog chamber measurements use aerosol concentrations considerably higher than typically found in the atmosphere, and gas concentrations are generally limited to the singular species under investigation. Moreover, recent evidence indicates that particulate oxidation can continue in the atmosphere following SOA formation particularly in regions where regional transport plays a key role (Robinson et al. 2006). Therefore, it is necessary to study the production and growth of SOA under comparable atmospheric aerosol loading conditions and gaseous concentrations. Such conditions may allow for a more accurate determination of atmospheric SOA yields (Kroll and Seinfeld 2008; Presto and Donahue 2006) and may also ensure that reactions leading to SOA production occur at rates relevant to the atmosphere (Kroll et al. 2007). Furthermore, chamber studies are generally carried out over a period less than 6 hours, with the majority of these only lasting from only 1 to 2 hours (Kroll and Seinfeld 2008). Since the reactions leading to aerosol aging can continue for days, it is necessary to study this process under atmospherically relevant timescales.

The absorption of visible radiation by atmospheric particulates is primarily due to soot and mineral dust. Soot is produced by incomplete combustion of fossil fuels and biomass burning with an estimated global emission rate of 8-24 Tg C yr^{-1} (Jacobson 2001). Unlike most other individual aerosol effects on radiation, soot aerosols are thought to have a significant atmospheric warming effect and a negative impact on visibility with increased concentrations. The absorption of visible radiation may be increased if the particles are incorporated into cloud droplets (Chylek and Hallett 1992)

by decreasing the cloud albedo, and may have an impact on photochemistry by reducing photolysis at the surface (Li et al. 2005). In addition, absorption and backscattering of solar radiation by soot aerosols may also alter the temperature profile of the atmosphere sufficiently to increase stability and decrease surface moisture fluxes, which may suppress convection and diminish cloud formation (Ackerman et al. 2000; Chung and Seinfeld 2002; Ramanathan et al. 2001); the so called "semi-direct effect" (Hansen et al. 1997; Johnson et al. 2004). Although fresh soot particles produced in the laboratory are typically hydrophobic and only activate at supersaturations exceeding 10% (Kotzick et al. 1997; Zuberi et al. 2005), aged soot particles may become efficient CCN due to an increase in the soluble fraction during the aging process, thereby modifying the microphysical and radiative properties and lifetime of clouds (Fan et al. 2008).

Soot particles in the atmosphere may undergo aging and become internally mixed by various processes including adsorption and condensation of nonvolatile and semivolatile vapors, coagulation with preexisting aerosol particles, heterogeneous reactions with atmospheric gases, and cloud processing. Such aging processes may occur upon source generation by mixing with unburned organics and sulfuric acid in diesel engine exhaust (Sakurai et al. 2003; Weingartner et al. 1997), or during atmospheric transport (Saathoff et al. 2003). Studies indicate that chemical and physical aging of soot in the atmosphere alters hygroscopicity, particle morphology, scattering and absorption, and composition of soot containing aerosols (Khalizov et al. 2009a; Khalizov et al. 2009b; Zhang and Zhang 2005; Zhang et al. 2008).

Soot particles are emitted into the atmosphere in the form of highly complex chain-like or compact aggregates. Compact aggregation can enhance absorption and scattering (Fuller 1995), and the intensity of these effects are dependent on both particle size and source generation (Fuller et al. 1999). Weingartner et al., 1997 observed the shrinking and restructuring of soot chain agglomerates when exposed to elevated RH. This finding was consistent with previous work by Crouzet and Marlow which suggested that the complex structure of soot aggregates provide possible active sites for water condensation (Crouzet and Marlow 1995). Non-reversible condensation may also occur during the sulfuric acid (Khalizov et al. 2009b; Xie and Marlow 1997) and organic acid (Levitt et al. 2007) uptake by soot. When enough liquid condenses into the small angle cavities present in soot chain aggregates, the branches of the agglomerated particle begin to collapse. However, despite the soot particles becoming more hydrophilic, the amount of water absorbed is insufficient for activation under atmospherically relevant critical supersaturations (Zuberi et al. 2005). Soot aging may increase the effect of this observed particle restructuring and lead to changes in the particle hygroscopic properties. Similarly, studies indicate that water-soluble compounds such as sulfuric acid may condense on the surface of soot particles leading to a collapse in the chain aggregate to a more spherical agglomerate, which alter the particle hygroscopicity, morphology and optical properties (Fuller et al. 1999; Khalizov et al. 2009a; Khalizov et al. 2009b; Zhang et al. 2008). Similar results have been observed for soot aging by nonvolatile organic condensation (Mikhailov et al. 2006; Saathoff et al. 2003; Schnaiter et al. 2005). Although such studies allow for the parameterization of singular processes leading to

atmospheric soot aging, the conditions involved with laboratory experimentations are often not representative of relevant ambient conditions as mentioned previously. Recent field experiments (Pósfai et al. 1999) and modeling investigations (Jacobson 2001) suggest that black carbon is commonly internally mixed with other compounds. Therefore it is desirable to isolate and study the physical effects of the soot aging process under ambient gaseous concentrations.

Numerous analytical difficulties arise when attempting to quantify aerosol evolution processes using ambient measurements. Due to the complex spatial and temporal variability in the atmospheric aerosol, it is often a challenge to decouple local variations from those changes in source regions and history prior to sampling, thereby complicating the extrapolation of SOA yields from data. Although laboratory measurements involving environmental smog chambers increase the overall understanding of processes leading to SOA and soot aging, the full range of atmospheric conditions has not been well represented. One chamber method which has been utilized to replicate ambient conditions is the Captive Air Chamber (Tanaka et al. 2003). Traditional captive air chambers consist of pulling ambient air into the chamber and then introducing gaseous and particulate variants to measure atmospheric response. Although such techniques are more representative of the natural environment, observational times needed for the study of SOA are limited by the initial concentration of ambient gases within the chamber, since the concentration of condensed species will decrease considerably over time.

In order to accurately represent aerosol evolution in the ambient environment, a new environmental chamber was developed allowing for continuous monitoring of the aerosol evolution process under ambient conditions for a period of greater than 12 hours, and field experiments investigating SOA production and growth as well as soot aging from seed particles was investigated. The Ambient Aerosol Chamber for Evolution Studies (AACES) was field deployed in two rural locations and one urban region, and the secondary organic aerosol production and soot aging process from seed particles were quantified using size and hygroscopic growth factor measurements obtained from a humidified Tandem Differential Mobility Analyzer (H-TDMA). The soot aging process was further examined for changes in particle mass and optical properties during periods of growth utilizing an Aerosol Particle Mass Analyzer (APM) and cavity ringdown system respectively. The results presented here show that AACES is a valuable tool that will bridge the gap between laboratory studies and atmospheric modeling.

2. THE AMBIENT AEROSOL CHAMBER FOR EVOLUTION STUDIES

2.1. ENVIRONMENTAL CHAMBER DESIGN

The Ambient Aerosol Chambers for Evolution Studies (AACES), shown in Figure 1, is a roughly 1.2 m^3 portable environmental chamber designed for the study of SOA production and soot aging under ambient conditions. Two individual sections make up the chamber as a whole; the lower section consisting of the flow region of the chamber where ambient air is pulled through continuously, and the upper section being composed of the actual environmental reaction chamber where experimental procedures are studied. The two regions of the chamber are separated using a 5 mil (.005") 0.2 μm expanded polytetrafluoroethylene (e-PTFE) membrane sheet manufactured by W. L. Gore & Associates. Unlike solid PTFE sheets, e-PTFE is created by heat treating and subsequently stretching the PTFE polymer which creates a woven micropourous sheet that maintains efficient particle filtration while simultaneously allowing gases to readily pass through, a property that makes e-PTFE popular in various filtration and pharmaceutical applications (Wikol et al. 2008). The e-PTFE membrane has an estimated 96% filtration efficiency for particles larger than 10nm. Because PTFE is widely known for its high degree of chemical resistivity, nonpolarity and thermal stability, it is desirable for long-term applications where harsh chemicals may be present.

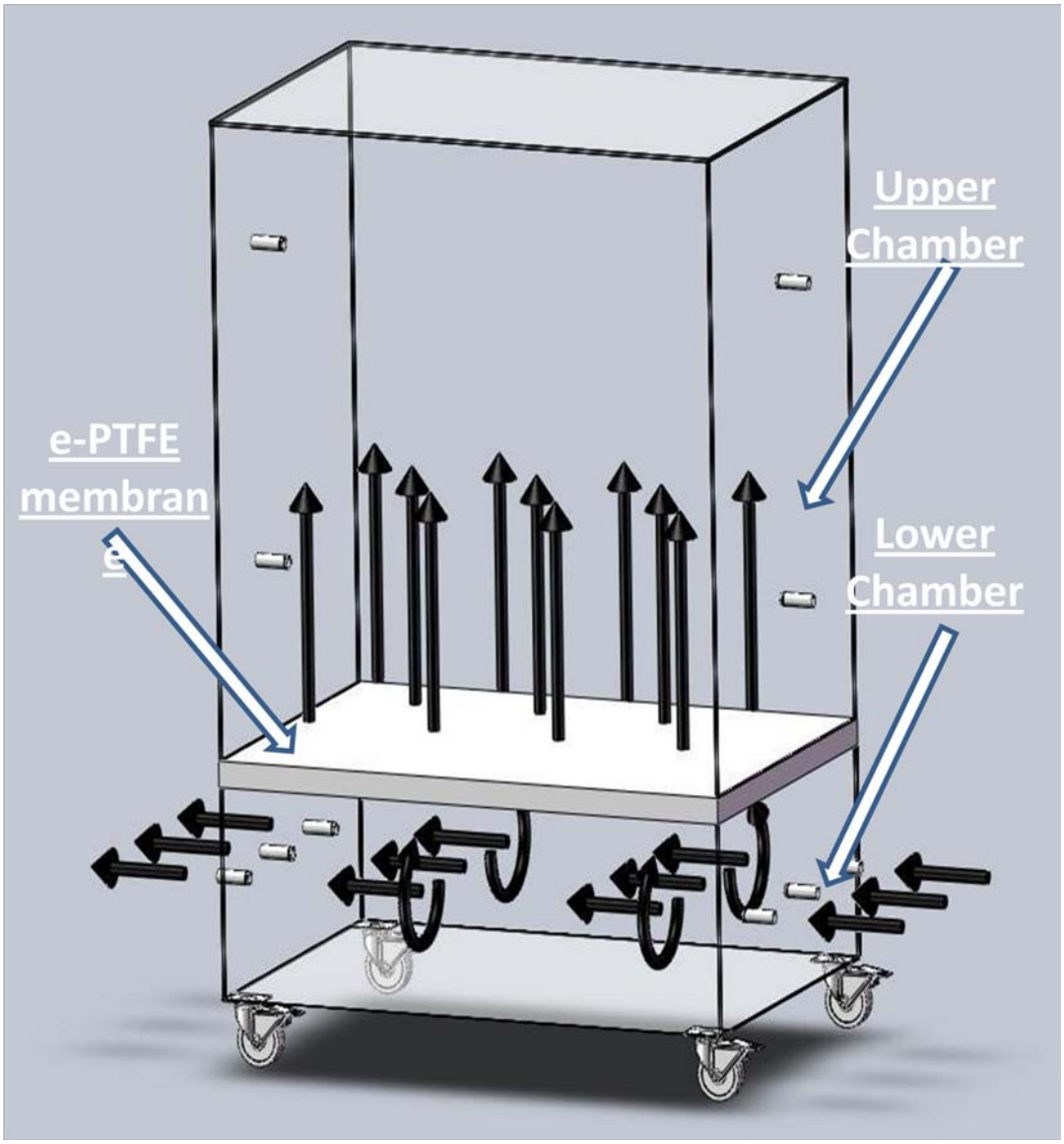

Figure 1. Schematic showing AACES and its operation. As air flows through the lower chamber, gases penetrate and diffuse across the ePTFE Teflon® membrane reaching the upper reaction chamber while ambient particles are trapped by the membrane. This creates an initial environment inside the reaction chamber that is free of particles while gas concentrations mimic ambient.

Furthermore, because e-PTFE is both microporous and hydrophobic, vapors penetrate the membrane by either bulk gas flow or diffusion while liquid droplets remain blocked from penetration (Wikol et al. 2008).

In a recent report by Botnen, 2006, the use of e-PTFE passive diffusion bag (PDB) samplers were tested for their ability to facilitate VOC diffusional transport for the measurement of contaminated groundwater (Botnen 2006). The measurement system consisted of two identical chambers separated by a 0.1 μm pore size e-PTFE membrane. One chamber was filled with sampled groundwater, while the other chamber was filled with deionized (DI) water and VOC vapors were allowed to diffuse across the membrane from the contaminated water to the DI water over a pre-determined period of time. The concentration of benzene, toluene, ethylbenzene, and xylenes were measured in both the contaminated water under pre-experimental conditions and in the DI water post-experimentally. The results showed that the system reached near equilibrium, with the measured VOC concentration in the DI water roughly half of the initial concentration of the contaminated water sample, yielding an overall conclusion that VOC molecules readily penetrate the e-PTFE membrane (Botnen 2006). Similar applications have been employed in direct analysis of ground water samples using gas chromatography (Magnusson 1989; Namieśnik et al. 2005). Therefore, by utilizing the e-PTFE membrane to separate the two portions of AACES, particulates are efficiently removed while facilitating gaseous transport across the membrane, creating an initial environment inside the upper portion of AACES that is free of particulates while continuously mimicking ambient gas concentrations.

The upper portion of AACES is constructed of a rigid 5.6 mm thick Cyro Industries Acrylite OP-4 Acrylic outer shell on all four sides and the top which is lined with American Durafilm 5 mil (0.13 mm) FEP Teflon, while the e-PTFE membrane alone makes up the bottom of the reaction chamber. The optical properties of both Acrylite OP-4 Acrylic and FEP Teflon allow for efficient UV transmission in both the UV-B (280-315nm) and UV-A(315-400nm) ranges as shown in Figure 2 when compared to the average global actinic flux allowing for ambient photochemical processes to take place within the chamber. In a technical data report by Cyro Industries, the UV transmission of Acrylite OP-4 Acrylic was measured before and after 10,000 hours of UV exposure by a 170 watt VHO lamp positioned 1.25" from the surface of the acrylic, and little difference was observed in the overall measured percent transmission as indicated in Figure 3 (Industries 2001).

During chamber operation, ambient air is pulled through the bottom portion of AACES at a constant rate allowing gases to move virtually unimpeded across the e-PTFE membrane to the upper portion of the chamber. Since the chamber environment is continuously exposed to ambient gas concentrations, gases lost due to deposition or adsorption to seed particles within the reaction chamber will be consistently replenished. By utilizing this novel chamber design, seed particles of known size and composition can be injected into the upper portion of AACES, and the physical and chemical properties of the aerosol monitored over longer timescales than previously allowed using traditional techniques.

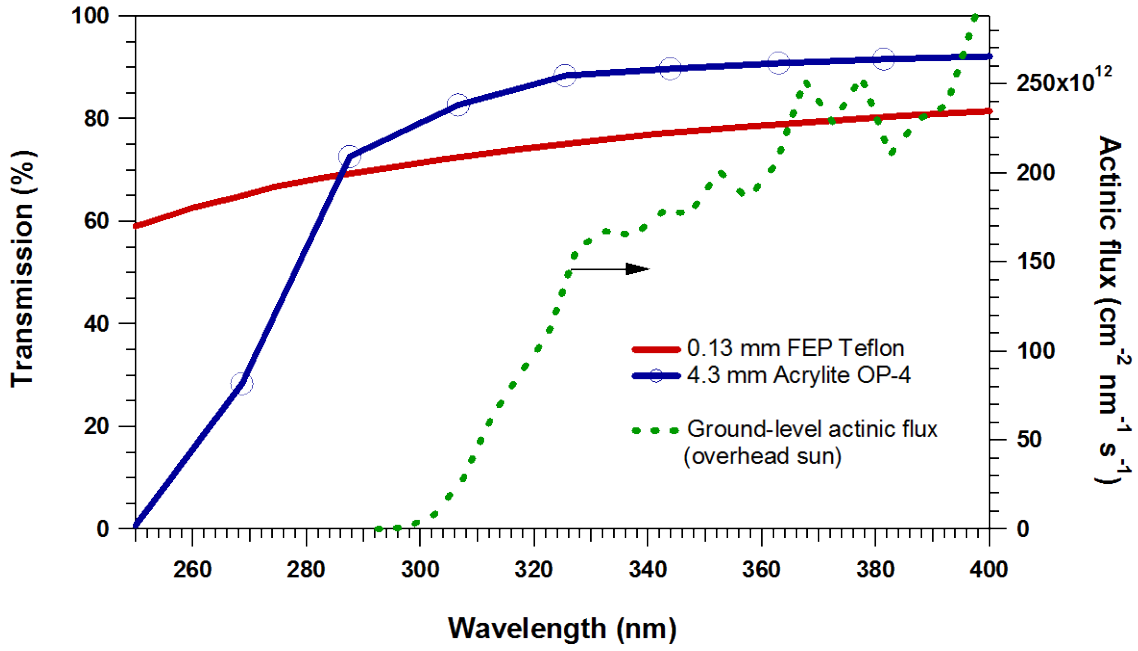

Figure 2. Materials transmission spectrum. Transmission spectrum for 0.13mm FEP Teflon®(red) and 4.3mm Acrylite OP-4 acrylic sheet (blue) plotted against typically measured ground-level actinic flux under clear sky conditions (green).

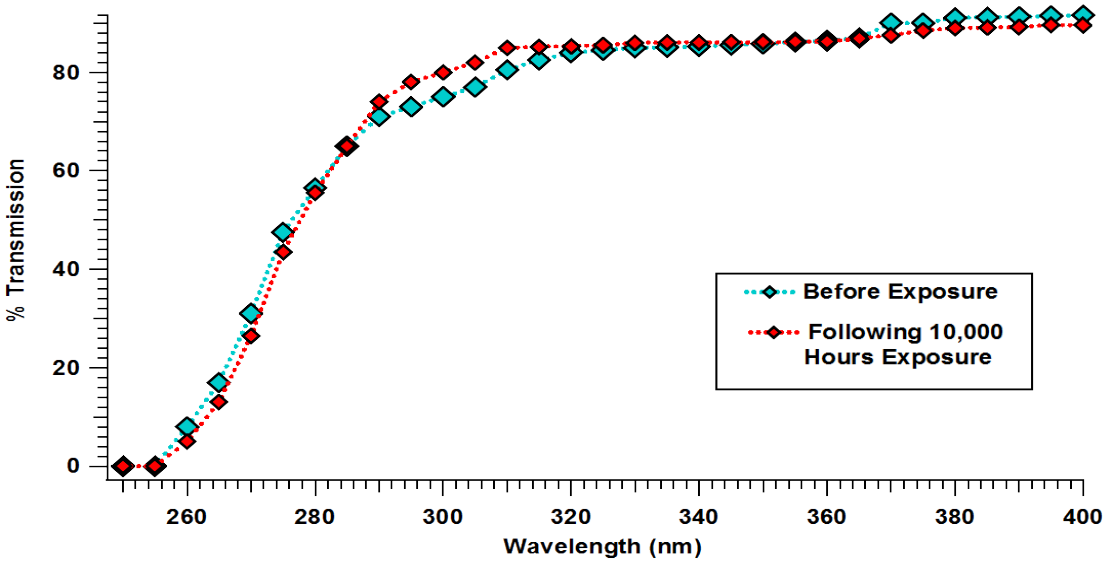

Figure 3. Percent transmission following UV exposure. Percent transmission vs. wavelength measured both before and after 10,000 hours of exposure to a high output 170 watt VHO lamp. Adapted from Cyro 2001 (Industries 2001).

2.2. ENVIRONMENTAL CHAMBER MIXING TECHNIQUE

Operational procedures for AACES include flowing ambient air through the lower chamber at a steady flow rate of approximately10 lpm. This air movement alone will lead to turbulent mixing in the lower chamber allowing for more efficient air penetration across the membrane. However, since the natural microporous structure of the e-PTFE leads to a slight pressure drop across the membrane, the turbulent mixing from the lower chamber will not effectively mix the upper portion of AACES. With a total chamber volume on the order of 1400 liters, additional mixing is required in order for the upper chamber to respond quickly to variations in ambient gas concentrations. Traditional mixing techniques used in environmental chamber applications include the use of air movement via internal mixing fans. This technique, although useful for efficient, timely mixing, can increase the particle coagulation effects within in the chamber as well as provide additional surfaces for heterogeneous reactions to occur as particles deposit to the surfaces of the fans. Therefore it is necessary, primarily in small volume chambers, to achieve non-invasive mixing. In order to do this, an external mixing technique was developed, tested and utilized. The method discussed below is analogous to that used by Luo et al., 1995 in which they manually flexed the Teflon chamber walls to achieve adequate mixing (Luo et al. 1995).

A sonic disturbance is propagated by the motion of molecules within the propagating medium. Using the concept of spherical harmonics and its relation to sound, an external subwoofer was placed alongside AACES and operated at a continuous

frequency of 20 Hz. This creates a small perturbation pressure wave whose behavior satisfies the spherical wave equation in scalar form:

$$\nabla^2\psi = \frac{1}{v^2}\frac{\partial^2\psi}{\partial t^2} \quad 2.1$$

With a general harmonic solution:

$$r\psi(r) = A\cos(\omega t - kr + \phi) \quad 2.2$$

where v is the speed of the wave, ω is the angular frequency, k is the wavenumber, and ϕ is the phase. By introducing a sonic disturbance of this form, particles and gaseous molecules will oscillate about a fixed point which will thereby enhance the diffusion of particles in space leading to a gentle mixing of the chamber environment. This method of mixing differs from traditional mixing techniques in that it is a simple enhancement of the already present diffusion and will not lead to an increase in particle coagulation rates.

In order to verify the effectiveness of this new mixing technique, carbon monoxide was continuously injected into one of the base inlets of the chamber under nominal operating conditions with a dilution flow rate of 10 lpm and intermittently sampled from the upper chamber using a Thermo Scientific Carbon Monoxide Analyzer. CO calibration gas was supplied using a compressed gas cylinder containing a concentration of 500 ppm, which was then diluted using the internal mass flow controllers housed within the calibration suite. During each mixing verification run, CO concentration was increased after roughly one hour, a time which enabled full mixing to take place, by employing a Thermo Scientific dynamic gas calibration system to vary the dilution rate while maintaining a near steady total flow rate entering the chamber resulting in a CO concentration vs. time given in Figure 4. As the CO gas flow was

stepwise increased, the zero air flow supplied to the internal mixing chamber was subsequently decreased to maintain a continuous flow into the bottom portion of AACES. Slight variations in the flow exiting the gas calibration system remained leading to fluctuations in total CO concentration over time. Plotted in Figure 5 are the results from six selected mixing segments during these stepwise increases in which the data has been quantified using exponential fits in order to retrieve the mixing time constant (τ):

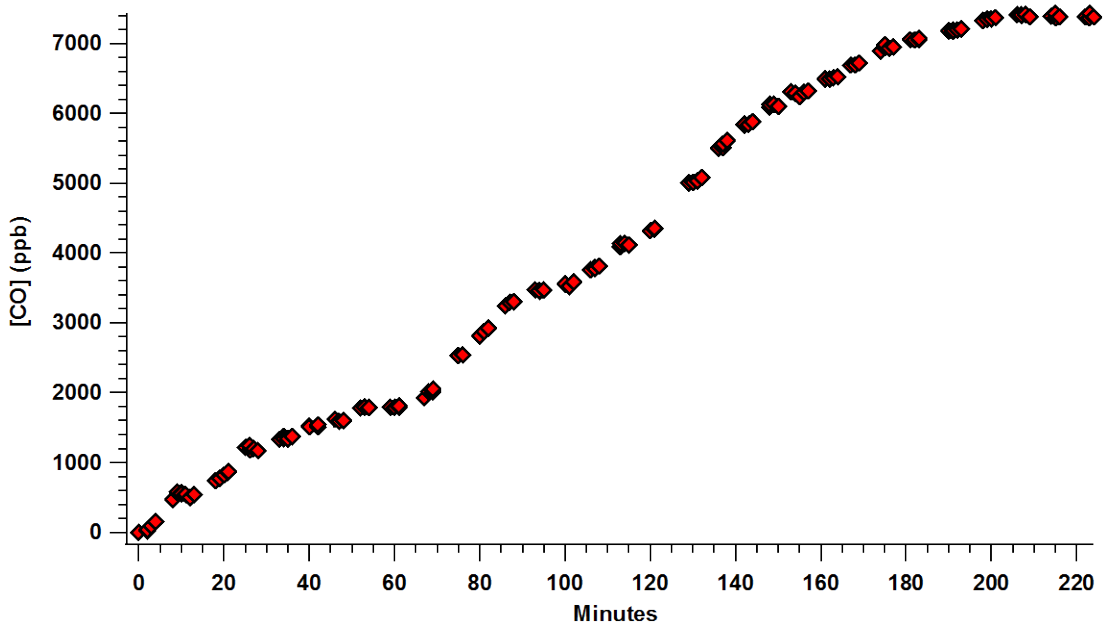

Figure 4. Aerosol Chamber Mixing. Plotted carbon monoxide concentration vs. time under fully mixed conditions. Each increase in concentration is representative of an intentional step change in CO concentration.

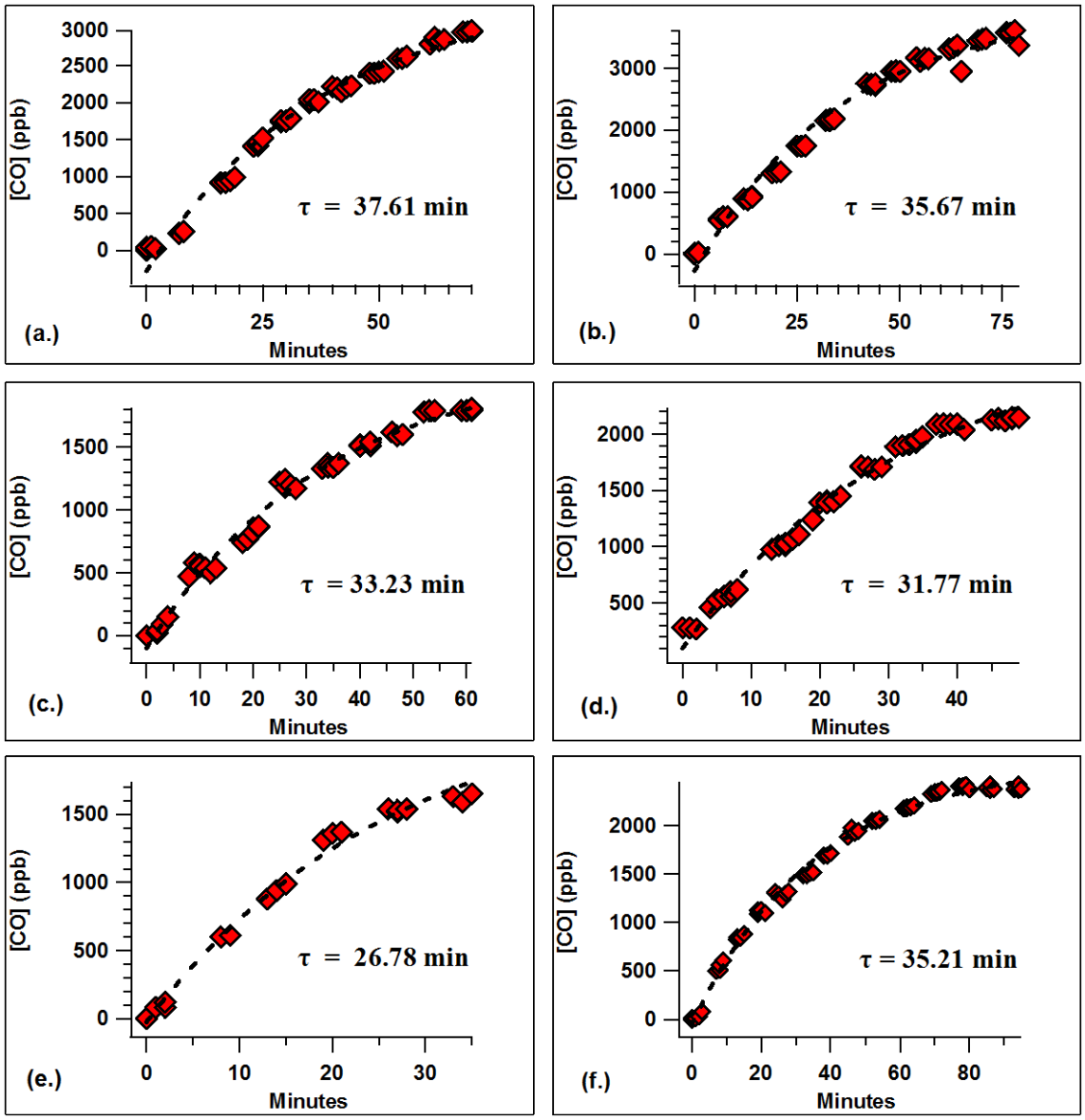

Figure 5. Mixing Timescales. Carbon monoxide concentration vs. time for 6 selected mixing periods fitted using exponentials to determine characteristic mixing time constants (τ).

The maximum observed mixing time constant was equal to 37.61 min. as indicated in Figure 5(a.), while the minimum measured time constant is recorded in Figure 5(d.) at 26.78 min with an average of roughly 33.8 min total. This data indicates that internal chamber concentrations under nominal operating conditions will be fully representative of ambient conditions within 30 min of a change in ambient concentrations.

2.3. EXPERIMENTAL CHAMBER PREPARATION

Laboratory evidence suggests that chambers constructed from FEP Teflon film off-gas NOx (Carter et al. 1982; Carter et al. 1995), and this may affect SOA production under high VOC/ NOx ratios (Presto et al. 2005). In order to limit the effects of Teflon® off-gassing on ambient measurements, a process was developed to both encourage Teflon® off-gassing and to react away products resulting from this off-gassing. For a period of about a week, AACES was flushed with zero air mixed with a high concentration of ozone atop the roof of the Eller O&M Building at Texas A&M University. This location provided optimal solar exposure during the daytime hours. Ozone was generated by modifying a Thermo Scientific NO-NO_2-NO_x Analyzer, Model 42i to isolate the ozone generation system housed with the instrument. At an average flow of 0.5 lpm, ozone was produced at a concentration of roughly 20 ppm as verified with a Thermo Scientific Ozone Analyzer Model 49i. The ozone flow was then diluted with zero air creating a steady ozone concentration of about 6ppm, which was then injected into the chamber and allowed to flush completely day and night for a period of

about a week. Following this baking process, NO_x concentrations were measured in both ambient and chamber hourly for 24 to 48 hours to determine if Teflon off-gassing was evident. In the event that chamber NO_x measurements were elevated, the process was repeated until NO_x concentrations inside the chamber were equal to or slightly less than that observed in ambient air. By limiting the effects of NOx off-gassing in the chamber environment, the impact on SOA formation and growth is restricted to ambient NOx concentrations (Presto et al. 2005).

2.4. PARTICLE FILTRATION AND GASEOUS PENETRATION EFFICIENCIES OF THE E-PTFE MEMBRANE

In order to determine the particle filtration efficiency of e-PTFE under chamber operational conditions, penetration experiments were conducted. The experimental setup involved connecting a TSI 3760A Condensation Nucleus Counter to a manual three way valve with one side of the valve sampling room air and the other connected to an inlet on the upper portion of the chamber. During the course of the experiment, the bottom portion of the chamber was continuously flushed with room air. Chamber air was sampled at 10 minute intervals and concentrations compared with that measured in room. The resulting particle filtration efficiency under chamber operating conditions yielded an average particle penetration of less than 0.1%. Since measurement of aerosol transformations within the chamber environment are based on the changes in particle properties observed over time relating to a monodisperse distribution of known size and

composition, it is imperative that ambient particles remain isolated from the chamber environment. These results show that when ambient concentrations are on the order of 10^3 cm^{-3}, the concentration of these ambient particles within the chamber is around 1 cm^{-3}, a value that is consistent with recent experimental filtration testing of e-PTFE in bag-house applications where a filtration efficiency exceeding 99.99% for particles 0.07 μm in diameter was observed (Wikol et al. 2008).

Similarly, the e-PTFE membrane is designed to allow for efficient gas flow while filtering particles. However, concerns regarding highly reactive species penetrating the membrane without reacting with existent trapped particles resulted in gas penetration tests in the laboratory. The gaseous species studied were ozone, carbon monoxide, sulfur dioxide, nitrogen oxides, toluene, acetic acid, and isoprene. In order to determine the penetration efficiency of ozone under normal chamber operating conditions, ambient air was pulled through the bottom portion of the chamber atop the roof of the Eller O&M building at Texas A&M University. The chamber was allowed to come to a steady mixed state, and ambient ozone concentrations were measured at roughly 30 min intervals using a Thermo Scientific Model 49i Ozone Analyzer. The resulting ozone concentration within the upper portion of the chamber, after passing through the membrane, was above 96% of ambient as indicated in Figure 6. The penetration efficiency of toluene, isoprene, carbon monoxide, sulfur dioxide, nitrogen oxides and

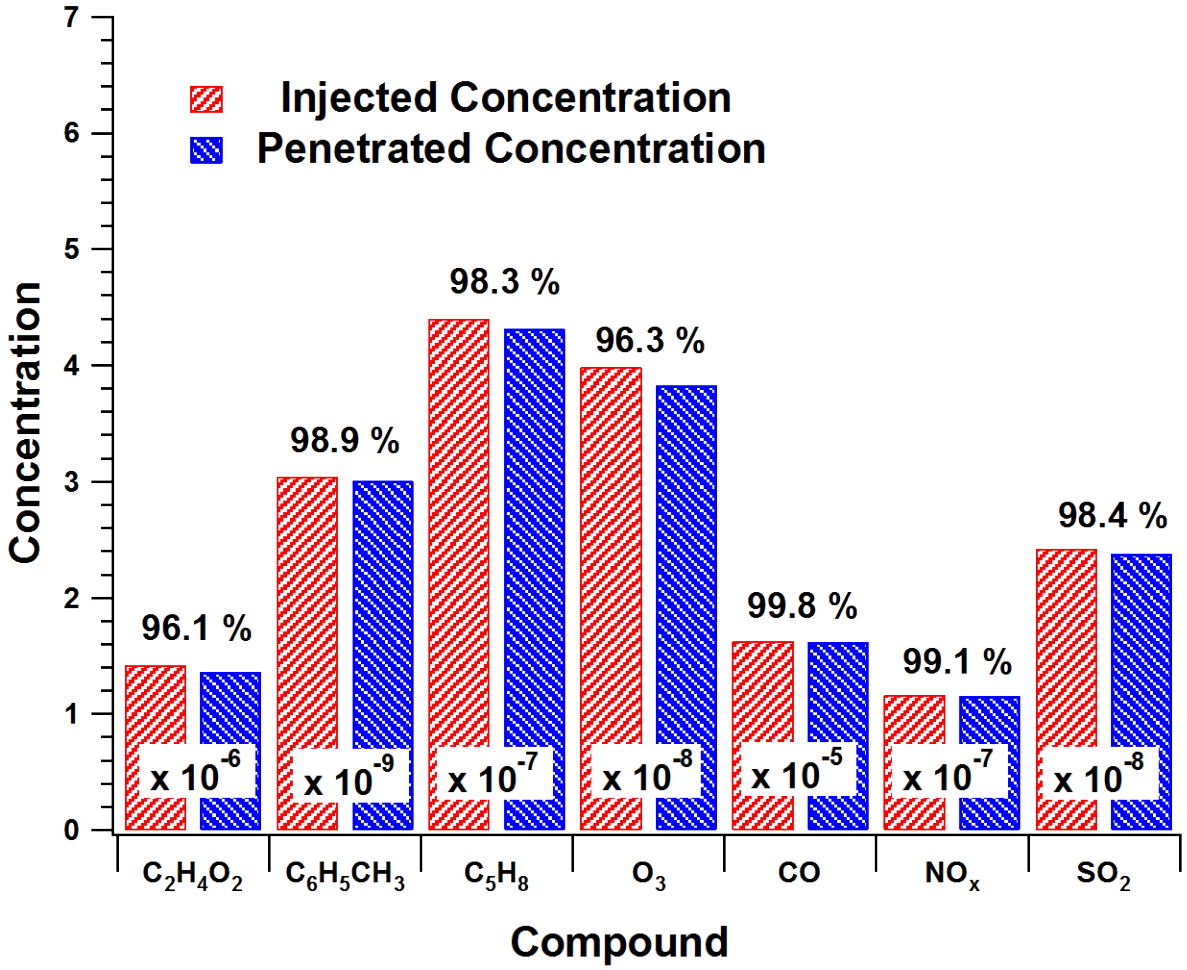

Figure 6. Penetration Efficiencies. Average concentration for acetic acid, toluene, and ozone both injected into the lower portion of AACES (red) and measured from the upper portion of AACES (blue). Resulting penetration efficiencies are depicted above each category as a percentage of that measured in the chamber compared with that injected.

acetic acid was conducted under a controlled laboratory setting. In order to generate acetic acid, zero air flow was subjected to a liquid bath containing the organic substance with a flow rate of 10 lpm. The air stream was then directed into the lower portion of AACES. Measurements of both the injected concentration and the concentration in the upper portion of AACES (past the e-PTFE membrane) were obtained at 15 min. intervals using a Proton-Transfer Mass Spectrometer (PTR-MS) for a period of at least 6 hours. In order to determine PTR-MS response time through the ¼" Teflon tubing used for both chamber and injection sampling, the inlet was disconnected from the chamber and exposed to room air. The measured response time was approximately 1 min so that the selected 15 min sampling intervals are sufficient to capture steady state concentrations for comparative purposes. Since acetic acid is a major contributor to the total atmospheric gas phase acidity (Grosjean 1992), high penetration efficiency supports the use of AACES to mimic the ambient environment.

Both toluene and isoprene were generated using Dynaco corp. permeation tubes housed in a glass temperature controlled u-tube, and 10 lpm zero air directed through the u-tube housing at 30°C. By using calibrated permeation tubes, a steady concentration is produced limiting fluctuations in injected concentration. The organic gas was then injected into the bottom portion of AACES, and concentrations sampled from the upper chamber using a PTR-MS at 15 min intervals once the chamber had reached a steady state concentration. Each measured concentration, both injected and in chamber, were averaged over the sampling period, and the resulting penetration efficiencies for toluene and acetic acid are 98.9% and 98.3% respectively as depicted in Figure 6. For each of the

gases shown, the concentrations were stable such that the resulting standard deviation was less than 1% of the total concentration. Toluene is a known contributor to SOA formation primarily through oxidation reactions yielding lower volatility products such as cresol. Although isoprene is only thought to be a small contributor to SOA formation, it accounts for a significant fraction of the total global BVOC budget. Therefore, determining the penetration efficiencies of these gases is crucial to verify the use of AACES in the study of ambient SOA production.

CO, SO_2, and NO_x injected concentrations were stabilized using a dynamic gas calibration system with the supply compressed gas flow rate set at 190 sccm diluted with 10 lpm zero air flow. Again, concentrations were allowed to reach a steady state within the upper chamber and concentrations measured at 15 min intervals upon injection into the lower chamber and from the upper chamber past the e-PTFE membrane. As indicated in Figure 6, CO exhibited a penetration efficiency of 99.8%, NO_x penetrated at 99.1 %, and SO_2 showed the least penetration efficiency of the three gases studied at 98.4%. Based on the above discussion it is determined that the e-PTFE Teflon membrane is efficient at removing ambient particles while allowing gases to readily penetrate creating an environment inside AACES that is free of particles and mimics ambient gas concentrations. This allows for the study of atmospheric particulate transformation under ambient conditions.

Temperature will have a significant impact on the SOA forming potential of organic vapors in the atmosphere. Sheehan and Bowman, 2001 reported a significant

decrease in SOA production (16 – 24 % decrease) following a 10 °C increase in temperature (Sheehan and Bowman 2001). Their modeled results agreed with experimental observations involving the effects of temperature on SOA production from m-xylene. Temperature measurements were obtained under normal chamber operating conditions outdoors at Lick Creek Park in College Station, TX using a suspended thermocouple. Since direct sunlight can influence readings from the thermocouple, a small portion of AACES near one of the upper inlets was shaded while the remainder of the chamber was exposed to solar heating. This allowed for accurate measurements of the actual temperature within the reaction chamber while allowing for a shaded region for temperature collection. Measurements of both temperature and relative humidity (measured in chamber by placing an RH probe immediately past the chamber inlet with a sampling flow rate of 1.0 lpm) both in chamber and in ambient during a roughly three hour period are shown in Figure 7. As is evident, the temperature within the reaction chamber is slightly higher (2.92 °F or 1.62 °C difference) on average, with the relative humidity in chamber 0.56% less than that of ambient, a value consistent with the increase in temperature measured. Based on these measurements, it is estimated that under normal chamber operating conditions outdoors, the gaseous vapor pressures will only be slightly higher than ambient.

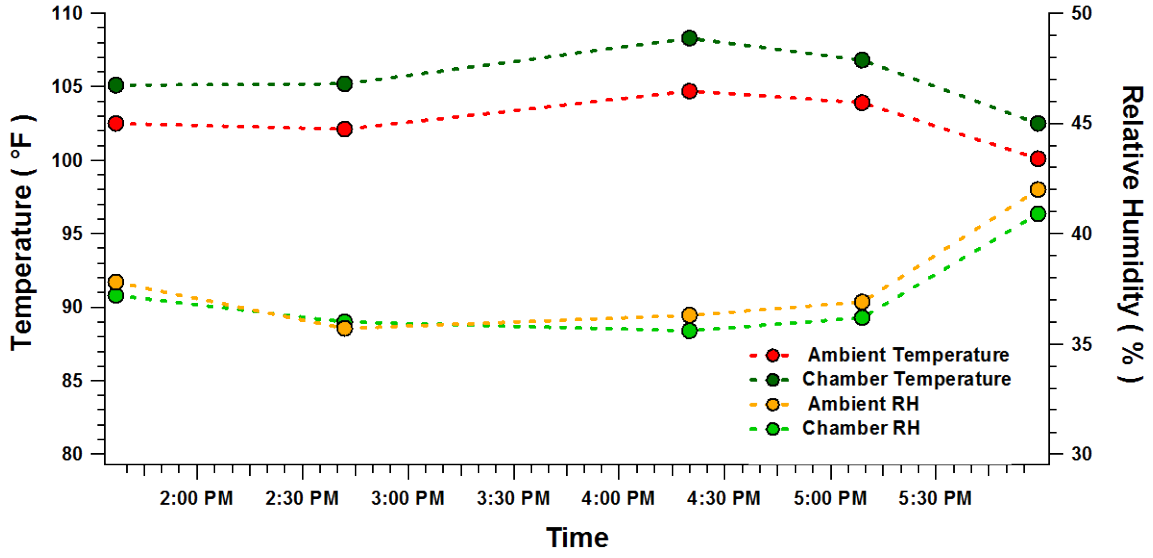

Figure 7. In Chamber Atmospheric Variability. Temperature and relative humidity vs. time measured both in chamber (green) and in ambient (red and yellow).

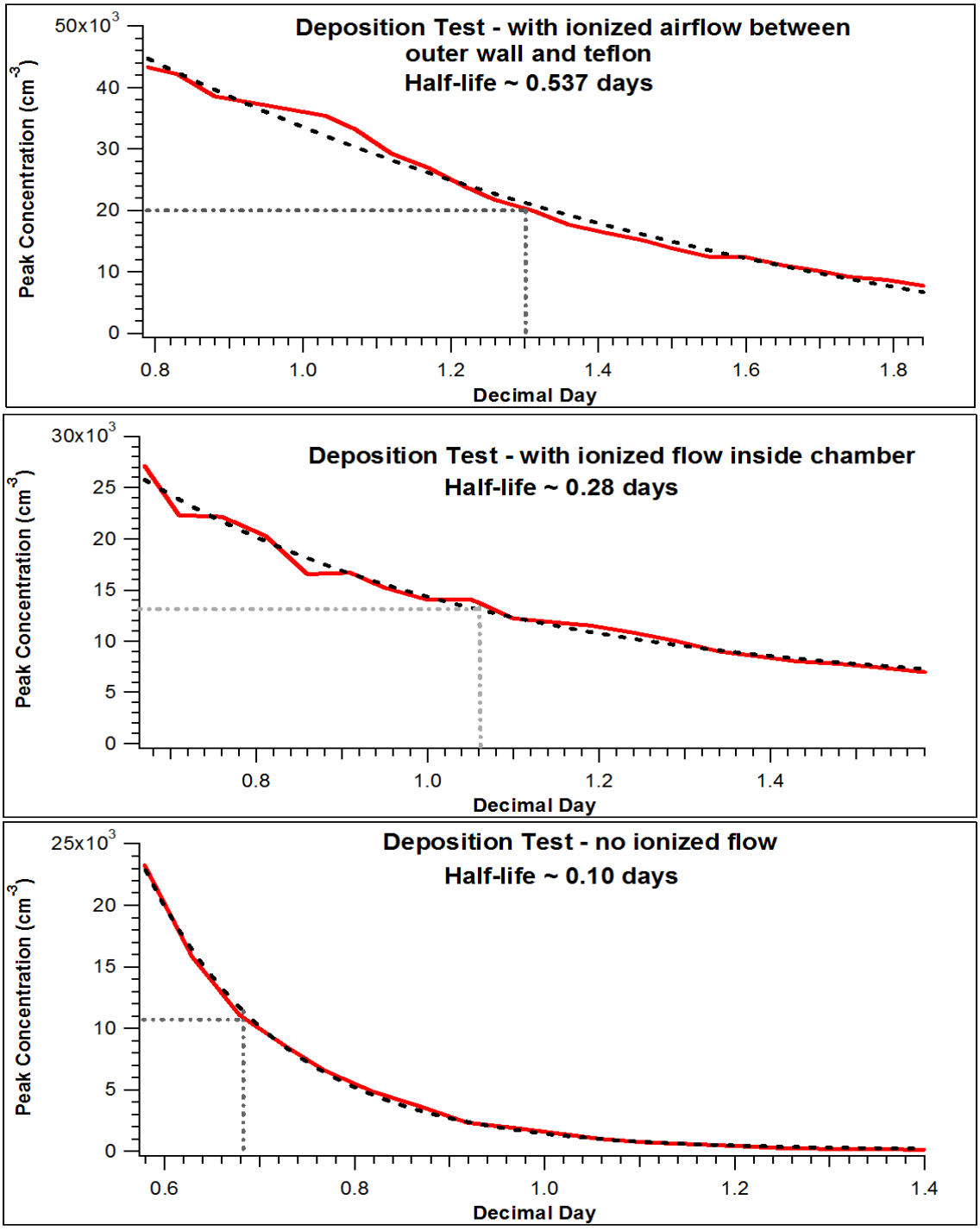

Figure 8. Particle Deposition Conditions. Deposition tests under the conditions of "no ionized flow" (bottom), ionized flow directly injected into the chamber (middle), and ionized flow injected in between the FEP Teflon® and the chamber outer wall (top).

2.5. IN-CHAMBER PARTICLE AND GASEOUS DEPOSITION RATES

Many processes that lead to particulate transformation occur within timescales on the order of hours to days. Moreover, since FEP Teflon is widely known to carry a natural static charge, experiments were carried out under non-mixed conditions to deterministically decrease the loss of particles to the walls within the chamber due to charge. In order to measure the depositional loss of particles, uncharged ammonium sulfate particles were generated and injected as described in sub-section 4.1, and the concentration monitored on an hourly basis using a DMA system. Figure 8 shows the depositional loss rates for each of three experimental observations on particle deposition within the chamber under non-mixed conditions. The first of three experiments involved injecting 0.075 μm uncharged particles into the upper portion of AACES with all but the injected port of the upper chamber plugged. Sampling was then conducted through hourly DMA scans, with each scan lasting roughly 5 min. The bottom portion of AACES remained open to room air allowing for any necessary dilution flow to be obtained without affecting particulate concentrations. This resulted in a particle concentration half-life of about 0.10 (2.4 hours). At a sampling flow rate of 1.5 lpm, the fraction of particles lost due to sampling is 0.625%, and therefore the measured loss within the chamber is a direct result of wall loss and gravitational settling. Since the settling velocity of particles smaller than 0.100 μm is on the order of 0.1 cm h^{-1} (Seinfeld and Pandis 1998), the conclusion can be drawn that since FEP Teflon maintains a natural static charge, regardless of the charging state of the aerosol, wall loss rates are enhanced

as the presence of cosmic rays in the atmosphere result in the re-charging of particles. To combat this effect, compressed air was passed through a ^{210}Po 200 mCi charging source which generated an ionized air flow. The air was then passed first into the reaction chamber itself and deposition scans repeated. The resulting half-life of the aerosol concentration increased to near 0.3 days (7.2 hours). This effect is likely due to a partial neutralization of the static charge carried by the FEP Teflon sheet. However, since the particles present in the chamber are also exposed to the ionized air flow, the particle distribution will also gain a uniform charging state through collisions with ionized molecules resulting in a loss enhancement of particles to the walls due to the attractive forces that exist between opposing charges. A third test involved injecting the ionized air flow between the outer acrylic walls of the chamber and the FEP Teflon and the experiment repeated. While continuously supplying ionized air to the Teflon outer surface, the depositional loss rate was decreased considerably, resulting in a concentration half-life of 0.54 days (12.96 hours) due to wall loss under non-mixed chamber conditions. Repeated tests yielded similar results.

Because AACES is operated under sonically mixed conditions which could have the potential to enhance particle concentrations near the Teflon walls, a series of depositional loss studies using various injected particle diameters was conducted under nominal chamber operation with ionized air flow being passed between the FEP Teflon bag and the outer acrylic sheet. Prior to each injection, AACES was continuously flushed with zero air to ensure a clean environment at the start of each experimental run. Monodisperse, uncharged ammonium sulfate particles having diameters of 0.050, 0.750,

0.150, or 0.200 μm were injected, and particle concentrations monitored hourly. These results are shown in Figure 9 and color specific arrows indicate the half-life of each respective particle size. As is evident, particles having small mobility diameters (0.050 and 0.075 μm) have an operational half-life of roughly 0.25 days (6 hours), while particles having relatively large diameters (0.150 and 0.200 μm) yield a half-life of about 0.2 days (4.8 hours) under normal chamber operation. This effect is likely a result in an increase in the settling velocity of the larger particles. Soot particles tended to behave more like the smaller diameter spherical ammonium sulfate particles, with a depositional half-life of roughly 0.3 days (7.2 hours) for soot particles having a mobility diameter of 0.150 μm. With a sampling rate of 1.5 lpm for roughly 2 minutes each hour during these experiments, it is calculated that fractional loss of particles due to sampling is equal to 0.004% of the original injected concentration. Despite the increase in depositional wall loss due to chamber mixing, measurable concentrations will be present within AACES longer than 12 hours. As an example, with an injected integrated concentration roughly equal to 1500 cm^{-3}, a total concentration of 375 cm^{-3} will still be present in measureable concentration within the chamber following 12 hours of intermittent sampling with the remaining portion of originally injected particles present on the chamber walls. It is important to note that the loss of particles to the flat surfaces of the chamber walls results in a lower available particle surface area exposed to the chemical environment which may lead to the particulate loading being less representative of actual ambient concentrations.

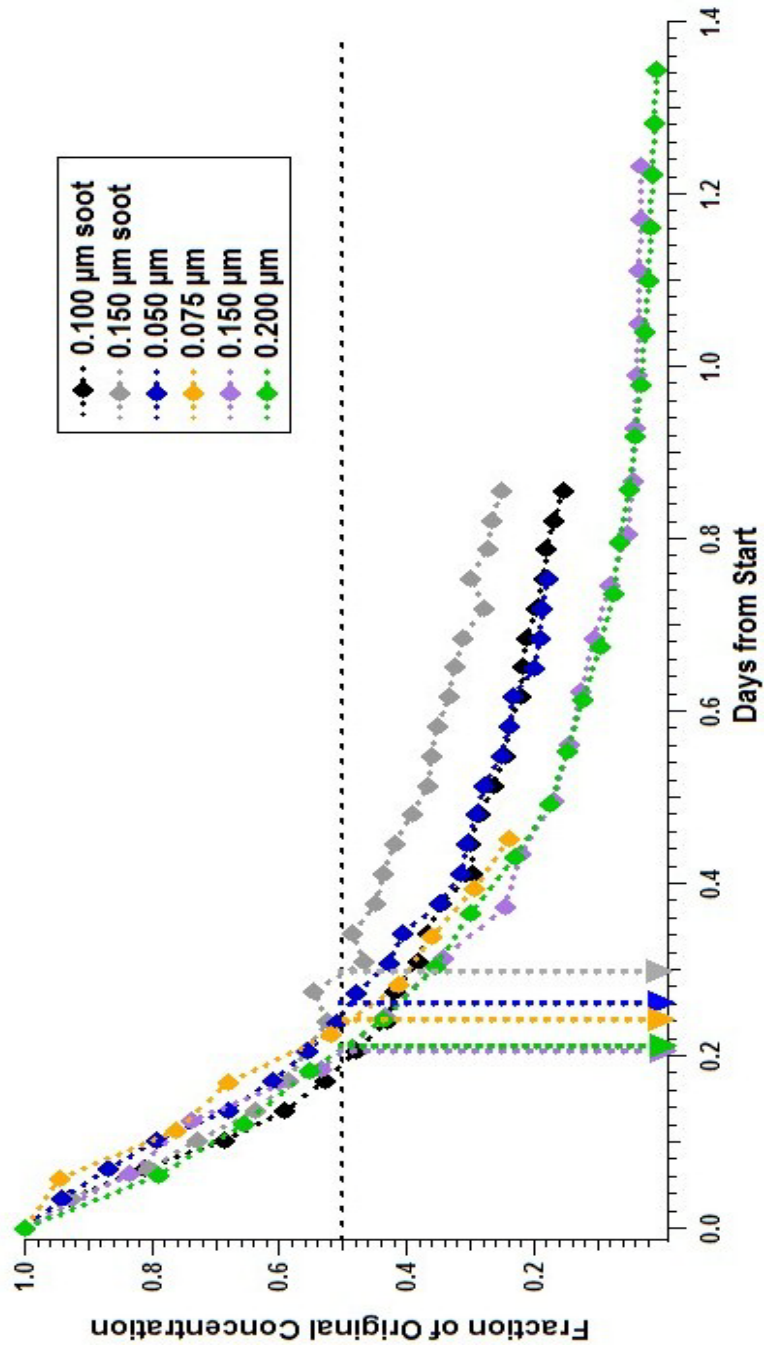

Figure 9. Particle Deposition Rates. Percent particle concentration vs. time for ammonium sulfate particles sized 0.050 (blue), 0.0750 (orange), 0.150 (lavender), and 0.200 µm (green) as well as soot particles sized 0.100 (black) and 0.150 µm (grey). Plot depicts depositional loss rate under normal chamber operating conditions with concentration half-life indicated by dashed color specific lines.

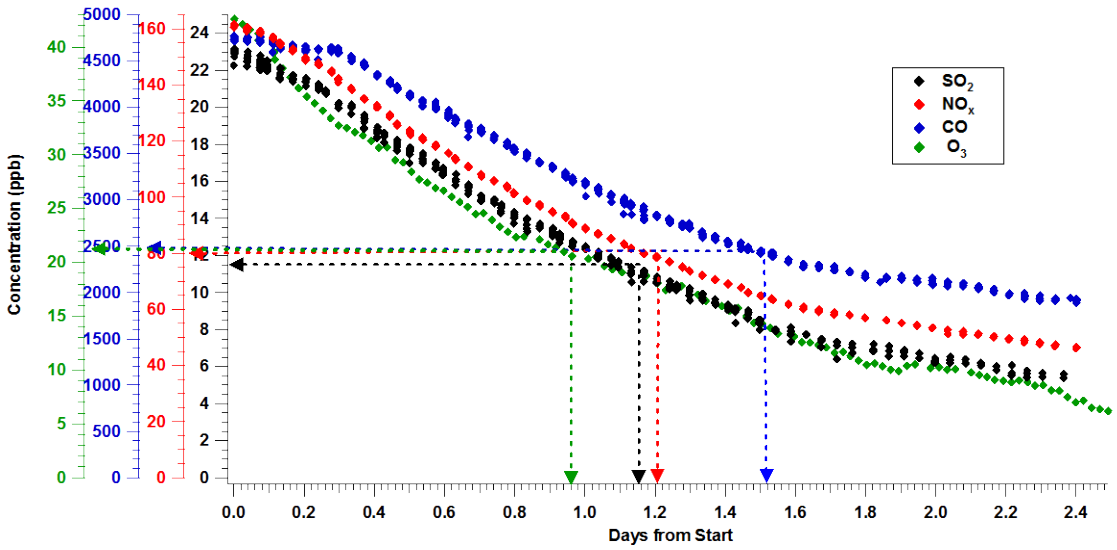

Figure 10. SO_2, NO_x, CO Deposition. Concentration vs. time for SO2 (black), NOx (red), CO (blue), and O3 (green). The y-axis are color coded for species, and the half-life indicated by the dashed lines.

Due to concerns regarding the loss of gaseous species to the Teflon surface during aging measurements, the depositional loss of ozone, carbon monoxide, nitrogen oxides, sulfur dioxide, toluene, and isoprene were examined. The resulting concentration vs. time for CO, O_3, SO_2, and NO_x is given in Figure 10. Ozone was generated by photolysis of diatomic oxygen using a mercury lamp source with a 185 nm cutoff and injected into the bottom portion of AACES until a steady concentration was reached. Following injection ozone was sampled using Thermo Ozone Analyzer Model 49i at roughly 30 minute intervals for duration no longer than 5 min to limit chamber loss due

to sampling. Because of the limited chamber volume, a dilution line was connected to the upper portion of AACES ensuring that long-term sampling would not lead to a significant pressure drop within the chamber which could lead to inaccurate gas measurements. Therefore, the results shown include a decrease in concentration due to dilution flow. Similarly, compressed CO, SO_2, and NO_x were injected using a dynamic gas calibration system to maintain a steady flow into the bottom portion of AACES until a steady concentration was reached, and sampling performed at roughly 50 min intervals. As used during O_3 sampling, a dilution line was connected to the chamber for the duration of the measurement period. Each gas sampled, as indicated by the color coded arrows in Figure 10, yielded a chamber loss with dilution flow greater than 0.9 days (21.6 hours) with CO exhibiting the slowest loss of 1.5 days (36 hours). In a recent study by Matsumaga and Ziemann, it was determined that although gases will deposit onto the Teflon walls, the process is completely reversible ((Matsumaga and Ziemann 2009). With the considerations that depositional loss of gases is reversible and that AACES is constantly supplied with ambient air and mixed such that the chamber turnover time is roughly 30 min, the effects of gaseous wall loss will not bias the aerosol growth measurements when utilizing AACES.

The depositional loss of both toluene and isoprene were also examined, and the results plotted in Figure 11. Both toluene and isoprene were generated using Dynaco Permeation tubes placed in a glass temperature controlled U-tube and injected by directing zero air flow through the housing at a flow rate of 10 lpm at 30°C. Concentrations were again allowed to reach steady state, and then sampled using a

commercial Proton-transfer Reaction Mass Spectrometer at roughly 50 min intervals. A dilution line was again supplied to the chamber. As shown in Figure 11 little depositional loss was observed with regards to either species. When comparing the loss rate of the organics studied with that of the previous gases mentioned, the PTR-MS flow rate of 0.5 lpm is significantly less than that of the gas analyzers used above (total combined flow rate of over 7 lpm). Therefore, there is a much smaller effect of any dilution flow that is present; however, the actual volumetric dilution flow rate was not quantified during the course of the experiments.

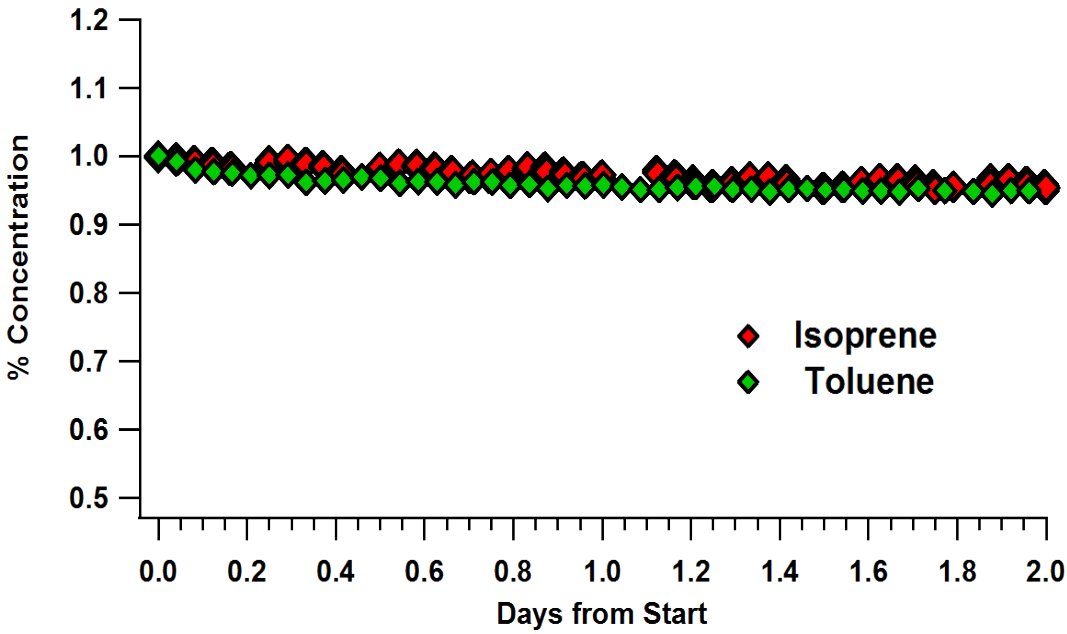

Figure 11. Toluene and Isoprene Deposition. Percent concentration vs. time for both toluene (green) and isoprene (red) gases in chamber.

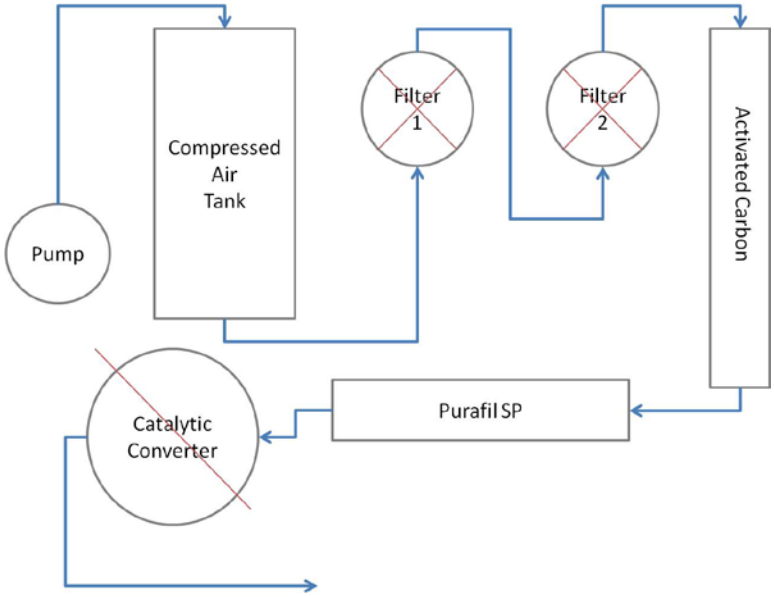

Figure 12. Zero Air Schematic. Flow schematic depicting the method of zero air generation.

2.6. ZERO GROWTH MEASUREMENTS UNDER AMBIENT CONDITIONS

A flow schematic depicting the method of zero air generation is shown in Figure12. In an attempt to limit the amount of unwanted products that may result from use of a typical compressed air system, an external high flow piston pump replaced the normal motor attached to a commercial air tank. To reduce excess back flow on the pump pistons, a check valve was installed on the tank inlet thereby reducing the work load on the pump and prolonging the lifetime of the pump pistons. Due to specifications requiring no more than 30psi of pressure be applied to the pump, a Swagelok adjustable excess pressure valve was installed in a tee with a regulator on the tank exit which

allowed excess pressure to be bled off. With this setup the pumps could run continuously, and the tank pressure was maintained at about 30psi depending on flow rates required for zero air generation.

In order to create zero air, the compressed air is first dried using a combination water trap to remove large water particles and a Perma Pure Nafion dryer in series. Dried air is then passed through a two stage micro filtration system designed to remove large particles from compressed air followed by an initial compressed air activated carbon scrubber. Following this initial scrubbing process, the air stream is passed through two 0.22 µm pore size Polypropylene Membrane filters in series resulting in the removal of any remaining small particles from the flow and then directed through a 4.0×10^3 cm^3 cylinder containing Purafil® SP, which effectively removes hydrogen sulfide, sulfur dioxide, nitric oxide, and formaldehyde from the gas stream. The next stage of air purification consists of a second 4.0×10^3 cm^3 cylinder containing General Carbon Corporation Spectrum XB-17 activated carbon blend. This blend consists of 50% Spectrum HS-600, a silicate compound impregnated with 6% potassium permanganate ($KMnO_4$), which is ideal for the absorption and oxidation of polar and lower molecular weight compounds. The remaining 50% is activated carbon. Spectrum XB-17 is efficient at the removal of numerous organic compounds including toluene, isoprene, acetic acid, and nitrobenzene as well as alcohols including isopropanol and methanol. The final stage of scrubbing consists of a heated stainless steel tube containing platinum coated aluminum spheres (Shimadzu Corp.) which acts as a catalytic converter.

Since AACES is designed specifically to study the evolution of atmospheric aerosols, growth scans under zero air conditions were conducted to ensure that ambient growth processes could be accurately represented, and Teflon off-gassing was not a significant contribution to observed growth. In order to obtain a zero growth scan, monodisperse ammonium sulfate particles containing no charge are injected into the upper portion of AACES during mid-morning for approximately one hour, and particle size and hygroscopic growth measured over time using an Humidified Tandem Differential Mobility Analyzer (H-TMDA) system, while zero air is supplied to the bottom portion of AACES throughout the measurement period. The process by which uncharged monodisperse particles are generated and injected into AACES and the H-TDMA operation are discussed in greater detail in 3.2. Prior to particle injections into the chamber, zero air was used to flush the chamber completely for a period of about four hours ensuring that all suspended ambient gases and any previously injected particles had been removed, and gases and particles which may have deposited to the walls were flushed out. Figure 13 shows the result of a zero growth scan, a process which was described previously, of a monodisperse ammonium sulfate aerosol distribution conducted at a rural location in Central Oklahoma plotted against an ambient growth event that occurred at the time of the measurements. The red diamonds indicate peak particle diameter log-normally fitted during the chamber measurements, and these are superimposed on top of contours (solid lines) showing relative concentration in chamber. Similarly, the blue open diamonds are the peak particle diameters observed in ambient during the same time period overlaid on ambient concentration contours (dashed lines).

While there was zero growth observed in the chamber being supplied zero air and separate from the ambient environment, ambient peak diameter exhibited a growth of roughly 0.024 µm over 2.5 hours, yielding a near linear 9.0 nm/hr growth rate. It is important to note that the comparisons between chamber and ambient are not exact as the ambient environment is uncontrolled yielding a higher concentration of small particles, the source of which is unknown, that may exhibit higher growth rates than those 0.075 µm particles injected into the chamber.

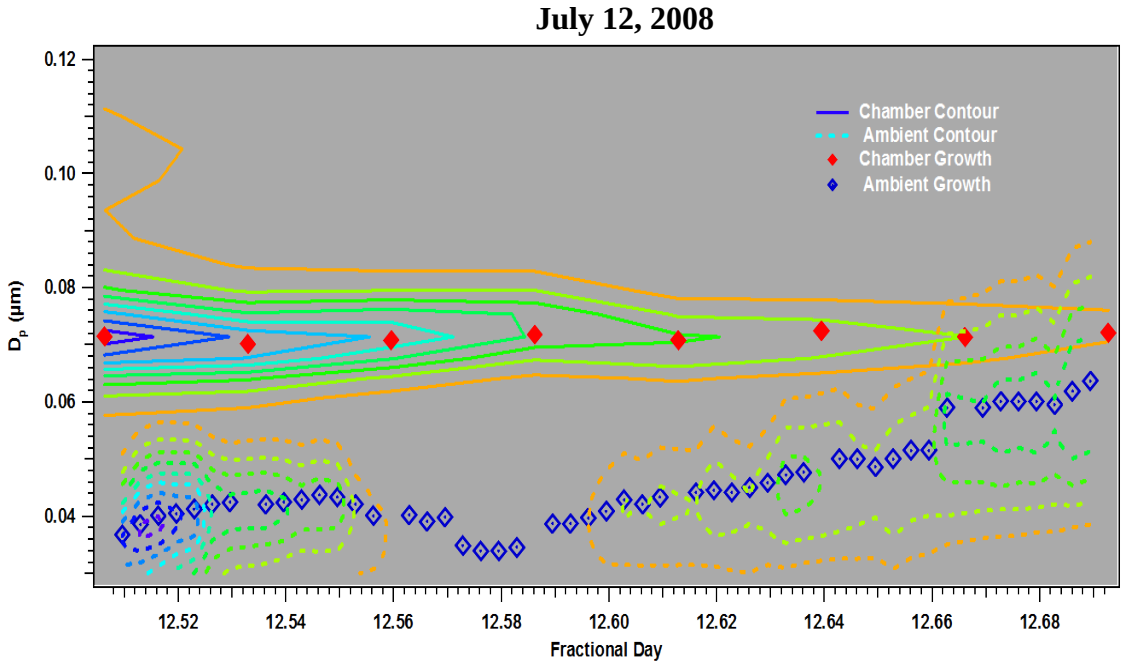

Figure 13. Zero Growth vs. Ambient Growth. Peak diameter for a zero growth measurement in chamber (red diamond) superimposed on measured chamber concentration (solid contour), and peak diameter determined for an ambient growth event (blue diamond) overlaid on ambient concentration (dashed contour).

Figure 14 shows the results of a zero growth scan involving a dual chamber setup conducted in a remote forested region in Colorado. The experimental setup involved continuously supplying zero air to the flow region of one chamber (chamber 1) as described above with the bottom portion of the other chamber (chamber 2) being supplied a constant flow ambient air. Chamber sampling occurred at hour intervals. Plot (a.) shows peak fitted diameter for zero growth (solid black dots) superimposed on contours of DMA measured concentration for comparative purposes, while plot (b.) shows the same for the chamber conducted under normal operating conditions. The results plotted in (a.) show no observable growth whereas the results given in (b.) yield a change in particle peak diameter from 0.076 μm to 0.097 μm over roughly 4.3 hours, culminating in a 4.9 nm/hr growth rate. As further evidence of zero growth observed under zero scan conditions, plot (c.) shows the hygroscopic growth factor (the ratio of measured wet diameter at 90% RH to initial dry diameter of the same size, D_p/D_p^*) for both chamber 1 and chamber 2. As chamber 1 exhibits zero growth, the hygroscopic growth factor remains constant at near 1.62, a value consistent with pure ammonium sulfate at 90% relative humidity; chamber 2 produced a measured growth factor that decreases from about 1.62 to less than 1.25, suggesting that the uptake of organics to the particle surface in chamber occurred. Based on the results from these zero growth scans, it is determined that there is little contribution of particle growth due to the off-gassing of VOC's to the chamber environment.

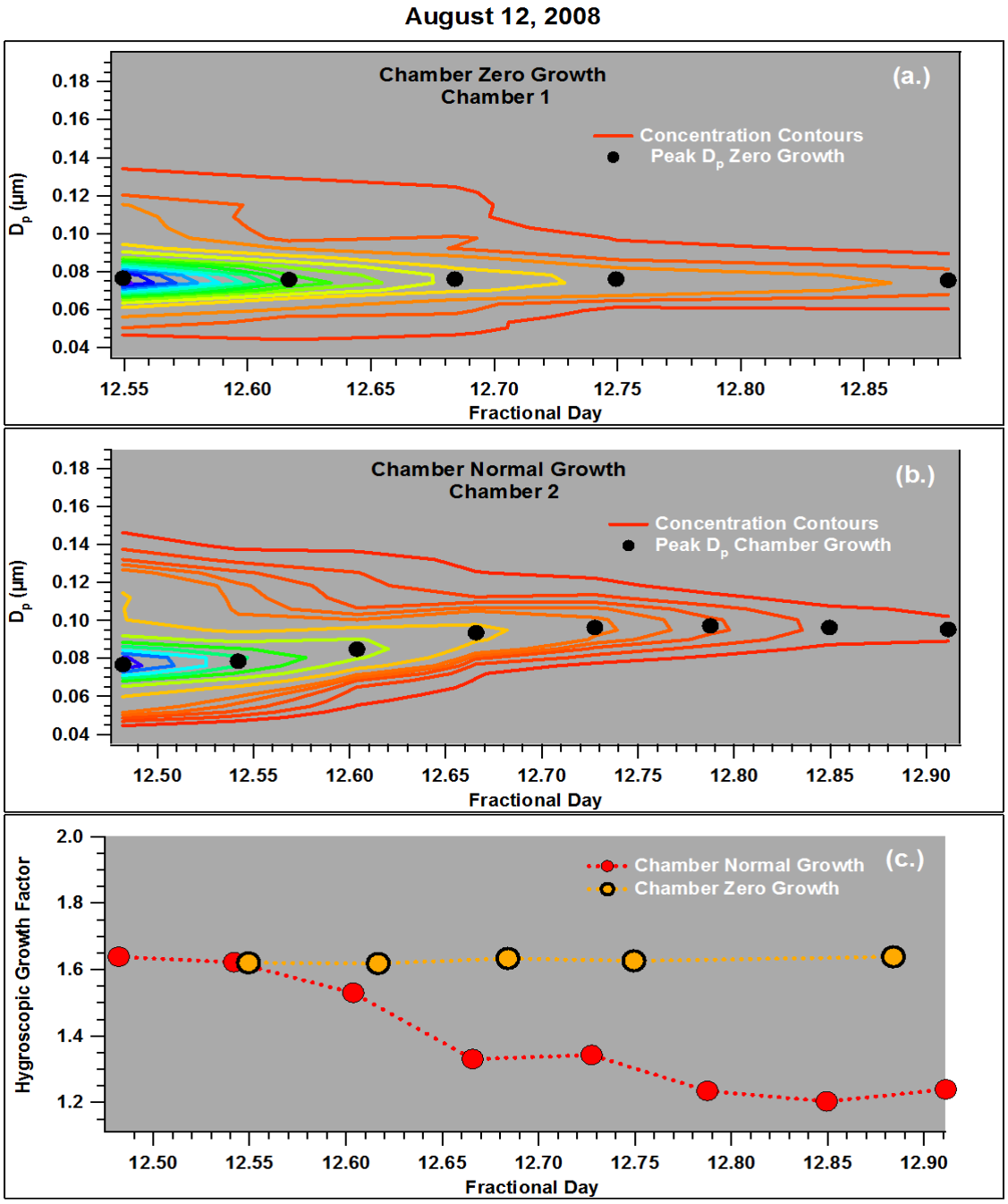

Figure 14. Zero Growth in Chamber vs. Growth in Chamber. Zero growth measurement under zero air chamber conditions showing peak diameter vs. time (plot a.), growth measurement under ambient air chamber conditions displaying peak diameter vs. time (plot b.), and hygroscopic growth factor measurements for both condition (a.) and (b.) above.

3. OBSERVED SOA PRODUCTION AND GROWTH FROM AMMONIUM SULFATE SEED PARTICLES UNDER AMBIENT CONDITIONS

3.1. SITE DESCRIPTION

AACES was deployed as an integral part of three major field studies from 2007 to 2009 and was utilized to investigate the production and growth of SOA from ammonium sulfate seed particles as a result of gas-to-particle partitioning in the ambient environment. The first field deployment occurred during the Cloud Land and Surface Interaction (CLASIC) field campaign from June to July 2007 at the Atmospheric Radiation Measurement (ARM) Southern Great Plains (SGP) Climate Research Facility located near Lamont, OK is tens of miles from the nearest urban area. The ARM SGP site is surrounded by agriculture, and natural grasslands, making this location ideal for measuring SOA production under rural, agricultural conditions. Combined measurements of VOC emissions in both agricultural areas and natural grasslands show that species known to contribute to SOA production, α-pinene, β-pinene, *d*-limonene, toluene, xylenes, and Δ^3-carene, are abundant (Fukui and Doskey 2000; Helmig et al. 1999; Ng et al. 2006). AACES was located on an outdoor platform at the guest facility near the North side of the complex, a location that provided ease of access to an H-TDMA system located inside while providing sufficient daytime solar exposure.

A second field deployment occurred from July to August, 2008 during the Bio-hydro-atmosphere interactions of Energy, Aerosols, Carbon, H_2O, Organics & Nitrogen (BEACHON) Project located North of Woodland Park, CO in the Manitou Experimental Forest. This was a rural location at elevation (7800 ft) surrounded by an evergreen National Forest, an area rich in isoprene, α-pinene, β-pinene, *d*-limonene, and some sesquiterpene emissions (Helmig et al. 1999). AACES was located under the canopy nearby an adjacent monitoring trailer which limited solar exposure during the daytime due to shading.

The third location studying the effects of the ambient environment on the transformation and growth of ammonium sulfate seed particles was from April to July, 2009 during the Study of Houston Atmospheric Radical Precursors (SHARP) field campaign located atop the South Moody Tower, a roughly 18 story tall dormitory, on the University of Houston campus in Houston, TX. The University of Houston is ideally located near two major highways, I-45 and Hwy 59, as well as northwest of the Houston Ship Channel, a major industrial area featuring numerous petrochemical refineries as well as other industrial manufacturing facilities. Although BVOC emissions are ubiquitous in Houston, the area is dominated by anthropogenic VOC emissions, with biogenic production of VOC's accounting for roughly 4% of the total measured VOC mass and direct anthropogenic contributions of up to 83% depending on location (Buzcu and Fraser 2006). Among the anthropogenic VOC's measured in Houston, those that have been shown to produce SOA are cyclohexane, ortho-xylene, toluene, ethyl benzene, and 1,3,5 trimethylbenzene, although many others may have SOA forming potential yet to be

determined (Buzcu and Fraser 2006; Grosjean and Seinfeld 1989). Furthermore, with the availability of sulfur dioxide, organosulfates may also be contributors to aerosol growth (Hallquist et al. 2009).

3.2. EXPERIMENTAL METHODS

During each of the three field experiments, AACES was placed outdoors in the ambient environment. Prior to field measurements, the chamber was flushed continuously with zero air for a period no less than 24 hours in order to ensure a clean environment prior to sampling. For the purposes of aerosol size classification and hygroscopic growth measurements, an H-TDMA system is employed and housed inside a temperature controlled measurement facility no more than 10 feet from AACES. Moreover, because typical aerosol generation methods result in a polydisperse distribution which, under environmental chamber conditions, will lead to a more complex analysis of particle growth processes, a monodisperse aerosol of know size and composition is injected allowing for efficient monitoring of the size and hygroscopic growth as well as many other aerosol properties over time. Furthermore, steps are taken to ensure that the injected aerosol is free of charge to minimize deposition to the chamber walls. In order to inject a monodisperse uncharged aerosol into the upper portion of AACES, a TDMA system was utilized. A schematic showing the operation of the H-TDMA system is shown in Figure 15.

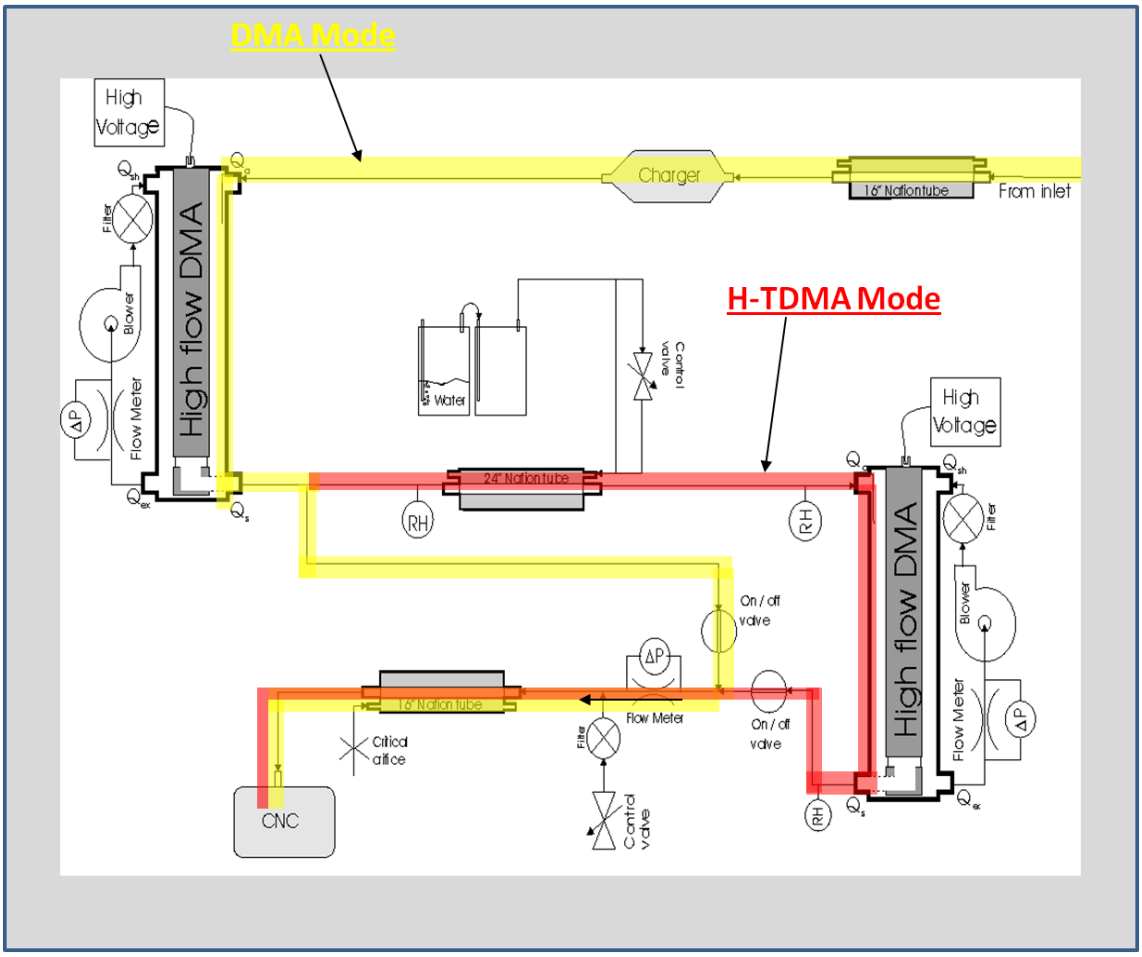

Figure 15. H-TDMA Schematic. Schematic depicting the operation of the humidified Tandem Differential Mobility Analyzer system. The yellow path indicated operation under DMA mode, while the red path shows the operation while operating in TDMA mode.

While in DMA operational mode, as indicated along the yellow path, the aerosol is first dried using a Perma Pure Nafion drier bringing the aerosol to a crystalline state at a stable RH of 15% and then directed through a ^{210}Po (400 μCi) charging source bringing the aerosol population to a predictable charged state. The aerosol is then sampled by the 1st DMA column where a high voltage is applied to the inner column and continuously ramped allowing for particles having diameters between 0.015 and 0.750 μm to be transmitted and counted using a TSI 3762 condensation particle counter (CPC). This produces a distribution of size-resolved aerosol concentration. While the system is in tandem mode as indicated by the red path, the voltage applied to the first DMA is held fixed in order to transmit a monodisperse crystalline aerosol. The size-classified aerosol is then exposed to a controlled RH ≥ 85% using a humidified Perma Pure Nafion drier, an RH that is sufficiently high to ensure deliquescence. Following humidification, the monodispersely distributed aerosol is then passed to the second DMA where the voltage is continuously varied, and transmitted particle concentrations are then measured using a TSI 3762 CPC. The final hydrated diameter D_p is then compared to the initial diameter D_p^* yielding the hygroscopic growth factor (HGF), D_p/D_p^*.

A schematic depicting the mechanism by which monodisperse particles are generated and injected is show in Figure 16. The polydisperse ammonium sulfate aerosol is generated using a solution of 1.0 g ammonium sulfate salt dissolved in 750 ml of 17 MΩ deionized water and atomized utilizing a TSI 3076 atomizer. The polydisperse aerosol spray exiting the atomizer is first dried using a Perma Pure Nafion drier then brought to a neutrally charged state using a ^{210}Po 400 μCi bipolar charging source and

sampled using the first DMA column at a specified fixed voltage, creating a monodispersely distributed aerosol. Upon size selection, the aerosol is directed through another ^{210}Po 400 μCi bipolar charging source bringing the aerosol back to a predictable charging state. The aerosol is then passed through the second DMA column with an applied voltage of 5000V and a sheath flow of zero, which removes charged aerosol from the flow while allowing only those aerosols containing effectively zero charge to be transmitted. This process creates a monodisperse uncharged aerosol distribution of known size and composition that is injected into the upper portion of AACES at a flow rate of 4 lpm. It is important to note that this method of monodisperse generation does not fully remove the multiply charged particles from the distribution as will be discussed in greater detail later in sub-section 3.3.

At the beginning of each sampling period, a monodisperse ammonium sulfate distribution is generated and injected into the upper portion of AACES for about 1 hour using the method described above. Typically, the injected particle size is around 0.075 μm. This size represents the peak of the atomized ammonium sulfate distribution allowing for shorter injection times and is sufficiently small to allow for the detection of minute changes to the aerosol diameter over time. Furthermore, in order to abate the effects of ambient nucleation within the chamber, seed particle concentrations having a peak diameter of 0.075 μm are on the order of 10^3. Such concentrations are also below the limit where coagulation becomes dominant, thereby minimizing effects from particle coagulation events within the chamber environment. Any effects of particle coagulation within the chamber should be reflected in the standard deviation of the monodispersely

distributed aerosol upon data parameterization techniques. During the injection period, the chamber remains isolated from the ambient air. This ensures that sampling begins under pure ammonium sulfate seed particle conditions and allows for any changes that occurred to the aerosol population during sampling to be attributed to ambient gaseous concentrations.

Immediately following the injection of a monodisperse seed ammonium sulfate aerosol, ambient air is pulled through the bottom portion of AACES resulting in the penetration of ambient gases through the ePTFE Teflon® membrane and mixed using the technique described in sub-section 2.2. Size and hygroscopic growth distributions are sampled from the chamber on a roughly hourly basis using an H-TDMA system. By sampling at hourly time intervals, particle loss within the chamber due to sampling is minimized and the majority of particle loss will be restricted to depositional processes (wall and membrane loss) within the chamber environment allowing for measurement periods to be optimized while still capturing the changes occurring to the aerosol over time. When the H-TDMA system is in chamber sampling mode, the peak diameter of the size distribution measured is determined using a peak-detecting algorithm and consequently used as the set point for humidified DMA measurements. This process enables the tracking of both the size of the particles within the chamber and the hygroscopic growth of those sized particles limiting measurement scan times and preserving chamber concentrations. The resulting particle size and hygroscopic growth distributions within the chamber are then log-normally parameterized in order to obtain the geometric mean diameter and standard deviation for each measurement. Upon the

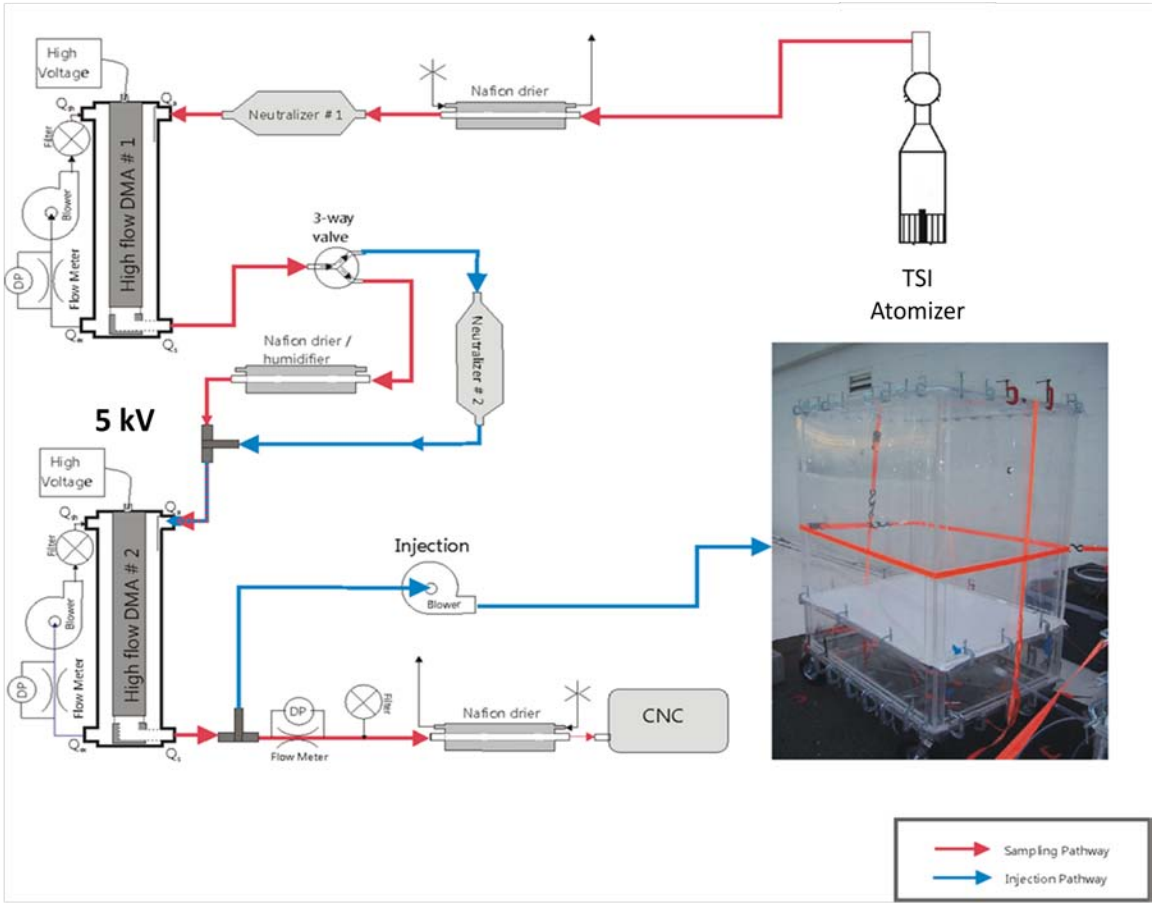

Figure 16. Ammonium Sulfate Injection Schematic. Schematic showing the monodisperse injection methods as well as the usual TDMA operation.

completion of each measurement cycle, AACES is again flushed with zero air for a minimum of 4 hours in order to remove any remaining particles and ensure a clean environment without ambient influences prior to the next measurement period.

3.3. MULTIPLY CHARGED PARTICLES IN THE INJECTED DISTRIBUTION

Figure 17 shows an example of an ammonium sulfate monodisperse distribution typical of that injected into the environmental chamber. As shown, there are three distinct modes in the resulting particle size distribution. This effect is partially the result of multiply charged particles transmitted by the first DMA during the size selection process described in sub-section 3.2. The DMA size selects particles according to their electrical mobility, Z_p, which is a function of number of charges the particle is carrying (n), the diameter of the particle (D_p), and a slip correction factor C_c

$$Z_p = \frac{neC_c}{3\pi\eta D_p} \quad 3.1$$

When particles of size D_p carrying n=1 charge are selected with the DMA, larger particles carrying n=2,3… charges may also be transmitted. The number and intensities of each mode transmitted will vary based on the size of selected singly charged particles as well as the shape of the polydisperse aerosol distribution generated.

For example, in the case of the distribution shown in Figure 17, 0.075 µm singly charged ammonium sulfate particles were selected (mode 1). However, a second mode of larger ~0.110 µm particles is evident (mode 2), which is caused by doubly charged particles being transmitted through the first DMA column upon the size selection of 0.075 µm particles. Since the distribution shown was that which was injected into the chamber, the ~0.110 µm mode is measured upon sampling, since these originally injected larger particles are passed through a bipolar ^{210}Po 400 µCi charging source prior to size classification where they gain only a single charge. Similarly, a third mode (mode 3) at D_p~.050 µm is measured due to the injected 0.075 µm particles becoming doubly charged upon sampling and having smaller mobility diameters. By employing the technique described above in order to inject only uncharged aerosol into the chamber, the concentration of the larger particle mode is minimized and therefore will have little influence on the primary 0.075 µm mode of interest during sampling. However, the presence of even a small fraction of these larger particles may bias optical measurements since light absorption and scattering vary nonlinearly with size.

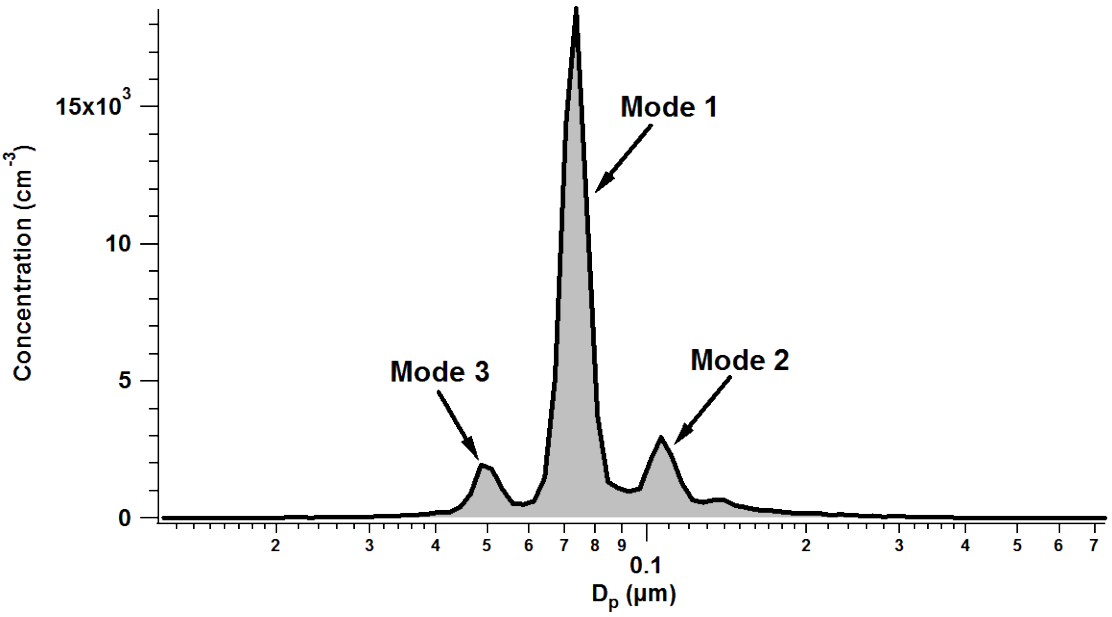

Figure 17. Multiply Charged Distribution. Monodisperse distribution showing the effects of multiple charging. Singly charged 75nm particles (Mode 1) represent the peak of the injected distribution while Mode 2 represents doubly charged larger particles present upon injection. Mode 3 represent doubly charged 75nm particles which are only evident upon sampling.

3.4. CONSIDERATIONS FOR CHAMBER NUCLEATION EVENTS

Although the injection of a monodisperse aerosol distribution allows for the isolation of a particle size of specific composition necessary to study evolutionary processes, the resulting integrated concentration remains low inside the environmental chamber. Furthermore, since the injected particle size is less than 0.100 µm, the available surface area is also small compared to typical ambient concentrations. Ideally, the particle size injected into the chamber would be >0.100 µm to increase surface area, but because aerosol evolution processes require the detection of minute changes to a particle size, particles of larger sizes are not desirable as they require a higher concentration of gases to adsorb on the surface in order to detect a measureable change in the particle diameter. Furthermore, theoretical growth calculations conducted by Fuchs and Sutugin show that the mass transfer rate of vapors to the particle surface assuming an accommodation coefficient of 1 drop off roughly 40% for particles with diameters between 0.100 µm and 0.130 µm, because of the Kelvin effect for vapor pressures above the surface of spherical particles (Fuchs and Sutugin 1971). Therefore, growth of these particles will be slow when compared with particles of smaller diameters leading to further difficulties in SOA detection. Because of these limitations, under high VOC loading conditions and lower injected surface area concentrations, nucleation events occur within the chamber frequently, particularly following particle loss within the chamber as those deposited particles will result in a still lower available surface area inside the chamber. Once a nucleation event does occur, the aerosol growth

measurement becomes biased because the probability of coagulation increases considerably, and the mechanism responsible for particle growth can no longer be identified with confidence. To combat these occurrences, particle injection times are increased allowing for increased particulate concentration within the chamber on initial sampling.

3.5. RESULTS AND DISCUSSION

Each size and HGF distribution obtained from chamber measurements was first inverted using a smoothing Twomey-based algorithm (Markowski 1987) and then parameterized using log-normal fits in order to obtain the mean diameter and HGF as well as the standard deviation for each property measured. Plotted in Figure 18 is the mean diameter and hygroscopic growth factor vs. fractional day for the measurement periods conducted on July 7th, 8th, and 21st measured under environmental chamber conditions at the SGP ARM Central facility in 2007. The initial diameter of seed particles injected was 0.075 µm for each day shown, and hygroscopic growth factors are given for an RH of 90%. Each experiment yielded a total increase in particle size under ambient conditions from the initial injected diameter of 0.075 µm to >0.110 µm. The days exhibiting the most prominent growth events were July 8th and 21st in which particles grew to sizes larger than 0.130 µm over a period of about 0.20 days, or roughly 5 hours. At the start of each experiment, accompanying hygroscopic growth factors for ammonium sulfate at 90% RH was consistent with calculated values for pure ammonium

sulfate at 0.075 μm. In conjunction with the accompanying growth of aerosol particles within the chamber, hygroscopic growth factors decreased consistently over time to values less than or equal to 1.35 meaning the resulting particles are significantly less hygroscopic culminating a growth event. During the two days in which a larger increase in particle size was observed, the hygroscopic growth factor decrease was also more prominent with values reaching 1.30 or less. On July 8, 2007, the measured HGF decreased from 1.67 to 1.20 over a period of about 5 hours. Deliquescence curves reported for pure SOA produced from various monoterpenes and oxygenated monoterpene photo-oxidation yield HGF values between 1.10 and 1.20 at 85% RH (Rudich et al. 2007).

An ambient growth event that occurred on July 7, 2007 is shown in Figure 19. Plotted is peak diameter vs. fractional day obtained from log-normal parameterization (grey dashed line) superimposed on the intensity distribution during the same time. The change in mean diameter of ambient particles over time was then compared to the growth observed in chamber on the same day with the results plotted in Figure 20. In order to directly compare the two growth modes, the most linear regions of growth were plotted against one another and linearly fit to obtain an estimated growth rate for the growth observed in both the ambient environment and in the chamber. The resulting growth rates (the slope of the linear fit) were comparable with the ambient growth rate being on the order of 4.25 nm /hr, and a measured growth rate under chamber conditions of approximately 4.0 nm/hr. This suggests that, as expected, chamber reasonably represents ambient growth under similar conditions.

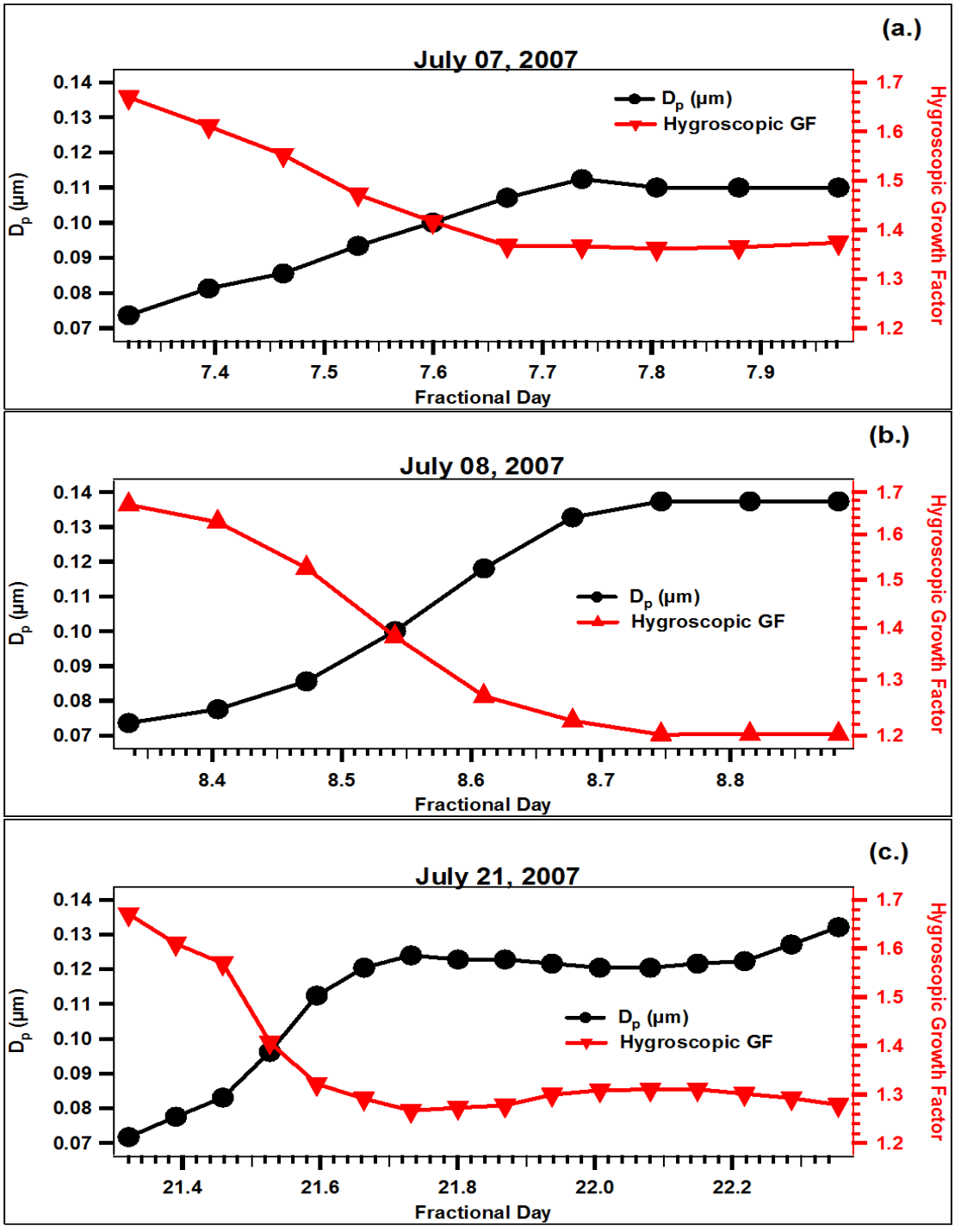

Figure 18. Chamber Growth Plots (ARM). Mean diameter and hygroscopic growth factor vs. time of day for July 7, 2007 (a.), July 8, 2007 (b.), and July 21, 2007 (c.). Measurements were conducted under chamber growth conditions at the ARM SGP Central Facility site.

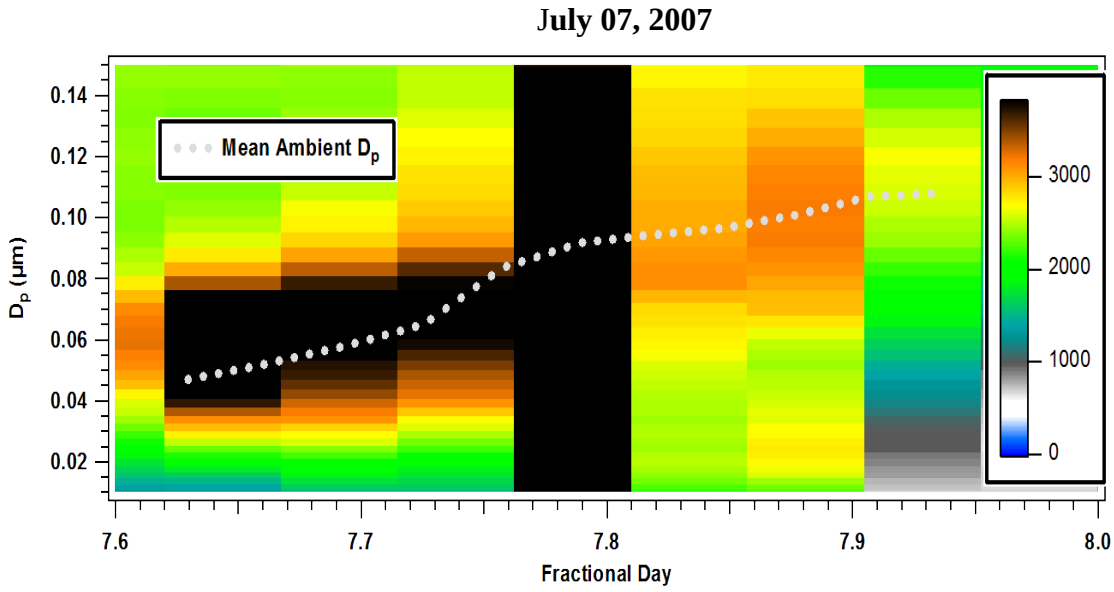

Figure 19. Ambient Growth (ARM). Ambient growth event and peak diameter (grey dashed line) measured at the ARM SGP site on July 07, 2007. The legend on the right indicates measured particulate concentrations.

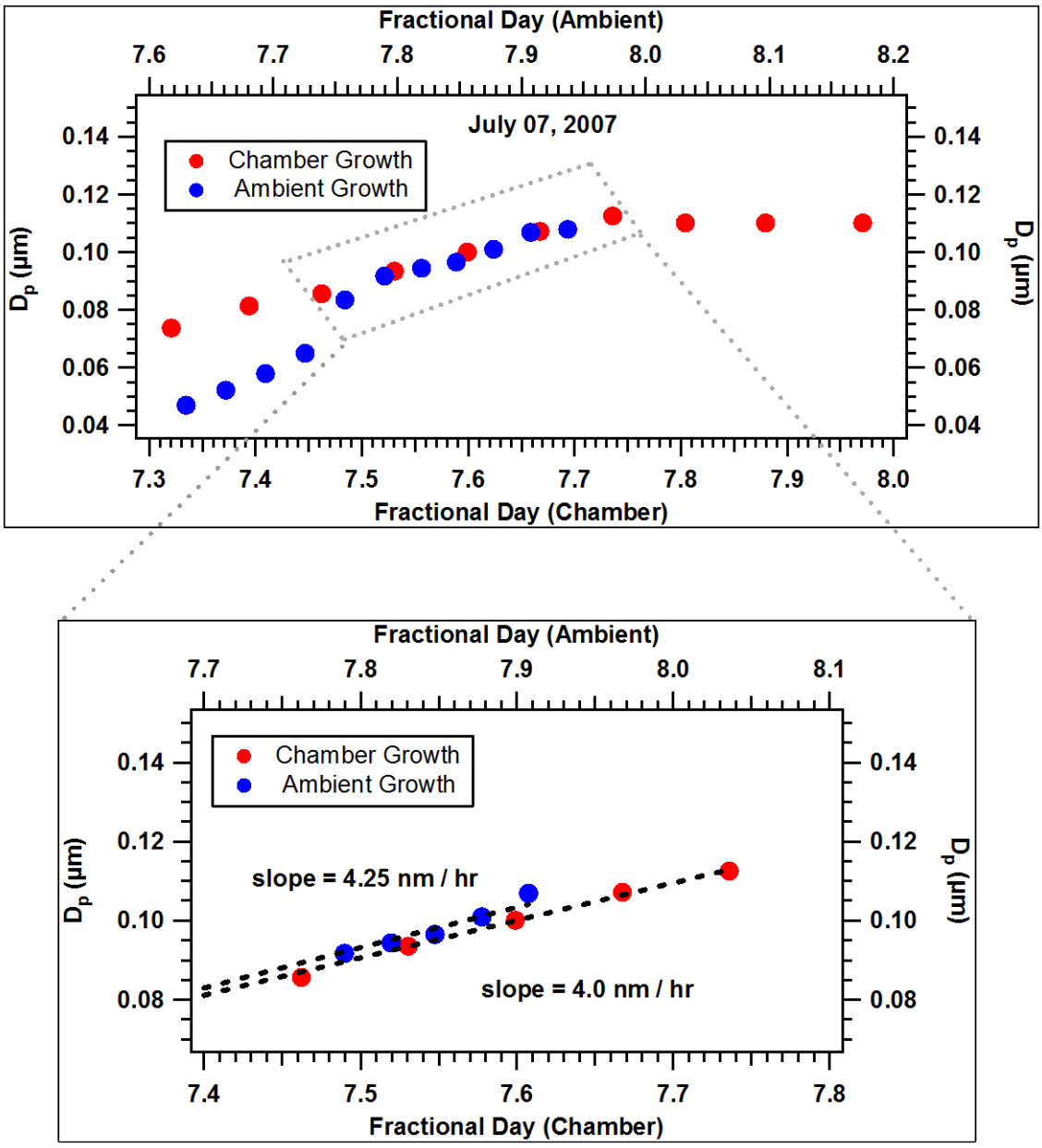

Figure 20. Ambient Growth Comparison July 07, 2007 (ARM). Measured peak diameter for both an ambient growth event (blue) and a chamber growth event under ambient condition (red) that occurred at roughly the same time. Data was collected at the ARM SGP site on July 07, 2007.

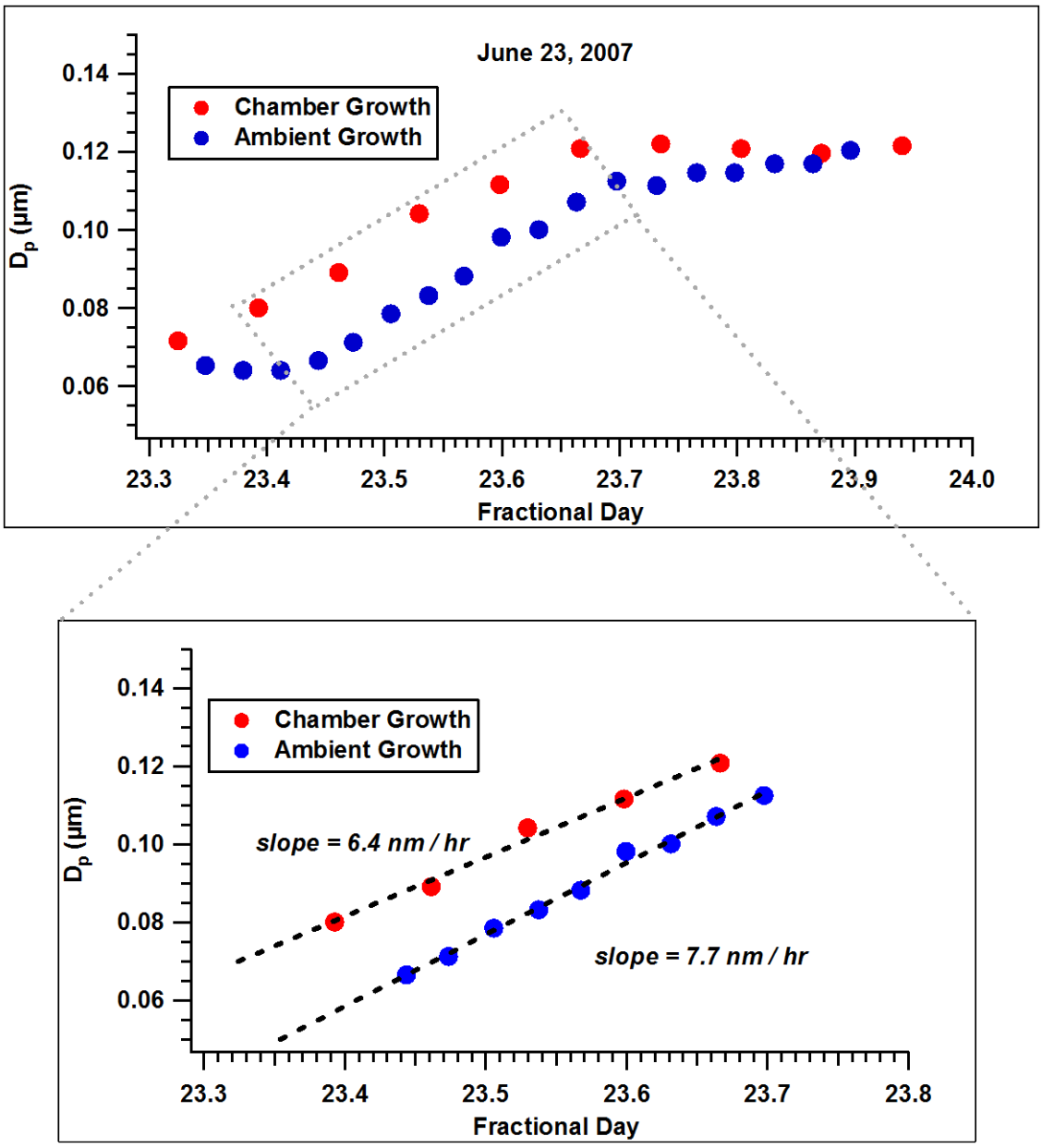

Figure 21. Ambient Growth Comparison July 23, 2007 (ARM). Measured peak diameter for both an ambient growth event (blue) and a chamber growth event under ambient condition (red). Data was collected at the ARM SGP site on June 23, 2007.

Plotted in Figure 21 is a growth comparison between that measured using AACES and in ambient on June 23, 2007 at the ARM site. The linear growth rate determined for the period of growth observed in ambient was 7.7 nm/hr while the growth measured under chamber conditions was 6.4 nm/hr. For the ambient growth period measured on June 24, 2007, as shown in Figure 22, a chamber growth rate of 5.92 nm/hr was measured. The linear ambient growth rate during the same time was 6.17 nm/hr.

Measured mean diameter and HGF for two selected periods during the BEACHON project in Colorado is shown in Figure 23. The most impressive growth period occurred on August 09, 2008. On this day, particle size increased from 0.075 μm to 0.112 μm with an accompanying hygroscopic growth decrease from approximately 1.67 to 1.30. This region had recently experienced a devastating fire which destroyed much of the piney forest to the north and west of the measurement site likely resulting in a reduction of biogenic VOC emission sources. Local meteorology was also an issue. Frequent cloudy days and afternoon rain events plagued the field campaign which limited the available UV radiation reaching the measurement site thereby reducing photolysis

rates at the surface. Furthermore, the experimental location was subject to daytime shadowing as the chamber was located under the tree canopy. These factors combined with the elevation of the field site may have contributed to the slower growth observed when compared with that measured in Oklahoma during 2007.

Plotted in Figure 24 are the results of data collected during the SHARP field campaign in Houston, TX. Despite the location being in an urban area, particle growth patterns are similar to those observed at both the ARM and Manitou Experimental Forest locations. Ammonium sulfate particles with mean diameters of 0.075 μm were injected in the morning hours and particle diameter and hygroscopic growth measured throughout the experimental period at a fixed RH of 90%. During each measurement period, the observed particle diameters increase from the injected initial diameter of 0.075 μm to a size equal to or larger than 0.110 μm. On May 2, chamber growth yielded a change in particle diameter of 27nm over roughly 7.32 hours. The accompanying hygroscopic growth factor decreased from 1.69 to 1.44 over the same time period.

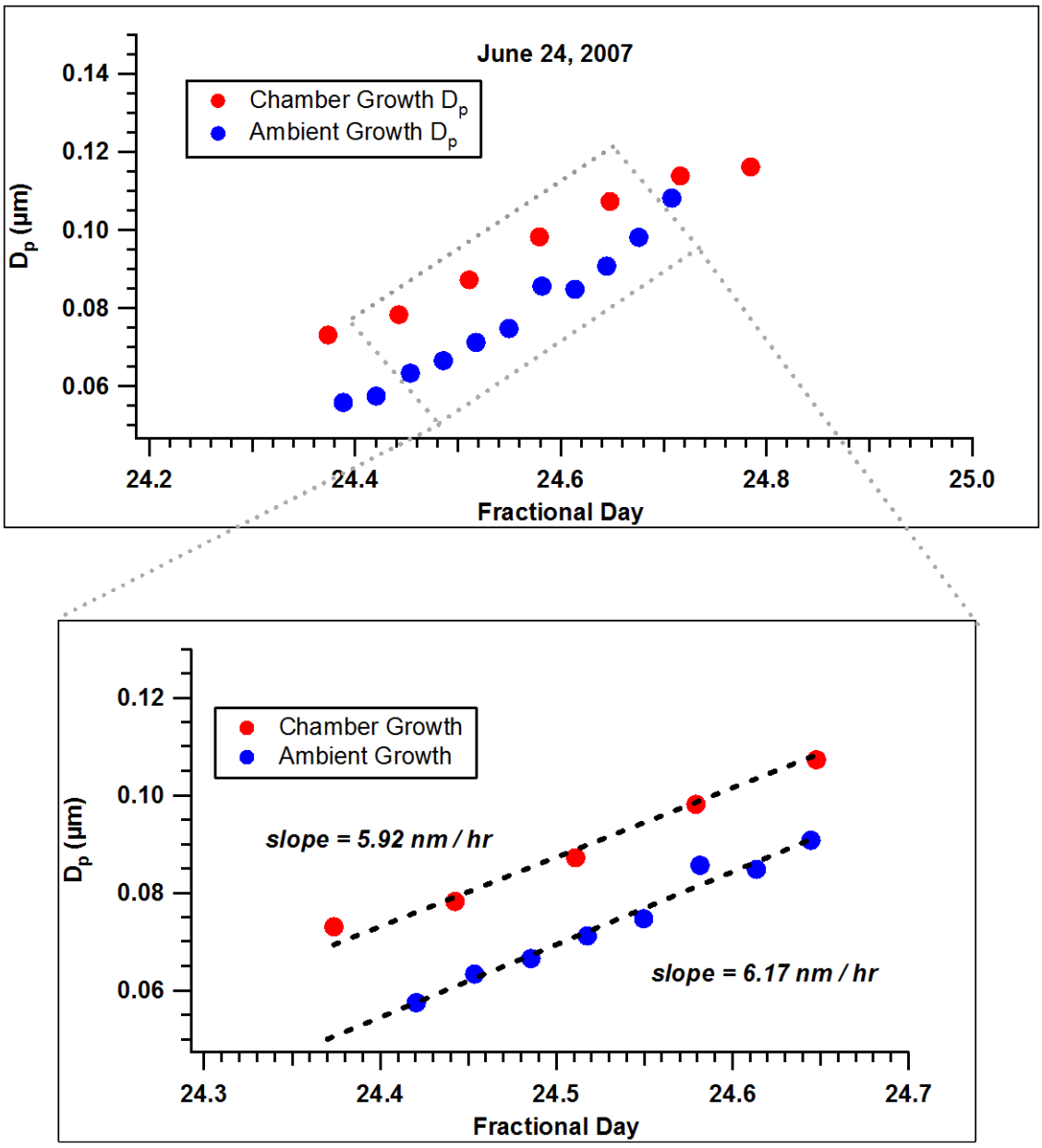

Figure 22. Ambient Growth Comparison June 24, 2007 (ARM). Measured peak diameter for both an ambient growth event (blue) and a chamber growth event under ambient condition (red). Data was collected at the ARM SGP site on June 24, 2007.

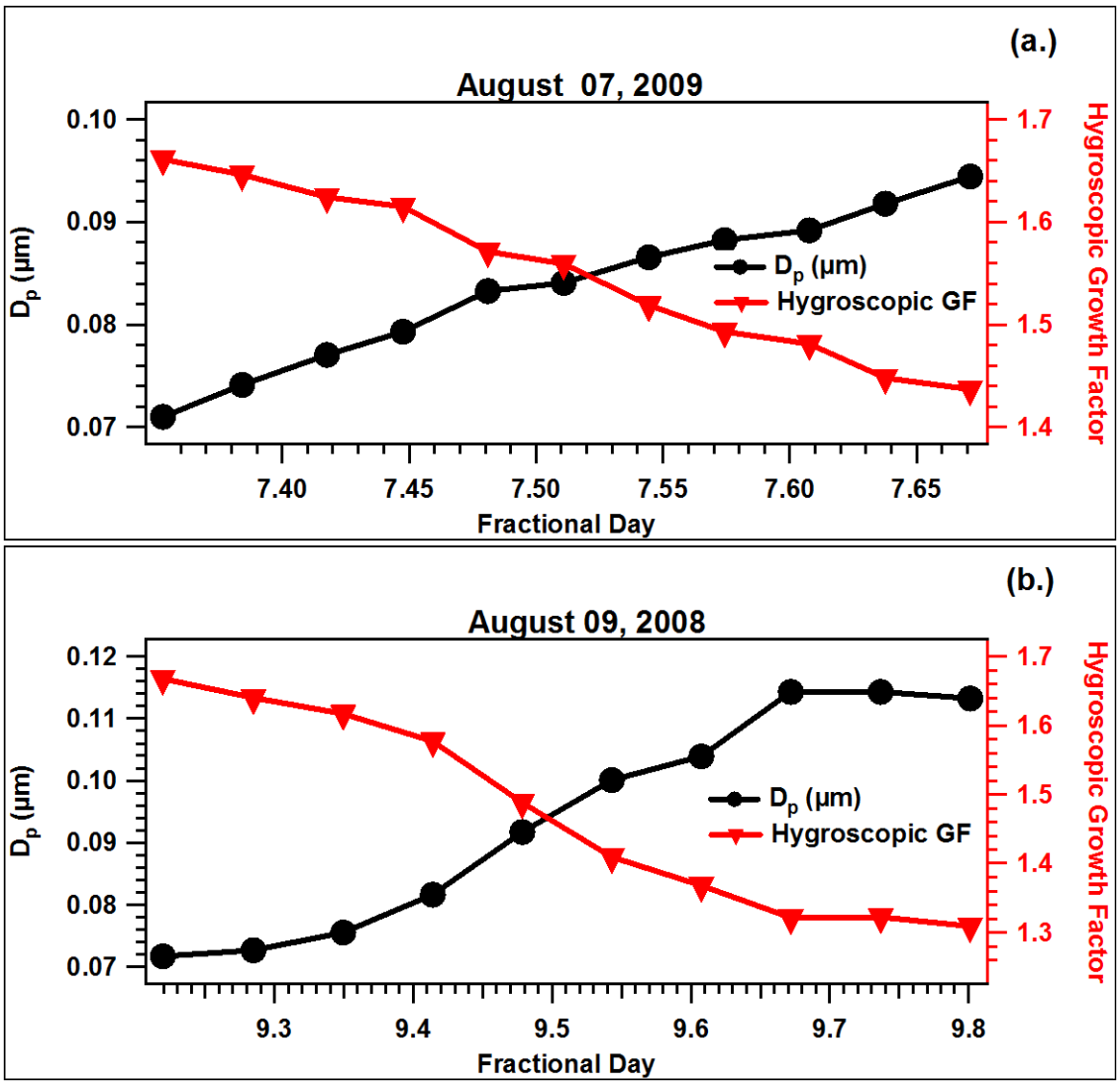

Figure 23. Chamber Growth (Colorado). Mean diameter and hygroscopic growth factor vs. time of day. Measurements were conducted under chamber growth conditions in the Manitou Experimental Forest in Colorado.

When comparing the observed change in hygroscopic growth factor in Houston, TX to that measured in previous rural locations, aerosol growth measured utilizing AACES in a rural setting resulted in particulates which exhibit more hydrophobic tendencies as evident from the HGF. This is likely caused by the availability of condensable sulfuric acid in Houston, TX compared to the previously mentioned rural locations.

Peak diameter vs. time for an ambient growth event that occurred on May 02, 2009 during the SHARP field campaign is plotted in Figure 25 against the intensity of the measured distribution. This growth episode corresponds to a chamber growth event measured during the same time period. As discussed previously, each growth episode was analyzed to extract the linear portion of the growth event in order to perform a direct comparison between the two environments. Figure 26 shows the results from this analysis. During the May 02, 2009 growth period, ambient particles grew at a rate of 6.67 nm/hr, which is comparable to the 6.33 nm/hr growth rate observed under chamber conditions. A similar analysis performed for the growth observed on May 01, 2009, as shown in Figure 27, yields an ambient growth rate equal to 5.29 nm/hr with a corresponding growth rate of 4.96 nm/hr measured using AACES.

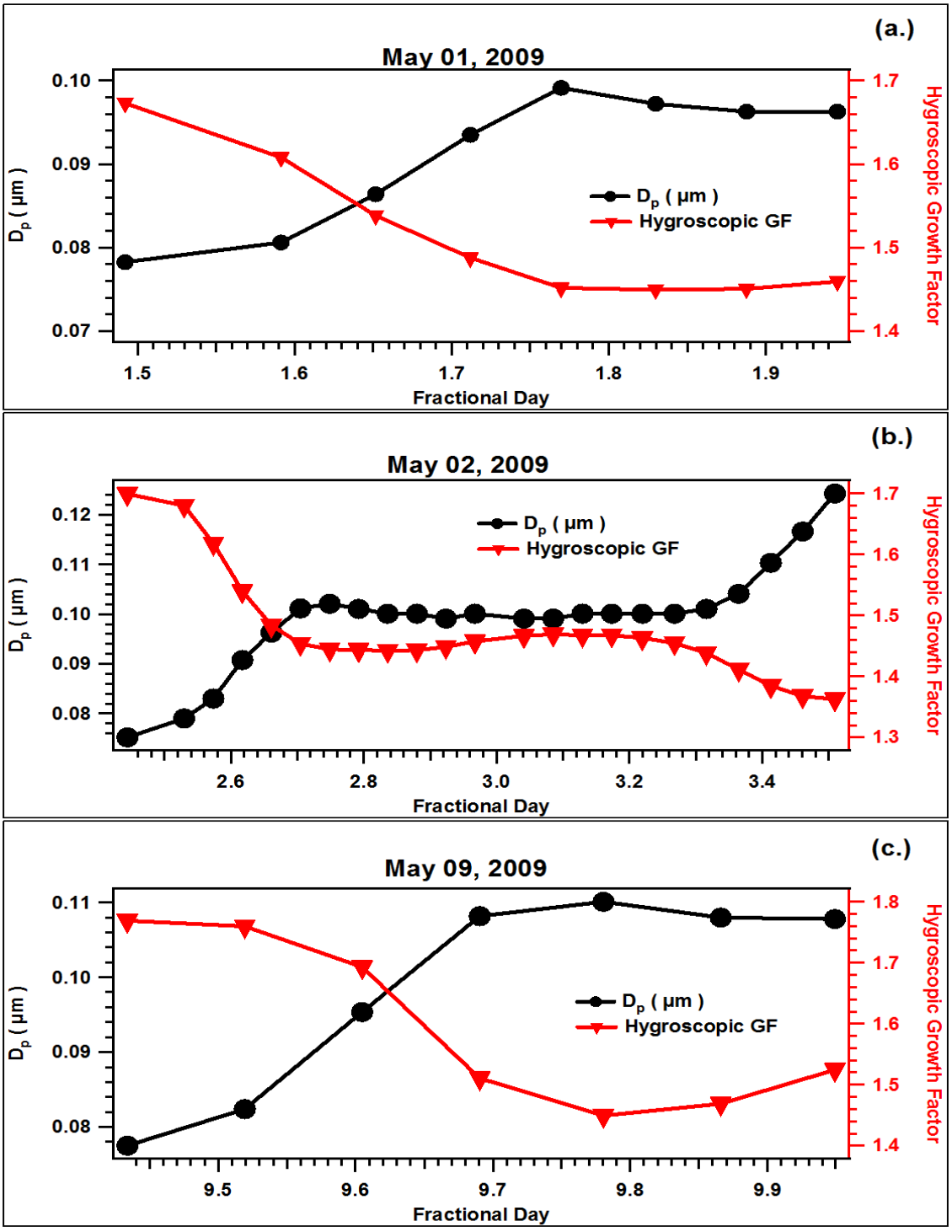

Figure 24. Chamber Growth (Houston, TX). Mean diameter and hygroscopic growth factor vs. time of day. Measurements were conducted under chamber growth conditions at the South Moody Tower on the University of Houston Campus in Houston, TX.

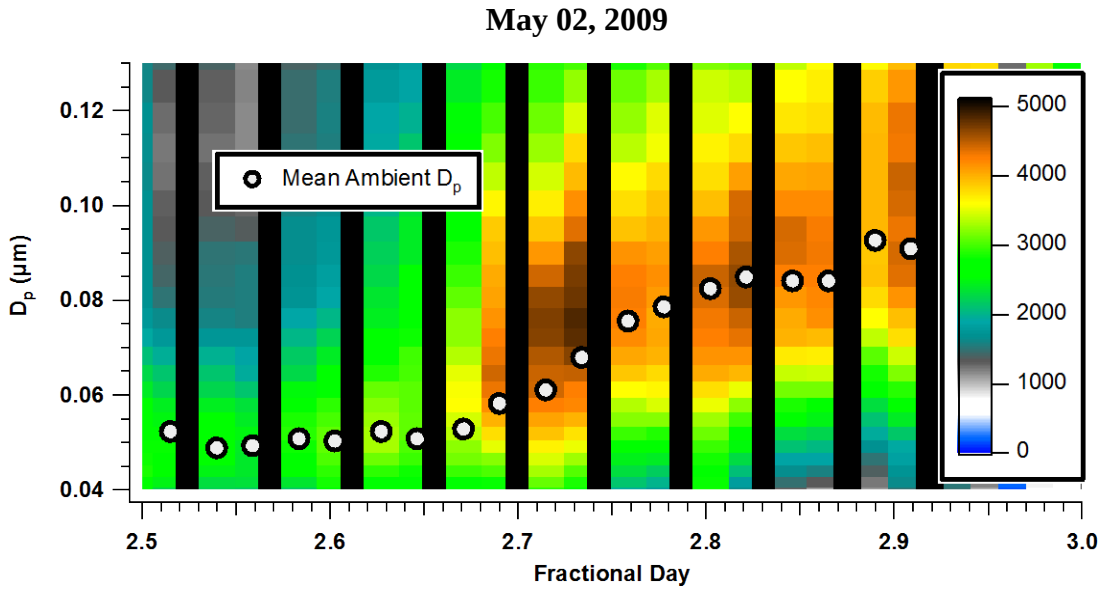

Figure 25. Ambient Growth May 02, 2009 (Houston, TX). Ambient growth event and peak diameter (grey dashed line) measured in Houston, TX on May 02, 2009. The legend on the right represents measured ambient particulate concentration.

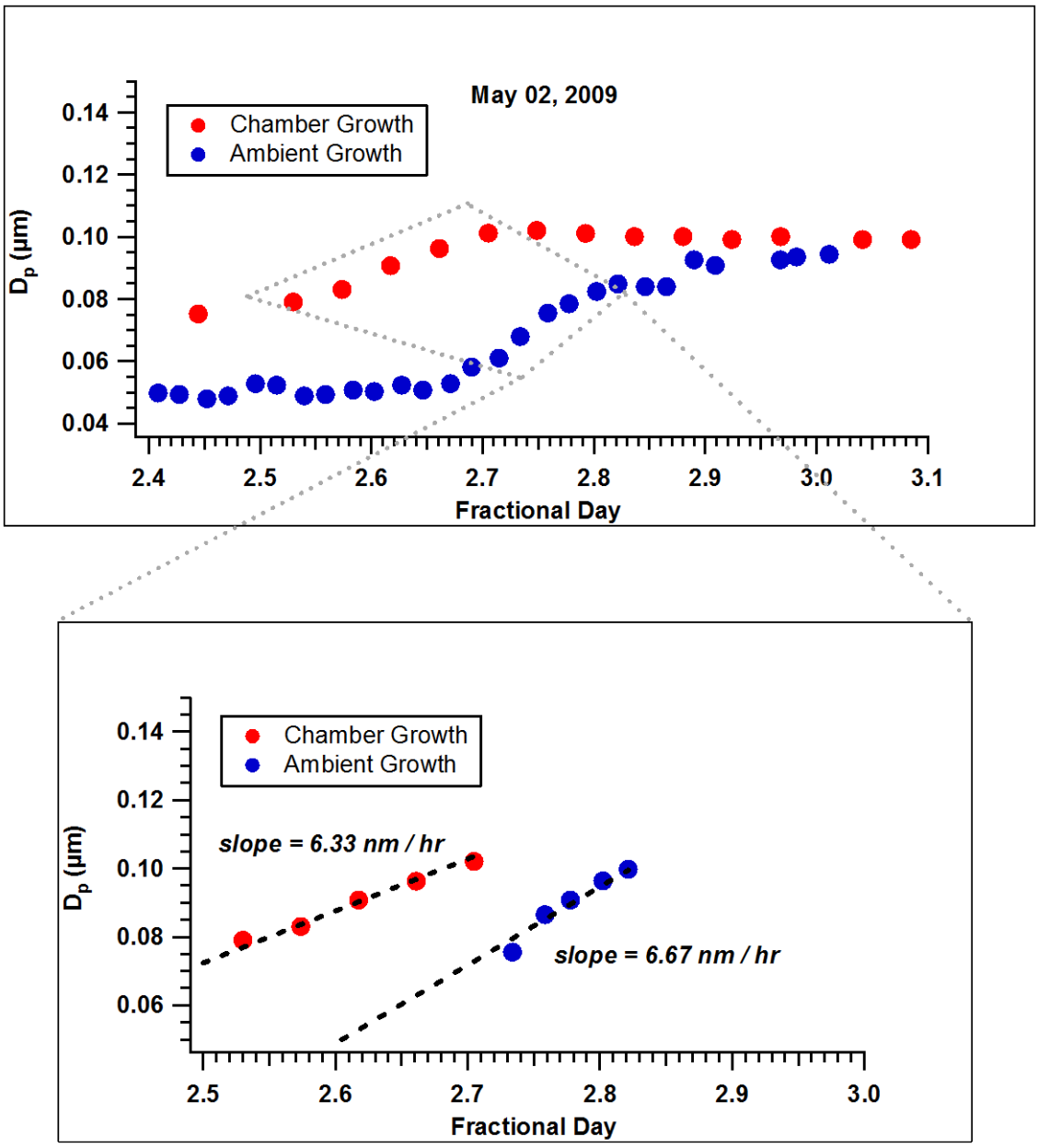

Figure 26. Ambient Growth Comparison May 02, 2009 (Houston, TX). Measured peak diameter for both an ambient growth event (blue) and a chamber growth event under ambient condition (red). Data was collected in Houston, TX on May 02, 2009.

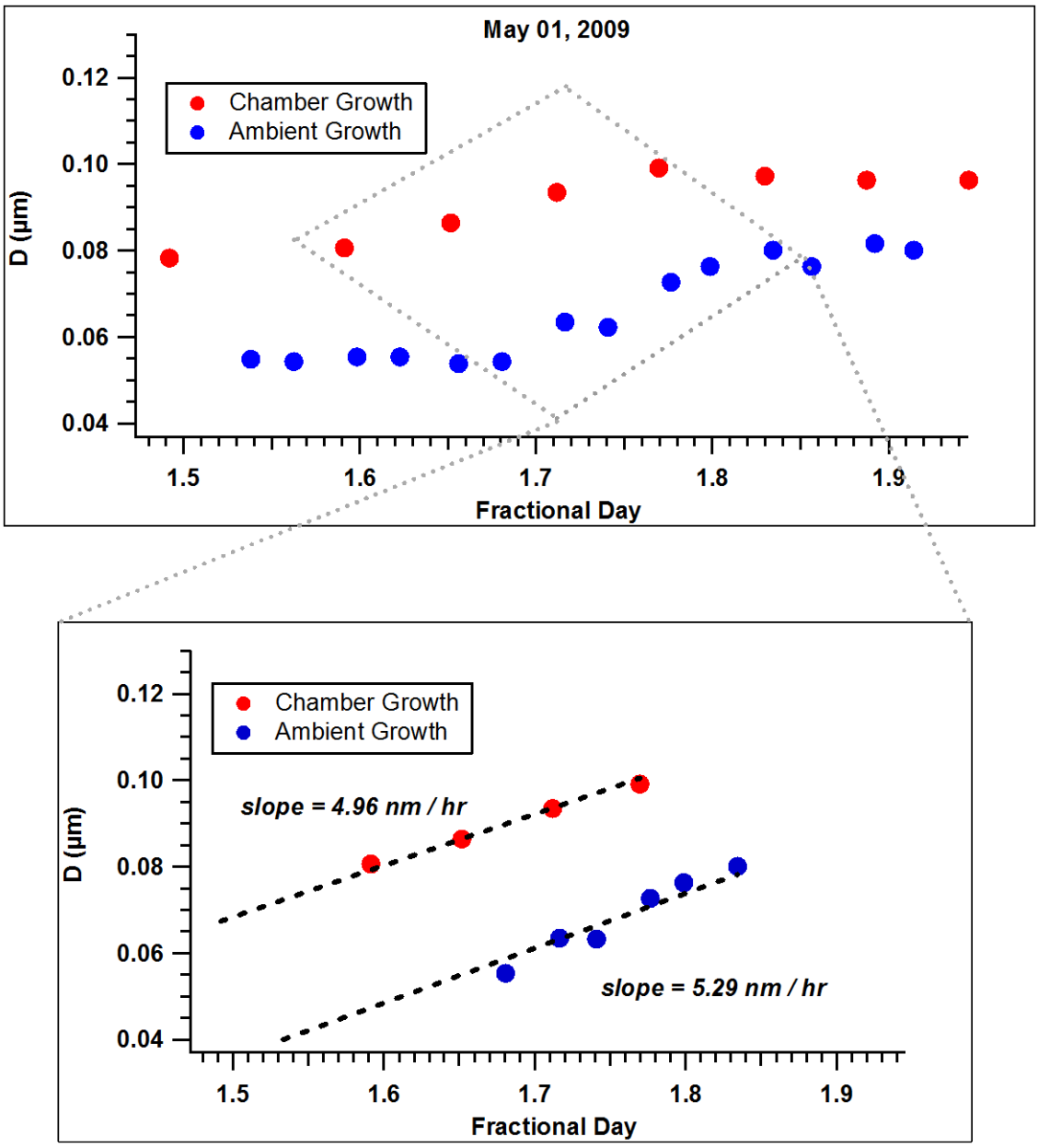

Figure 27. Ambient Growth Comparison May 01, 2009 (Houston, TX). Measured peak diameter for both an ambient growth event (blue) and a chamber growth event under ambient condition (red). Data was collected in Houston, TX on May 01, 2009.

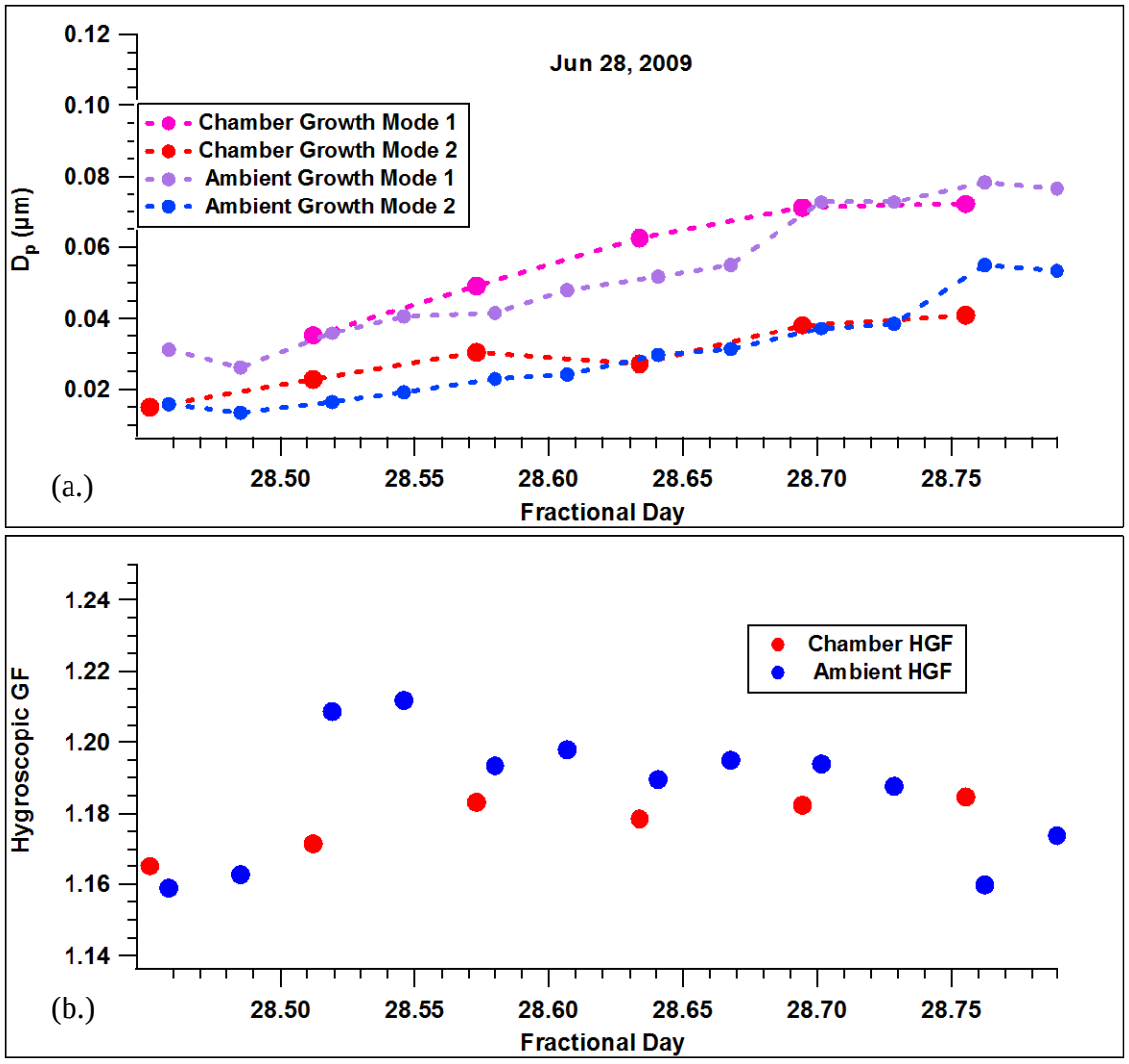

Figure 28. Ambient Growth Comparison June 28, 2009 (Houston, TX). Measured peak diameter for both an ambient nucleation and growth event (blue) and a chamber nucleation and growth event under ambient condition (red). Data was collected in Houston, TX on June 28, 2009.

Further evidence of the viability of AACES for the measurement of aerosol transformation processes under ambient conditions is presented in Figure 28. Plotted are the results from a chamber nucleation and growth event that occurred at the same time as a nucleation and growth event that was measured in the ambient environment on June 28, 2009 in Houston, TX. Each peak of the distribution, both in chamber and ambient, was log-normally parameterized for mean diameter and HGF. The change in mean particle diameter over time measured using AACES is consistent with that observed in ambient throughout the measurement period. Accompanying HGF measurements also yield similar characteristics between the two environments. Ambient HGF measurements were obtained for particles sized 0.013, 0.025, 0.050, 0.100, 0.200, and 0.400 μm. Therefore, ambient measurements of HGF were linearly interpolated to correspond to mean diameter for each log-normal fit at a given time in order to compare measured chamber mean HGF with that in ambient as shown in Figure 28(b.).

Although the estimated linear growth rates discussed above allow for a comparative extrapolation of aerosol properties, a more accurate quantification of aerosol growth is desirable. Therefore, the resulting growth curves associated with the observed SOA production from seed ammonium sulfate particles under ambient conditions within the chamber environment were parameterized using a sigmoid type function in which the particle diameter (D_p) for a given time of day can be expressed as

$$D_p(t) = D_{p_0}(t_0) + \frac{D_{p_{max}} - D_{p_0}(t_0)}{1 + exp\left(\frac{t_{1/2} - t}{c_m}\right)} \qquad 3.2$$

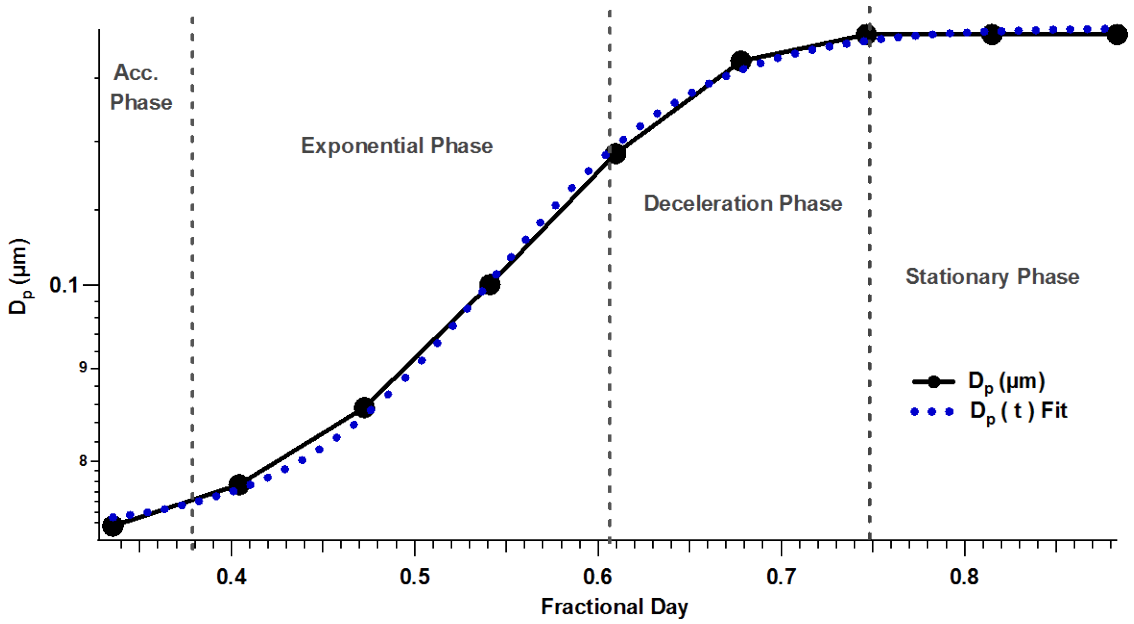

Figure 29. Growth Curve Fitting Example. Plot depicting data growth parameterization. The growth curve represents four phases of growth and are separated by the dashed grey vertical lines.

where $t_{1/2}$ is the time at which D_p is equal to $(D_{p_{max}} - D_{p_0}(t_0))/2$ and $c_m$represents the rate of rise during which the linear growth observed is at a maximum. By using a sigmoid function to determine the data characteristics, the particle growth can be separated into four distinct periods. The first as indicated in Figure 29 is the acceleration phase of growth in which the seed aerosol particles are beginning to grow by gas-to-particle partitioning. This slower growth is consistent with model calculations by Pankow (1994) where the modeled growth of a particle due to organic condensation was dependant on the organic mass concentration within the particle phase (Pankow 1994). As was observed from that modeling study, the addition of a monolayer consisting of

organic acids accelerated the growth of the aerosol population under investigation. A second phase, referred to as the exponential phase of growth, occurs following the initial acceleration period in which a relatively constant growth rate is observed. During the third phase of growth, a lag in the change of particle diameter over time is evident followed by a Stationary period in phase four. During phase two, the peak growth rate of particles can be determined by differentiating the equation above with respect to time to determine slope at $t = t_{1/2}$.

Maximum calculated growth rates from parameterized fits were observed during the measurement period on July 8, 2007 at the ARM SGP central facility with a linear (exponential phase) growth rate roughly equal to 12 nm/hr and in Houston, TX on May 09, 2009 with a growth rate of 9 nm/hr. Table 1 summarizes the parameterized growth rates for each of the measurement period throughout the three separate field locations. The growth rates reported here are on average significantly lower than the values reported by Leskinen et al., 2008 recorded from the photo-oxiation of xylene/NO_x mixtures in which particle growth rates ranged from 10.6 to 18.6 nm/hr (Leskinen et al. 2008). Ambient growth events can also be parameterized using this method as shown in Figure 30.

Table 1. Growth Summary Table. Summary of the results from chamber growth analysis during three separate field campaigns; the CLASSIC field campaign which took place in Oklahoma at the ARM SGP Central Facility, the BEACHON field project located in the Manitou Experimental Forest in Colorado, and the SHARP field intensive in Houston, TX.

Date Measured	Location	Final Growth Diameter (μm)	Final HGF	Growth Rate (nm/hr)	Organic Mass Fraction (%)	Rate of Mass Addition 10^{-10} (μg/hr)
07-07-07	ARM, OK	0.110	1.37	5.17	53.7	1.20
07-08-07	ARM, OK	0.137	1.20	12.00	76.4	3.98
07-21-07	ARM, OK	0.132	1.28	10.20	65.5	2.75
08-07-07	Manitou, CO	0.094	1.44	2.93	40.5	0.52
08-09-07	Manitou, CO	0.113	1.31	6.19	60.4	1.41
05-01-09	Houston, TX	0.096	1.46	6.41	36.7	1.69
05-02-09	Houston, TX	0.124	1.36	7.80	54.0	1.33
05-09-09	Houston, TX	0.108	1.52	8.97	51.9	2.40

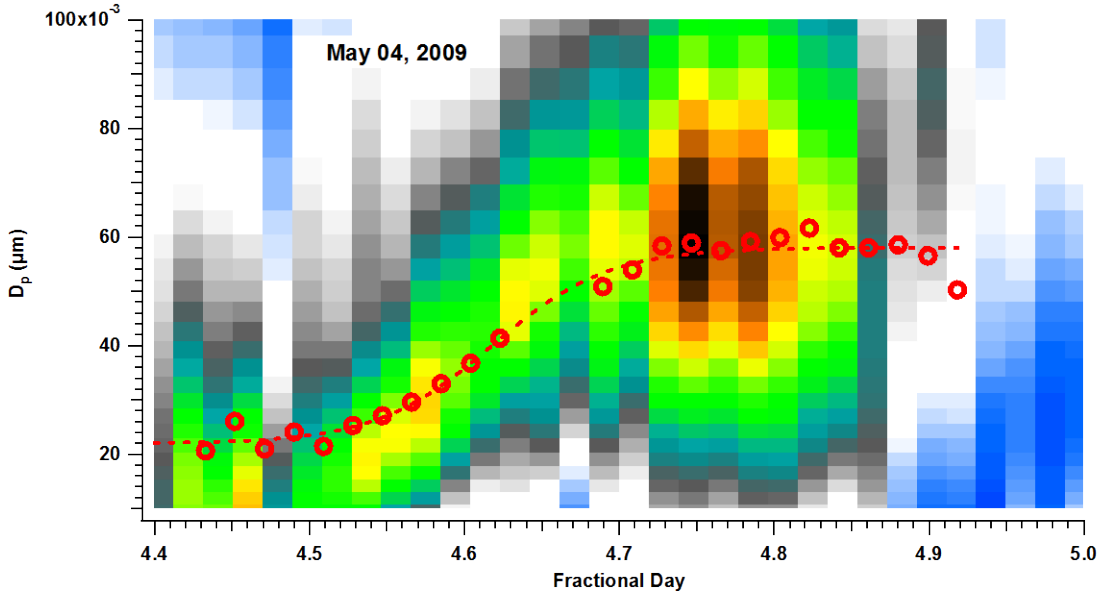

Figure 30. Ambient Growth Curve Fit Example. Ambient growth event analyzed for peak diameter (red circle) and fit using a sigmoid type data parameterization curve (red dashed).

The mass of organic material internally mixed within a solution droplet can be calculated from the measured HGF at 90% RH through the following expression (Gasparini et al. 2004):

$$m_i = \rho_i \frac{\pi}{6}(D_p^3 - \alpha D_p^{*3})\left(\frac{1}{\beta^3 - \alpha}\right) \quad 3.3$$

where D_p^* refers to the dry particle diameter, D_p to the hydrated particle diameter, ρ_i is the density of insoluble organic material, β is the growth factor of pure insoluble material contained within the solution droplet for the given dry diameter and HGF, and α is defined as:

$$\alpha = \frac{\rho_s}{\chi_s \rho_{as}} \quad 3.4$$

Here ρ_s refers to the density of the dry soluble material (1.76 g cm^{-3} for ammonium sulfate), χ_s is the mass fraction of solute in the hydrated particle, and ρ_{as} is the density of an aqueous solution composed of water and ammonium sulfate. For the purposes of this work, the density of insoluble material is taken as 1.4 g cm^{-3} (Hallquist et al. 2009; Hu and Kamens 2007) and the hygroscopic growth factor for a particle composed of pure insoluble material to be 1.2 (Cruz and Pandis 2000). Following the calculations for insoluble mass contained within a particle, the amount of soluble mass present can then be determined through the following relation:

$$m_s = \rho_s \left(\frac{\pi}{6} D_p^{*3} - \frac{m_i}{\rho_i} \right) \quad 3.5$$

It follows then that the organic mass fraction can be calculated by computing the portion of insoluble mass contained in the total mass (soluble + insoluble) within the particle:

$$\chi_i = \frac{m_i}{m_s + m_i} \quad 3.6$$

The above equations are iteratively solved using measured dry particle diameter and HGF, empirical relations, and taking into account the effect of water activity and solution density (Tang and Munkelwitz 1994).

Calculated mass fractions for the periods of growth observed at the ARM SGP site are plotted in Figure 31. Each measurement period resulted in calculated organic mass fractions greater than 50%, with the highest percentage of 76% occurring following the particle growth observed on July 08, 2007. The rate of addition of organic mass to the particle phase was calculated by parameterizing the change in organic mass over time using the fitting method described above. As indicated in Table 1, the rate of organic

mass addition for each of the three periods was on the order of 10^{-10} µg/hr, while the highest rate calculated was for the July 08, 2010 growth event at approximately 4.0×10^{-10} µg/hr. Mass fraction calculations for data collected in both Colorado and Texas revealed similar trends as indicated in Figure 32 and Figure 33 respectively. Although the rate of change in particle size measured in Houston, TX was comparable to that observed using AACES at the ARM site, calculated organic mass fractions in Houston, TX were consistently below 60%. This result supports the initial determination that sulfuric acid or other more soluble material is likely a significant contributor to the particle mass in Houston, TX. All calculated organic mass fractions and rates of organic mass addition are summarized in Table 1.

Nighttime measurements of particle growth in both Texas and Oklahoma resulted in a decrease in particle diameter and an increase in particle hygroscopicity as indicated in Figure 24 and Figure 22. This effect is likely due to the re-emission of semi-volatile organics to the gas phase which may indicate that gas-to-particle partitioning may be reversible for some species in the atmosphere. Recent evidence shows that for SOA formed via ozonolysis of α-pinene repartitions reversibly upon systematic dilution, however on much longer time scales that had been previously observed with other singular systems (Grieshop et al. 2007). This slower evaporation rate will likely influence the observable behavior of SOA in the atmosphere as well as the interpretation of laboratory SOA data (An et al. 2007).

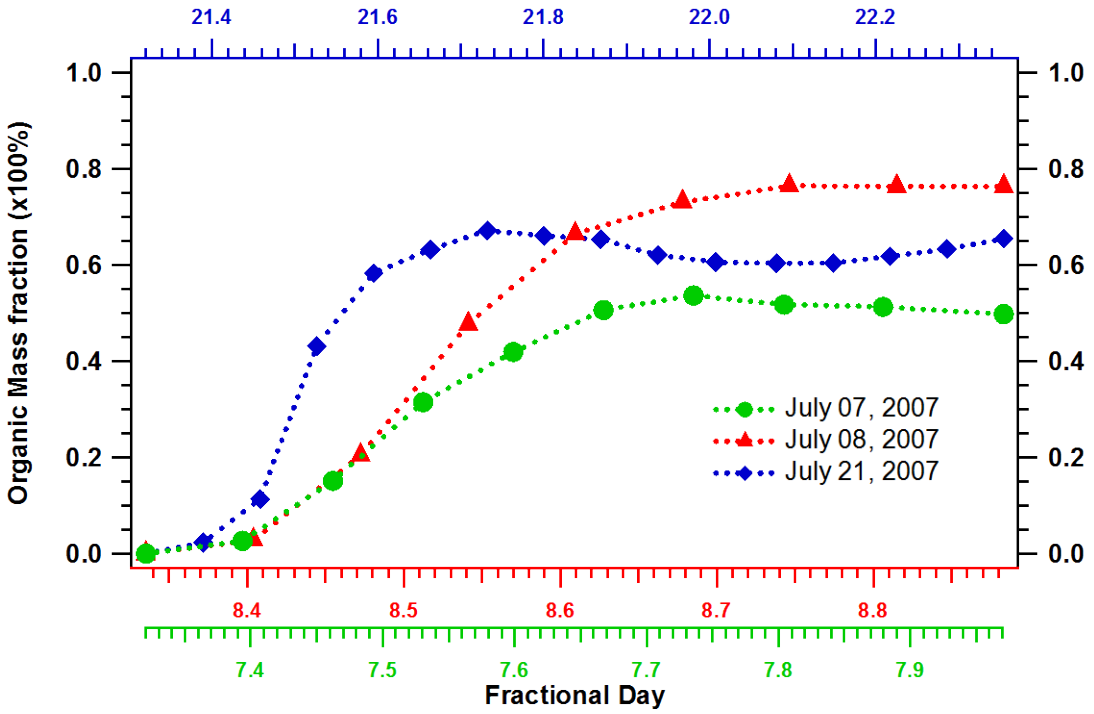

Figure 31. Mass Fractions (ARM). Time resolved calculated organic mass fractions from measured hygroscopic growth factor and mean particle diameters during chamber growth experiments. Measurements were obtained during the CLASIC field campaign at the ARM SGP Central Facility.

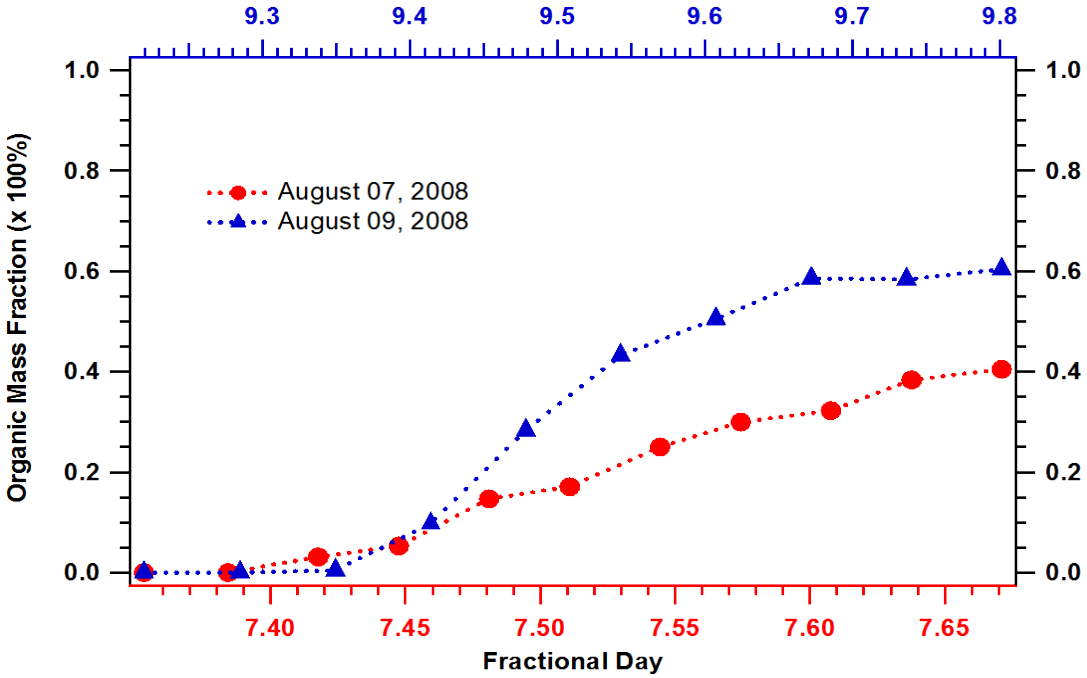

Figure 32. Mass Fractions (Colorado). Time resolved calculated organic mass fractions from measured hygroscopic growth factor and mean particle diameters during chamber growth experiments. Measurements were obtained during the BEACHON field campaign in the Manitou Experimental Forest, CO.

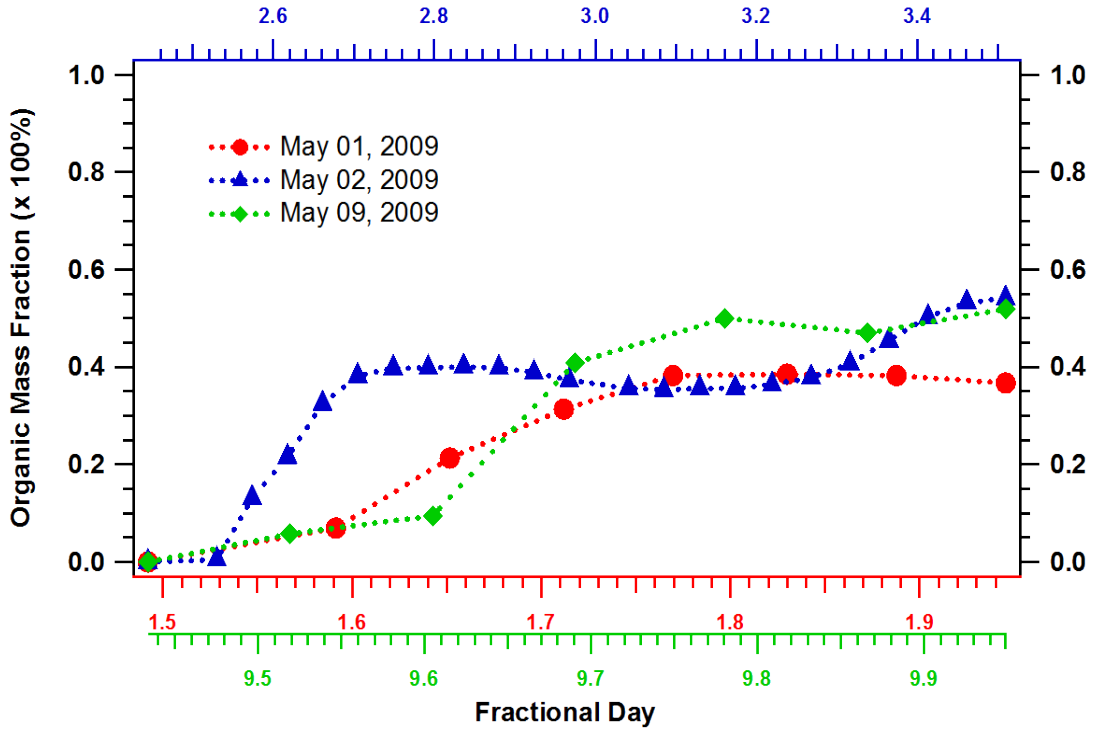

Figure 33. Mass Fractions (Houston, TX). Time resolved calculated organic mass fractions from measured hygroscopic growth factor and mean particle diameters during chamber growth experiments. Measurements were obtained during the SHARP field campaign Houston, TX.

Various model simulations involving the production and growth of SOA use a partitioning model in which the gaseous species are assumed to partition between the gas and liquid phases under equilibrium (Anttila and Kerminen 2003; Pankow 1994) (Pankow, 1994; Antilla and Kerminen, 2003). More recently, a volatility basis-set approach has been used as a framework for the modeling of SOA (Donahue et al. 2009; Lane et al. 2008; Robinson et al. 2007; Stanier et al. 2008). This method involves grouping compounds by their volatility: low volatility organic compounds are those compounds which are primarily in the condensed phase, semi-volatile organic compounds are those which will be found in both phases, and intermediate volatility organic compounds are those which are primarily in the gas phase but comprise a substantial fraction of difficult to measure compounds. The results from the measurements in both Oklahoma and Texas suggest that a large fraction of the species contributing to particle growth irreversibly condense to the particle phase under atmospheric conditions, while only a small fraction are in partitioning equilibrium. The data reported here support the use of the volatility basis set approach as full partitioning reversibility was not observed. It is therefore recommended that further investigation into vapor partitioning be employed and the volatility basis set approach adapted by the organic modeling community for the prediction of SOA production and growth.

4. OBSERVATIONS OF THE AMBIENT SOOT AGING PROCESS DURING THE STUDY OF HOUSTON ATMOSPHERIC RADICAL PRECURSORS (SHARP) FIELD CAMPAIGN

4.1. EXPERIMENTAL METHODS

The soot aging process was investigated during the SHARP intensive field campaign, a location which was previously described in sub-section 3.1, and pre-experimental chamber preparations were identical to those mentioned in sub-section 3.2. For the purposes of monitoring soot aging under ambient conditions, AACES was deployed atop the Moody Tower on the University of Houston Campus on an outdoor platform adjacent to an indoor temperature controlled facility which housed the instrumentation. A polydisperse carbon soot aerosol distribution was generated by incomplete combustion of Propane fuel in a laminar diffusion burner (Santoro et al. 1983) and sampled using a pinhole diluter. This method of soot generation tends to produce a stable soot concentration with a geometric mean diameter near 0.130 μm. The fresh soot laden aerosol stream was then passed through a silica gel diffusion dryer in order to remove excess moisture from the flow. Following the initial drying stage, the aerosol was then passed through a 4×10^{-3} cm^3 cylinder containing both General Carbon Corporation Spectrum XB-17 activated carbon blend to remove any unwanted VOCs produced during the combustion process and Purafil® SP, which effectively removes hydrogen sulfide, sulfur dioxide, nitric oxide, and formaldehyde.

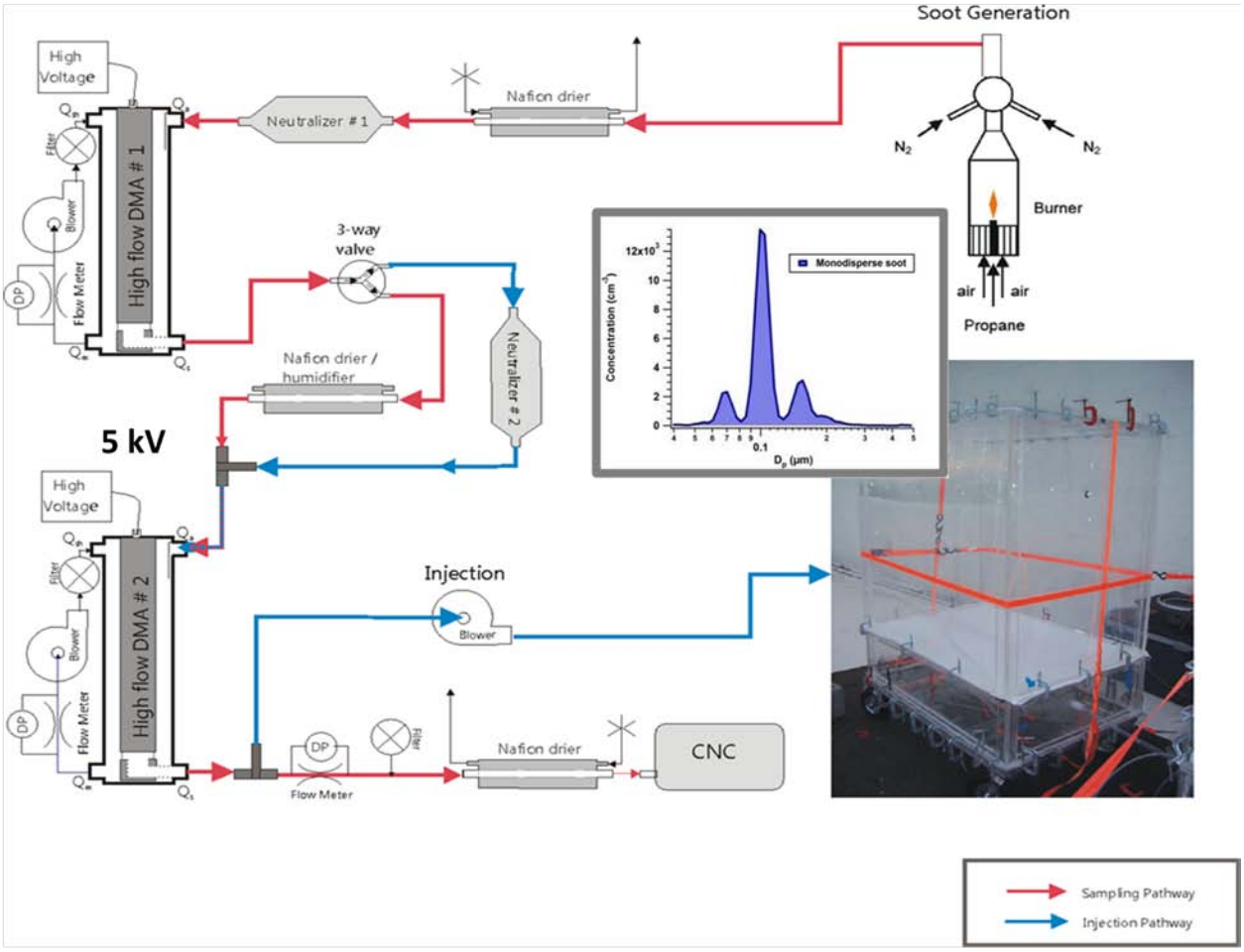

Figure 34. Soot Injection Schematic. Schematic of the monodisperse soot generation and injection.

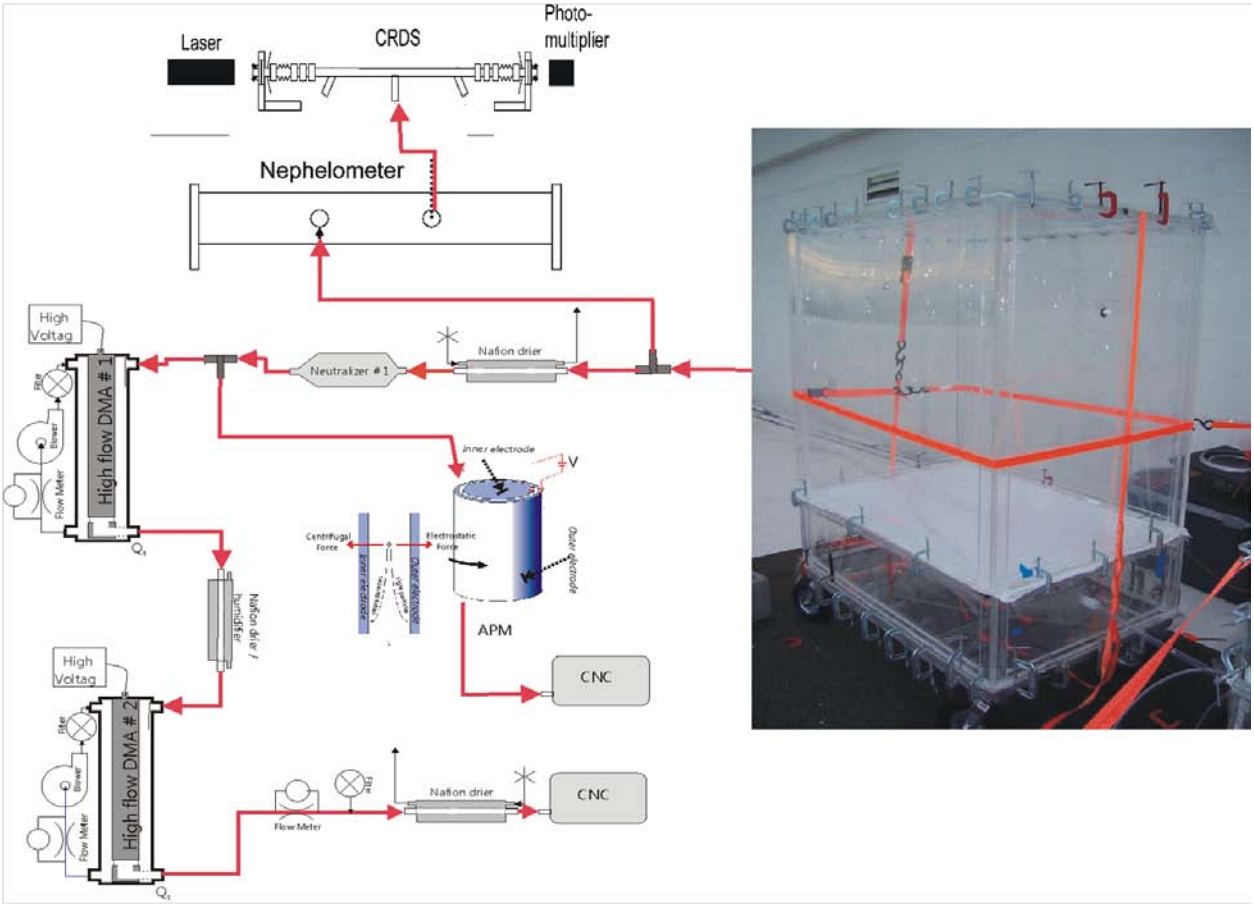

Figure 35. Soot Sampling Schematic. Schematic showing the chamber soot sampling setup.

Following gas scrubbing, a monodisperse soot distribution was generated and injected into the reaction chamber as described sub-section 3.2. A schematic of the monodisperse soot injection method is show in Figure 34.

Upon injection of the seed soot aerosol, hourly measurements of particle size, hygroscopic growth factor, particle mass, and particle optical properties were taken. In order to monitor both particle size and hygroscopic growth factor, an H-TDMA system was used as discussed in sub-section 3.2. For the purposes of measuring particle mass and optical properties, a commercial Aerosol Particle Mass Analyzer (APM) and cavity ringdown / nephelometer system was employed respectively, in collaboration with Dr. Renyi Zhang. The soot-chamber sampling system schematic is displayed in Figure 35. Such a combination of measurements is unique to the study of the ambient soot aging process and has the ability to provide insight into the physical changes that occur to soot particles as aging occurs.

The DMA-APM method has been previously employed by various authors (Khalizov et al. 2009b; McMurry et al. 2002; Park et al. 2002). In order to obtain a mass measurement of an aerosol, the sample is first brought to charge equilibrium and then size selected by the DMA set at a steady voltage to generate a monodisperse distribution, a technique which was discussed previously in sub-section 3.2. After exiting the DMA column, the monodispersely distributed aerosol is directed through the APM system. The operation of the APM is based on the theory proposed by Ehara (Ehara et al. 1996). The system consists of two concentric cylindrical electrodes that rotate together about a common axis at the same speed. The outer cylinder is maintained at ground while a

voltage is applied to the inner cylinder. Charged particles are introduced into the annular gap between the two cylinders and rotate at a common angular speed with the system. Therefore, the particles experience opposing electrostatic and centrifugal forces. When particles of a specific mass-to-charge ratio experience a balance of these forces, they will penetrate through the APM where they can then be passed to a detector. The mass of particles carrying n charges can be calculated according to the following force balance (Ehara et al. 1996):

$$m\omega^2 r = \frac{\pi D_{ve}^3}{6}\rho_{true}\omega^2 r = \frac{\pi D_{me}^3}{6}\rho_{eff}\omega^2 r = neE_{APM} \quad 4.1$$

where *m* is the particle mass, ω is the rotational speed of the concentric cylinders, ρ_{true} and ρ_{eff} are the true material and effective density of the particles respectively, r is the radial distance to the annular gap from the axis of rotation, E_{APM} is the magnitude of the electric field in the annular gap, and D_{ve} and D_{me} are the volume equivalent and mobility equivalent diameters respectively. In the case of spherical particles, D_{ve}=D_{me}. By stepping the voltage applied to the APM inner cylinder, a mass distribution can be obtained. Because the densities obtained using this equation vary in proportion to D_{me}^3, a small error in mobility diameter yielded from electrical mobility separation may lead to much larger calculated density errors primarily for non-spherical particles where the error in electrically classified mobility is high. Because of this, the APM system is calibrated using PSL spheres of know size (McMurry et al. 2002). PSL spheres are generated and brought to a charge equilibrium state then size selected by a DMA column and passed to the APM to quantify the APM voltage for a given size of PSL particles. The true

material density of the aerosol of interest can then be found by comparing the APM voltage between that aerosol and the calibrated PSL spheres. It holds then, that:

$$\frac{m_{test}\omega^2 r}{m_{PSL}\omega^2 r} = \frac{\rho_{true}(\frac{\pi D_{ve}^3}{6})}{\rho_{PSL}(\frac{\pi D_{PSL}^3}{6})} = \frac{neE_{APM\ test}}{neE_{APM\ PSL}} = \frac{V_{APM\ test}}{V_{APM\ PSL}} \quad 4.2$$

where m_{test} and m_{PSL} are the mass of the aerosol of interest (test aerosol) and the mass of the PSL spheres respectively. This equation assumes that particles carry a single charge (n =1), however, particles classified by the DMA generally contain both singly and multiply charged particles which could lead to error in measurements as previously discussed. For the purposes of our study, monodisperse soot aerosol distributions with a mean mobility diameter of 0.100 μm were used, which in turn yields a second mode with a mean mobility diameter of 0.155 μm. As was found by McMurry, et al. 2002, the APM voltages required to classify these more massive doubly charged particles are roughly 2 to 2.5 times the values required to classify the singly charged particles of interest, therefore, the APM will cleanly separate out multiply charged particles from the aerosol flow and measure the mass distribution of only the singly charged soot aerosol. Therefore, for the purposes of this study, any effects of the presence of multiply charged particles in the distribution can be neglected when considering mass measured by the APM.

Aerosol optical properties were measured using a combination system of a Cavity Ringdown Spectrometer (CRDS) and a nephelometer This method of retrieving aerosol scattering and extinction related to soot particle aging under laboratory controlled conditions has been previously used (Zhang et al. 2008). In order to measure aerosol

extinction, the CRDS is employed. During operation, a 532 nm light pulse with 11 ns duration is injected into a cavity formed by two mirrors which have 99.9985% reflectivity (Los Gatos Research, Inc.) housed within a stainless steel cell. Light exiting the cavity is detected with a Hamamatsu H6780-02 photomultiplier. Decay times are calculated by fitting the decay data, and the light extinction coefficient, b_{ext}, is calculated by comparing the decay times of the cavity with and without the aerosol sample according to:

$$b_{ext} = \frac{R_L}{c}\left(\frac{1}{\tau} - \frac{1}{\tau_0}\right) \quad 4.3$$

where R_L is the ratio of optical cavity length to sample length, c is the speed of light, τ is the ring-down time with aerosol sample, and τ_0 is the reference filtered ring-down time. In order to prevent the mirrors from aerosol contamination, a small flow (2-4% of sample flow) of dry nitrogen is used to purge the mirror region. Total scattering is measured using a commercial three color integrating nephelometer (TSI 3563) at wavelengths equal to 450, 550, and 700 nm. The scattering coefficient at 532 nm is calculated by fitting the scattering coefficients measured at the three nephelometer wavelengths using a power law. If follows then, that the single scattering albedo (SSA) can be calculed by directly comparing the scattering coefficient to the extinction coefficient:

$$\boldsymbol{SSA} = \frac{\boldsymbol{C_{sca}}}{\boldsymbol{C_{ext}}} \quad 4.4$$

As was discussed in sub-section 3.3, the presence of larger particles in the injected aerosol distribution due to effects from multiple charging can lead to substantial errors in aerosol scattering properties. This is because multiply charged particles scatter

and absorb light more efficiently than singly charged particles because of their larger effective size. Due to a nonlinear relation between scattering and particle size, a small fraction of these multiply charged particles in the distribution can lead to a significant overestimation of the scattering cross-section. Khalizov et al., 2009 investigated the effects of the presence of multiply charged ammonium sulfate, soot and PSL particles and determined that the bias in the optical measurements due to multiply charged particles is significantly less for soot vs. ammonium sulfate. Furthermore, this study focuses primarily on the soot aging process in which the relative changes to the scattering properties over time are of primary interest, a general property that would be reflected in both the singly charged particles and the larger multiply charged mode of the distribution. Since the objective of this study is to examine the relative physical changes that soot particles undergo as they age in the ambient environment, it is determined that the presence of multiply charged particles in the aerosol will not significantly bias the aerosol optical data as the change in optical properties will still be well represented.

4.2. RESULTS AND DISCUSSION

Monodisperse soot particles were injected having mean mobility diameters of 0.100 μm, and particle size, HGF, mass, and extinction and scattering measured hourly as ambient aging occurred under chamber conditions using AACES. Each size and HGF measurement retrieved was fit with log-normal distributions in order to recover geometric mean mobility diameter and mean HGF corresponding to mean diameter. Moreover, near

linear growth rates were determined using sigmoid growth curve fits to the measured change in particle mass over time, a technique that was discussed in sub-section 3.5. Since soot particles are initially chain-like aggregates, the mobility diameter as measured using a DMA does not reflect the true particle diameter since fresh soot particles are not likely spherical on initial generation. Because of this, the growth rate calculated using a change in particle size does not accurately reflect the physical evolution of soot particles under ambient conditions. This analysis will focus on three primary growth periods that were observed; June 05, 2009, June 19, 2009, and June 27, 2009.

Figure 36 displays peak mobility diameter (black), HGF (red), particle effective density (green), and SSA (blue) for the growth period measured on June 05, 2009. During the observed soot aging under ambient conditions using AACES, measured mobility diameter increased from the injected value of 0.100 μm to approximately 0.133 μm throughout a 5 hour period. Similarly, the HGF increased from 1.07 upon injection to 1.15 by the end of the measurement period yielding evidence that as soot particles.

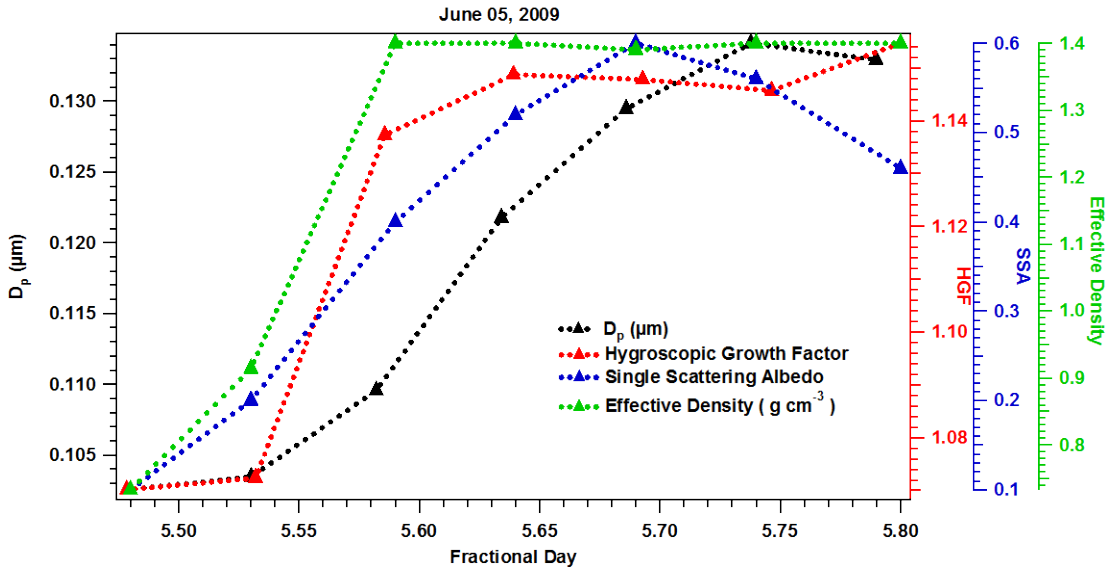

Figure 36. Chamber Soot Growth June 05, 2009. Plotted values of soot particle diameter (black), hygroscopic growth factor (HGF)(red), single scattering albedo (SSA) (blue), and particle effective density (green) vs. fractional day for the measurement period of June 05, 2009 in Houston, TX.

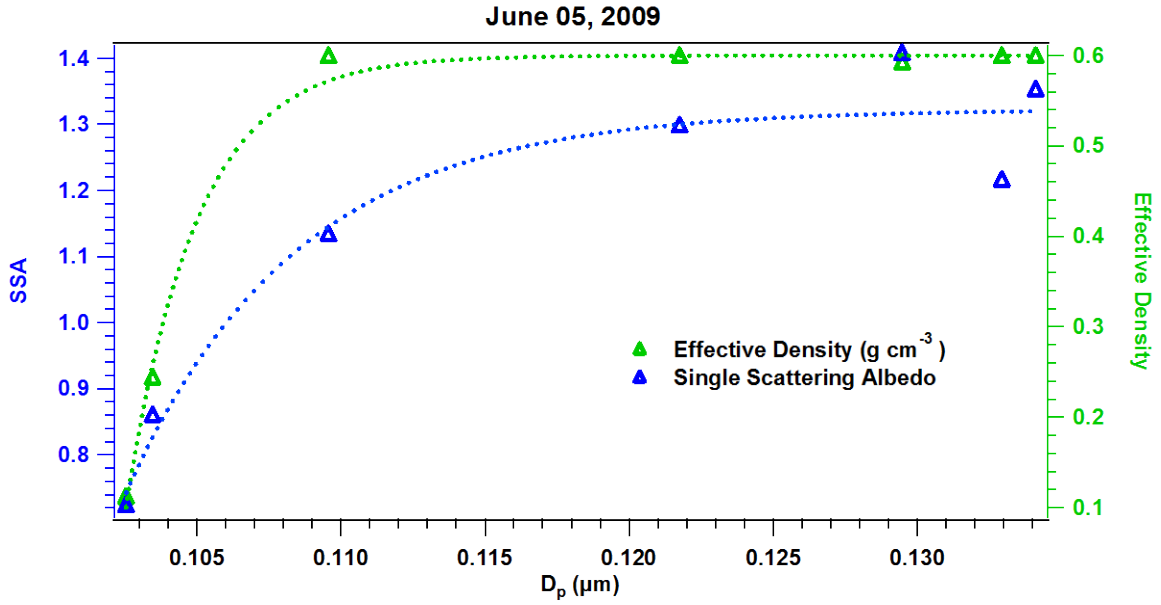

Figure 37. Density and SSA vs. Particle Size June 05, 2009. Effective density and single scattering albedo (SSA) plotted against mean particle diameter during the measurement period of June 05, 2009. Measurements were made during the SHARP field campaign in Houston, TX.

age under ambient conditions, they become more hygroscopic. Despite the measured HGF increasing over time during chamber measurements, it is important to note that evidence supports the collapse and restructuring of soot particles when exposed to high RH (Crouzet and Marlow 1995), and since the measured HGF utilizing the H-TDMA depends on the electric mobility of a particle and not the actual soot particle size, a change in soot particle diameter of 1.15 times the original dry diameter under 90% RH may in fact be unrepresentative of the actual HGF. As is shown in Figure 37, an exponential relationship exists when both measured SSA and effective density are

directly compared to mobility diameter during the course of the soot aging experiment on June 05, 2009.

In contrast, evidence associated with the restructuring of soot particles as they are aged under high sulfuric acid concentrations in the laboratory may indicate that following ambient aging, the core soot particle is more spherical (Zhang et al. 2008), thereby validating HGF measurements following chamber aging under atmospheric conditions. This restructuring may also be a valid explanation for the observed exponential relations indicated in Figure 37. Over the course of the measurement period on June 05, 2009, the effective density of the soot particles increased from 0.75 g cm^{-3} to roughly 1.4 g cm^{-3}, and the SSA increased from 0.1 to 0.6.

Although slower growth was observed on June 19, 2009, similar patterns are evident as shown in Figure 38. On this day, peak measured mobility diameter increased from the injected 0.100 µm to near 0.115 µm during a 6 hour time frame. Accompanying HGF measured at the end of the growth period roughly equal 1.13. The effective density of the soot particles within the chamber also increased from 0.73 to 1.32 g cm^{-3}, and SSA increased from 0.23 to 0.70. Also similar to that observed on June 05, an exponential relation between both SSA and effective density compared with measured mobility diameter exists as indicated in Figure 39.

The results from ambient soot aging utilizing AACES measured on June 27, 2009 are given in Figure 40. Although the measured mobility diameter only increases from 0.100 µm to 0.113 µm, the particle effective density increases from 0.86 g cm^{-3} to over

1.60 g cm^{-3}. Measured HGF at the end of the measurement period was roughly 1.2, and SSA was near 0.5.

The temporally resolved change in observed soot particle mass for each of the three selected measurement periods is given in Figure 41. Rate of mass additions were calculated using the method detailed in sub-section 3.5, in which the differential of sigmoid curve fits to measured growth data provides the near linear rate of change of mass during the exponential phase of growth. Consistent with observations made on June 05, 2009, the calculated growth rate was the most prominent of the three days with a change in particle mass over time equal to 6.33 x 10^{-10} µg hr^{-1}. This rate of growth results in a change in particle mass equal to 4.2 times the initial particle mass concentration, a property which is referred to as the mass growth factor (MGF). As defined, the MGF is equal to the measured particle mass over the initial particle mass (M_p/M_{p0}), and these are plotted for each measurement period in Figure 42. The resultant calculated mass growth rates for the observations obtained on June 19, 2009 and June 27, 2009 were 1.65 x 10^{-10} and 2.88 x 10^{-10} µg hr^{-1} respectively with final MGF values of 2.6 and 2.5.

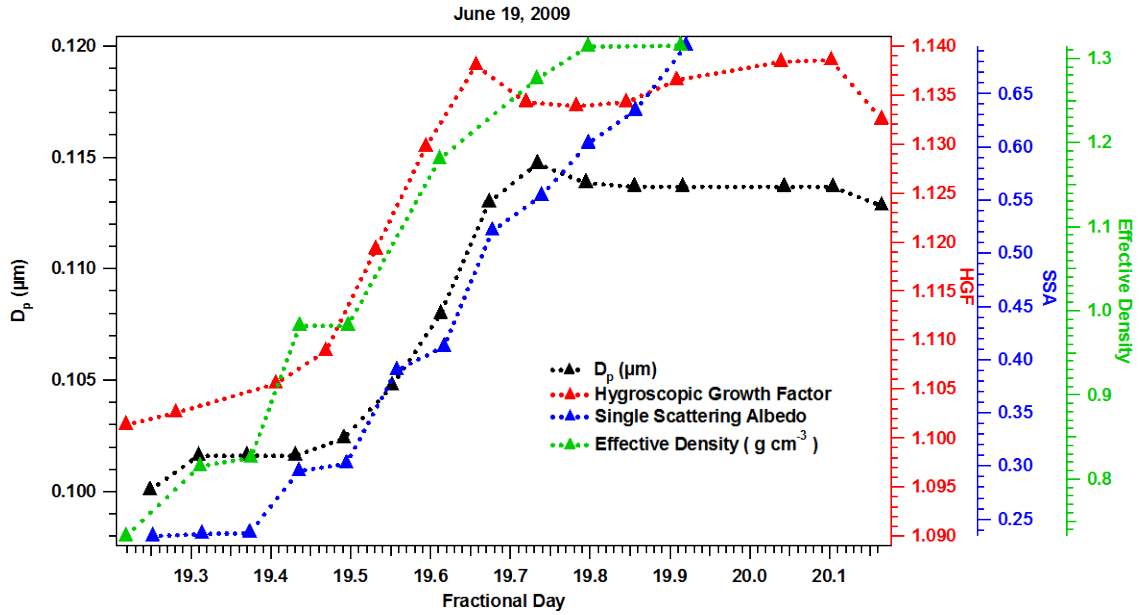

Figure 38. Chamber Soot Growth June 19, 2009. Plotted values of soot particle diameter (black), hygroscopic growth factor (HGF)(red), single scattering albedo (SSA) (blue), and particle effective density (green) vs. fractional day for the measurement period of June 19, 2009 in Houston, TX.

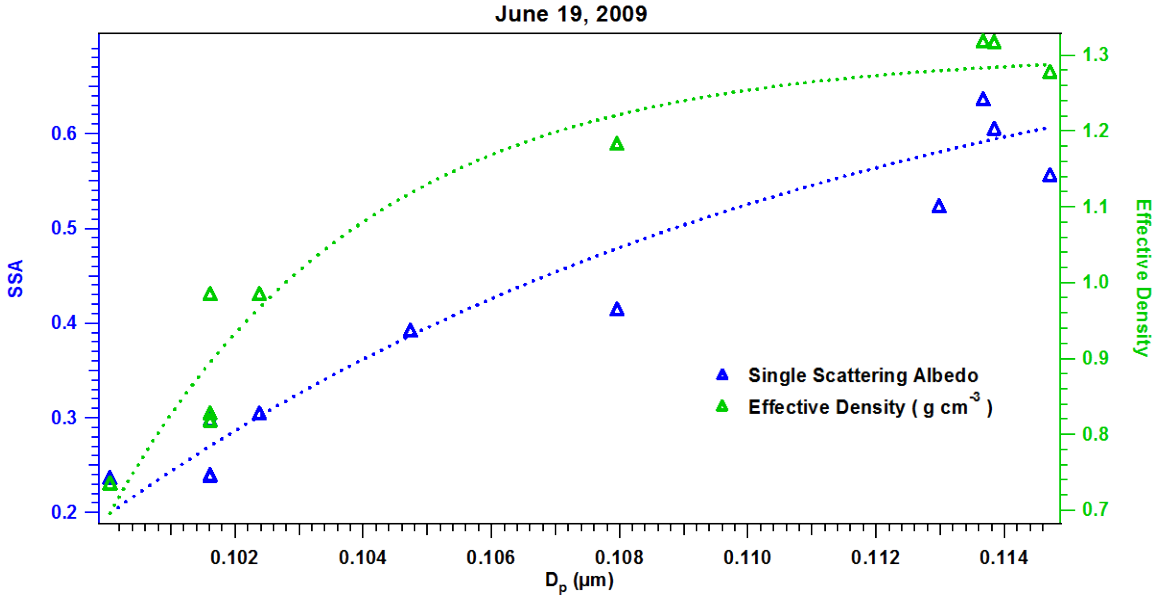

Figure 39. Density and SSA vs. Particle Size June 19, 2009. Effective density and single scattering albedo (SSA) plotted against mean particle diameter during the measurement period of June 19, 2009. Measurements were made during the SHARP field campaign in Houston, TX.

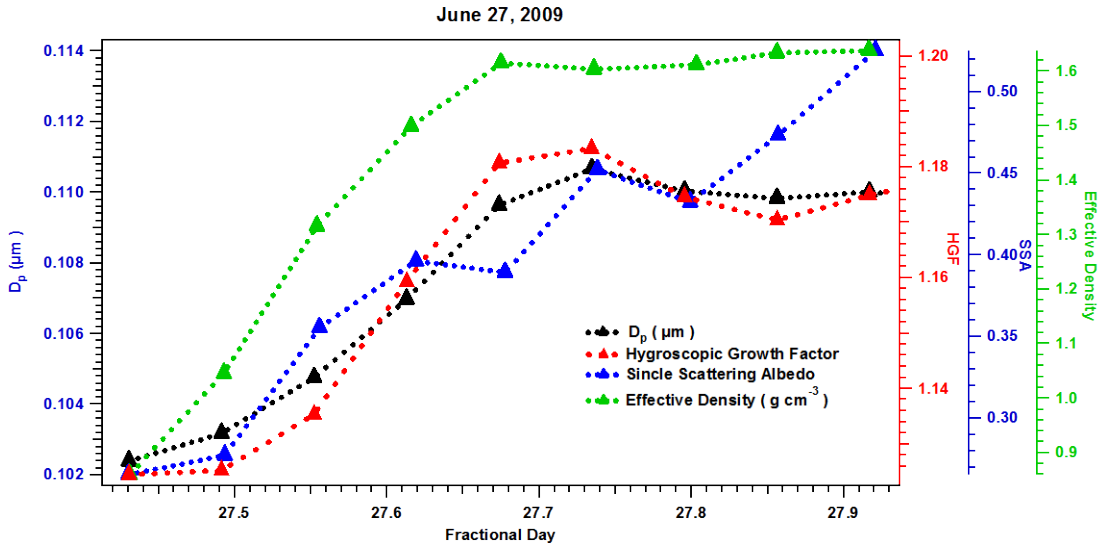

Figure 40. Chamber Soot Growth June 27, 2009. Plotted values of soot particle diameter (black), hygroscopic growth factor (HGF)(red), single scattering albedo (SSA) (blue), and particle effective density (green) vs. fractional day for the measurement period of June 27, 2009 in Houston, TX.

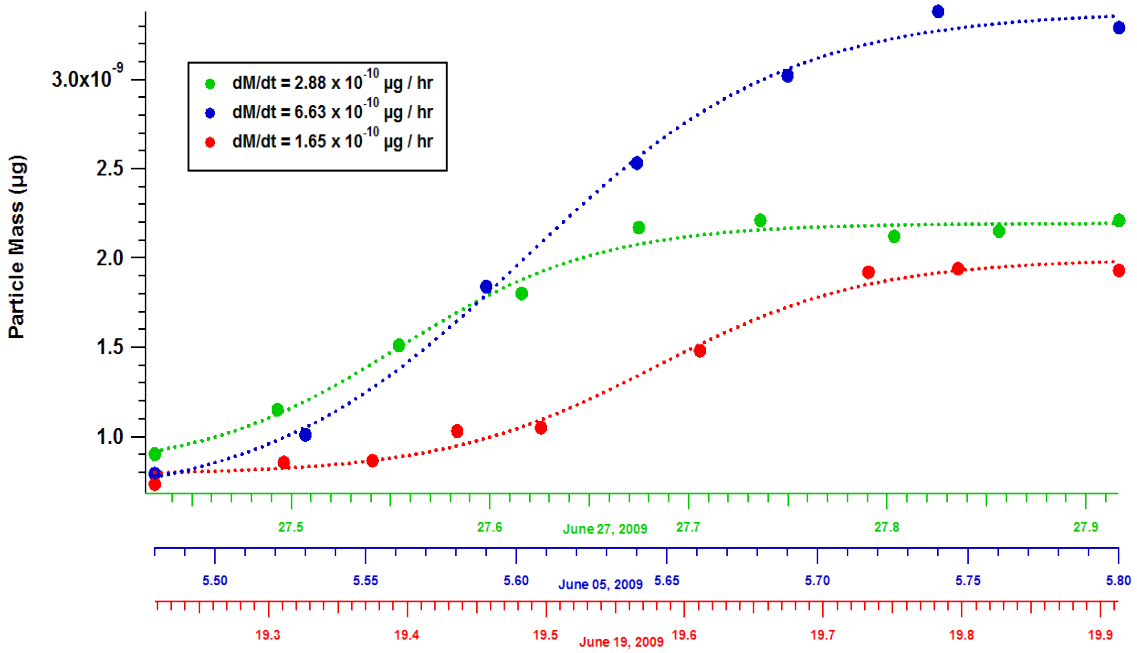

Figure 41. Soot Mass Growth Rates. Particle mass vs. fractional day for the measurement periods of June 05, 2009 (blue), June 19, 2009 (red), and June 27, 2009 (green). Observations are fit using a sigmoid type fitting function (dashed lines) in order to retrieve near linear rate of mass addition to the particle.

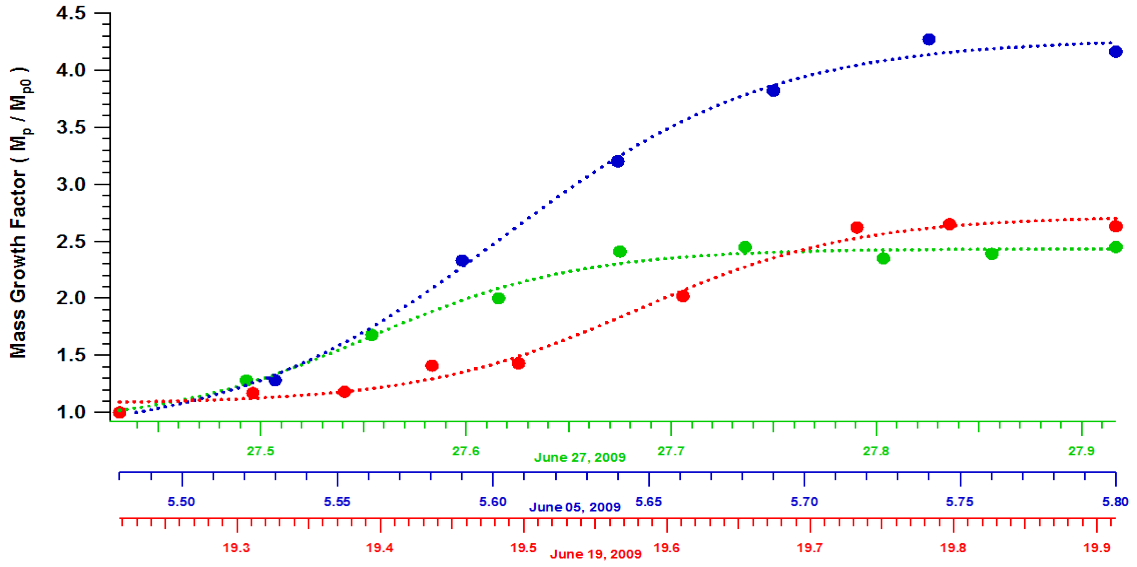

Figure 42. Soot Mass Growth Factor. Calculated mass growth factor (MGF) for each measurement period. The MGF is defined as the measured mass corresponding to a point of time during growth to the initial mass injected into the chamber.

5. SUMMARY AND CONCLUSIONS

With an increased need to study the atmospheric aging of particulates and its impact on the environment and human health, an innovative aerosol chamber was developed. AACES is a fully portable ambient aerosol chamber constructed with both FEP Teflon and UV transparent acrylic designed to measure SOA production and soot aging under atmospherically relevant conditions. The chamber utilizes the exceptional chemical and physical properties of e-PTFE to provide an environment in which gaseous concentrations mimic ambient while maintaining efficient particle filtration. Chamber characterization tests measuring the permeation of various gases across the membrane revealed penetration efficiencies greater that 96% for each of the compounds studied while particle filtration was above 99.9%. Furthermore, the depositional loss of both gases and particulates in the chamber environment allow for sustainable measurement periods exceeding 12 hours dependant on initial injected particle concentrations.

AACES was field deployed during three separate campaigns beginning with CLASIC in Ponca City, Oklahoma during the summer of 2007 and ending with SHARP in Houston, TX during the summer of 2009. For the majority of measurements, monodisperse ammonium sulfate seed aerosols were injected and particle size and hygroscopic growth factor monitored hourly using an H-TDMA system. When studying the atmospheric aging of soot particles under ambient conditions, measurements of mass and optical properties using an APM and a combined nephelometer / CRDS complimented data obtained from H-TDMA measurements. Growth rates were acquired

by differentiating sigmoid type growth curve fits to the measured particle size over time. Resulting growth rates varied by day and location and ranged from 3 nm/hr in Colorado to 12 nm/hr in Oklahoma. Final hygroscopic growth factors at the end of a measurement cycle also varied considerably as indicated in Table 1. Growth rates measured in Colorado at elevation tended to be lower than those observed at both the Oklahoma field site and in Texas, while the final HGF measured at the urban location in Texas were consistently higher than the other two locations. These results agree with calculated values for the final organic mass fractions. Calculations utilizing data from Houston, TX yielded an average percent organic mass fraction around 50% compared with 65% determined from the Oklahoma data. Average percent mass calculations were not conducted from the Colorado dataset due to the limited number of observations collected at that site. Growth rates measured using AACES were directly compared to observed ambient growth with good agreement in selected cases concluding that the environment created using AACES mimics that of the ambient environment in which the chamber is located. Therefore it is concluded that AACES is a valuable tool to allow for the measurement of the atmospheric aging process under ambient conditions. Partial SOA reversibility appears to have been observed during four of the measurement periods reported. This evidence contradicts earlier modeling studies in which organic vapors are assumed to fully partition between the gas and condensed phase. However, recent models have incorporated a volatility basis-set approach to modeling SOA production and growth in the atmosphere. Based on the results from this study, it is recommended that future models adapt the methods of the volatility basis-set approach for the

prediction of SOA under atmospheric conditions, although further examination of the partitioning of known SOA precursors between the gas and particle phases is required.

Investigations into the ambient soot aging process utilizing AACES were conducted atop the South Moody Tower on the University of Houston campus during the SHARP field project. Monodisperse soot seed particles were injected and mobility diameter and hygroscopic growth factor, mass, and optical properties measured hourly using an H-TDMA system, an APM, and a nephelometer / CRDS system respectively. As the soot particle aged under ambient conditions in the environmental chamber, an increase in all measured properties was observed. Furthermore, it is likely the data obtained indicates the restructuring of the initially injected chain aggregates over time as sulfuric acid and non-volatile organics deposit onto the particle surface. Although calculated growth rates were similar to that of ammonium sulfate seed particles, official reported growth is in the form of a change in particle mass. This is due to the inaccuracies surrounding mobility diameter measurements of soot particles. Change in particle mass varied by day with values of mass growth factor (M_p/M_{p0}) ranging from 2.5 to a maximum of 4.2. Future studies investigating the soot aging process using AACES are recommended.

REFERENCES

Ackerman, A. S., Toon, O. B., Stevens, D. E., Heymsfield, A. J., Ramanathan, V. and Welton, E. J. (2000). Reduction of Tropical Cloudiness by Soot. *Science* 288:1042-1047.

An, W. J., Pathak, R. K., Lee, B.-H. and Pandis, S. N. (2007). Aerosol Volatility Measurement Using an Improved Thermodenuder: Application to Secondary Organic Aerosol. *Journal of Aerosol Science* 38:305-314.

Anttila, T. and Kerminen, V.-M. (2003). Condensational Growth of Atmospheric Nuclei by Organic Vapours. *Journal of AErosol Science* 34:20.

Botnen, B. W. (2006). Subtask 1.15 - Passive Diffusion Sample Bags Made from Expanded Polytetrafluoroethylene (Eptfe) to Measure Voc Concentrations in Groudwater, U.S. Department of Energy, 81.

Buzcu, B. and Fraser, M. P. (2006). Source Identification and Apportionment of Volatile Organic Compounds in Houston, Tx. *Atmospheric Environment* 40:2385-2400.

Cai, X., Ziemba, L. D. and Griffin, R. J. (2008). Secondary Aerosol Formation from the Oxidation of Toluene by Chlorine Atoms. *Atmospheric Environment* 42:7348-7359.

Carter, W. P. L., Atkinson, R., Winer, A. M. and Jr., J. N. P. (1982). Experimental Investigation of Chamber-Dependent Radical Sources. *International Journal of Chemical Kinetics* 14:1071-1103.

Carter, W. P. L., Luo, D., Malkina, I. L. and Fitz, D. (1995). The University of California, Riverside Environmental Chamber Data Base for Evaluating Oxidant Mechanisms - Indoor Chamber Experiments through 1993, U.S. Environment Protection Agency, 240.

Chen, J. and Griffin, R. J. (2005). Modeling Secondary Organic Aerosol Formation from Oxidation of [Alpha]-Pinene, [Beta]-Pinene, and D-Limonene. *Atmospheric Environment* 39:7731-7744.

Chung, S. H. and Seinfeld, J. H. (2002). Global Distribution and Climate Forcing of Carbonaceous Aerosols. *J. Geophys. Res.* 107:4407.

Chylek, P. and Hallett, J. (1992). Enhanced Absorption of Solar Radiation by Cloud Droplets Containing Soot Particles in Their Surface. *Quarterly Journal of the Royal Meteorological Society* 118:167-172.

Cocker, D. R., Clegg, S. L., Flagan, R. C. and Seinfeld, J. H. (2001). The Effect of Water on Gas-Particle Partitioning of Secondary Organic Aerosol. Part I: A-Pinene/Ozone System. *Atmospheric Environment* 35:23.

Colville, J. C. and Griffin, R. J. (2004). The Roles of Individual Oxidants in Secondary Organic Aerosol Formation from Δ3-Carene: 2. Soa Formation and Oxidant Contribution. *Atmospheric Environment* 28:10.

Crouzet, Y. and Marlow, W. H. (1995). Calculations of the Equilibrium Vapor Pressure of Water over Adhering 50–200-Nm Spheres. *Aerosol Science and Technology* 22:43 - 59.

Cruz, C. N. and Pandis, S. N. (2000). Deliquescence and Hygroscopic Growth of Mixed Inorganic−Organic Atmospheric Aerosol. *Environmental Science & Technology* 34:4313-4319.

Dockery, D. W., Pope, C. A., Xu, X., Spengler, J. D., Ware, J. H., Fay, M. E., Ferris, B. G. and Speizer, F. E. (1993). An Association between Air Pollution and Mortality in Six U.S. Cities. *The New England Journal of Medicine* 329:6.

Donahue, N. M., Robinson, A. L. and Pandis, S. N. (2009). Atmospheric Organic Particulate Matter: From Smoke to Secondary Organic Aerosol. *Atmospheric Environment* 43:94-106.

Ehara, K., Hagwood, C. and Coakley, K. J. (1996). Novel Method to Classify Aerosol Particles According to Their Mass-to-Charge Ratio--Aerosol Particle Mass Analyser. *Journal of Aerosol Science* 27:217-234.

Fan, J., Zhang, R., Tao, W.-K. and Mohr, K. I. (2008). Effects of Aerosol Optical Properties on Deep Convective Clouds and Radiative Forcing. *J. Geophys. Res.* 113:D08209.

Fuchs, N. A. and Sutugin, A. G. (1971). *Highly Dispersed Aerosol, In: Topics in Current Aerosol Research*. Pergamon, New York.

Fukui, Y. and Doskey, P. V. (2000). Identification of Nonmethane Organic Compound Emissions from Grassland Vegetation. *Atmospheric Environment* 34:2947-2956.

Fuller, K. A. (1995). Scattering and Absorption Cross Sections of Compounded Spheres. Ii. Calculations for External Aggregation. *J. Opt. Soc. Am. A* 12:881-892.

Fuller, K. A., Malm, W. C. and Kreidenweis, S. M. (1999). Effects of Mixing on Extinction by Carbonaceous Particles. *J. Geophys. Res.* 104:15941-15954.

Gasparini, R., Li, R. and Collins, D. R. (2004). Integration of Size Distributions and Size-Resolved Hygroscopicity Measured During the Houston Supersite for Compositional Categorization of the Aerosol. *Atmospheric Environment* 38:3285-3303.

Goldstein, A. H. and Galbally, I. E. (2007). Known and Unexplored Organic Constituents in the Earth's Atmosphere. *Environmental Science & Technology* 41:1514-1521.

Goodman, P. G., Dockery, D. W. and Clancy, L. (2004). Cause-Specific Mortality and the Extended Effects of Particulate Pollution and Temperature Exposure. *Environmental Health Perspectives* 112.

Gouw, J. A. d., Middlebrook, A. M., Warneke, C., Goldan, P. D., Kuster, W. C., Roberts, J. M., Fehsenfeld, R. C., Worsnop, D. R., Canagaratna, M. R., Pszenny, A. A. P., Keene, W. C., Marchewka, M., Bertman, S. B. and Bates, T. S. (2005). Budget of Organic Carbon in a Polluted Atmosphere: Results from the

NOAA Report, New England Air Quality Study in 2002. *Journal of Geophysical Research* 110:22.

Grieshop, A. P., Donahue, N. M. and Robinson, A. L. (2007). Is the Gas-Particle Partitioning in Alpha-Pinene Secondary Organic Aerosol Reversible? *Geophys. Res. Lett.* 34:L14810.

Griffin, R. J., Cocker, D. R., III, Flagan, R. C. and Seinfeld, J. H. (1999a). Organic Aerosol Formation from the Oxidation of Biogenic Hydrocarbons. *J. Geophys. Res.* 104:3555-3567.

Griffin, R. J., Cocker, D. R., III, Seinfeld, J. H. and Dabdub, D. (1999b). Estimate of Global Atmospheric Organic Aerosol from Oxidation of Biogenic Hydrocarbons. *Geophys. Res. Lett.* 26:2721-2724.

Grosjean, D. (1992). Formic Acid and Acetic Acid: Emissions, Atmospheric Formation and Dry Deposition at Two Southern California Locations. *Atmospheric Environment. Part A. General Topics* 26:3279-3286.

Grosjean, D. and Seinfeld, J. H. (1989). Parameterization of the Formation Potential of Secondary Organic Aerosols. *Atmospheric Environment (1967)* 23:1733-1747.

Hallquist, M., Wenger, J. C., Baltensperger, U., Rudich, Y., Simpson, D., Claeys, M., Dommen, J., Donahue, N. M., George, C., Goldstein, A. H., Hamilton, J. F., Herrmann, H., Hoffmann, T., Iinuma, Y., Jang, M., Jenkin, M. E., Jimenez, J. L., Kiendler-Scharr, A., Maenhaut, W., McFiggans, G., Mentel, T. F., Monod, A., Prevot, A. S. H., Seinfeld, J. H., Surratt, J. D., Szmigielski, R. and Wildt, J.

(2009). The Formation, Properties and Impact of Secondary Organic Aerosol: Current and Emerging Issues. *Atmospheric Chemistry and Physics* 9:81.

Hansen, J., Sato, M. and Ruedy, R. (1997). Radiative Forcing and Climate Response. *J. Geophys. Res.* 102:6831-6864.

Hauser, R., Godleski, J. J., Hatch, V. and Christiani, D. (2001). Ultrafine Particles in Human Lung Macrophages. *Archives of Environmental Health: An International Journal* 56.

Heald, C. L., Jacob, D. J., Park, R. J., Russell, L. M., Huebert, B. J., Seinfeld, J. H., Liao, H. and Weber, R. J. (2005). A Large Organic Aerosol Source in the Free Troposphere Missing from Current Models. *Geophys. Res. Lett.* 32:L18809.

Helmig, D., Klinger, L. F., Guenther, A., Vierling, L., Geron, C. and Zimmerman, P. (1999). Biogenic Volatile Organic Compound Emissions (Bvocs) I. Identifications from Three Continental Sites in the U.S. *Chemosphere* 38:2163-2187.

Hu, D. and Kamens, R. M. (2007). Evaluation of the Unc Toluene-Soa Mechanism with Respect to Other Chamber Studies and Key Model Parameters. *Atmospheric Environment* 41:6465-6477.

Industries, C. (2001). Acrylite Op-4 Acrilic Scheet: Ultraviolet-Transmitting Acrylic Sheet, in *Technical Data*, C. Industries, ed., New Jersey, 4.

Jacobson, M. Z. (2001). Strong Radiative Heating Due to the Mixing State of Black Carbon in Atmospheric Aerosols. *Nature* 409:695-697.

Jenkin, M. E. (2004). Modelling the Formation and Composition of Secondary Organic Aerosol from A- and B-Pinene Ozonolysis Using Mcm V3. *Atmospheric Chemistry and Physcis Discussions* 4:43.

Johnson, B. T., Shine, K. P. and Forster, P. M. (2004). The Semi-Direct Aerosol Effect: Impact of Absorbing Aerosols on Marine Stratocumulus. *Quarterly Journal of the Royal Meteorological Society* 130:1407-1422.

Johnson, D., Jenkin, M. E., Wirtz, K. and Martin-Reviejo, M. (2005). Simulating the Formation of Secondary Organic Aerosol from the Photooxidation of Aromatic Hydrocarbons. *Environmental Chemistry* 2:35-48.

Kanakidou, M., J. H. Seinfeld, Pandis, S. N., Barnes, I., Dentener, F. J., Facchini, M. C., Dingenen, R. v., Ervens, B., Nenes, A., Nielsen, C. J., Swietlicki, E., Putaud, J. P., Balkanski, Y., Fuzzi, S., Horth, J., Moortgat, G. K., Winterhalter, R., Myhre, C. E. L., Tsigaridis, K., Vignati, E., Stephanou, E. G. and Wilson, a. J. (2005).

Organic Aerosol and Global Climate Modelling: A Review. *Atmospheric Chemistry and Physcis* 5.

Khalizov, A. F., Xue, H., Wang, L., Zheng, J. and Zhang, R. (2009a). Enhanced Light Absorption and Scattering by Carbon Soot Aerosol Internally Mixed with Sulfuric Acid. *The Journal of Physical Chemistry A* 113:1066-1074.

Khalizov, A. F., Zhang, R., Zhang, D., Xue, H., Pagels, J. and McMurry, P. H. (2009b). Formation of Highly Hygroscopic Soot Aerosols Upon Internal Mixing with Sulfuric Acid Vapor. *J. Geophys. Res.* 114:D05208.

Kotzick, R., Panne, U. and Niessner, R. (1997). Changes in Condensation Properties of Ultrafine Carbon Particles Subjected to Oxidation by Ozone. *Journal of Aerosol Science* 28:725-735.

Kroll, J. H., Chan, A. W. H., Ng, N. L., Flagan, R. C. and Seinfeld, J. H. (2007). Reactions of Semivolatile Organics and Their Effects on Secondary Organic Aerosol Formation. *Environmental Science & Technology* 41:3545-3550.

Kroll, J. H. and Seinfeld, J. H. (2008). Chemistry of Secondary Organic Aerosol: Formation and Evolution of Low-Volatility Organics in the Atmosphere. *Atmospheric Environment* 42:3593-3624.

Lane, T. E., Donahue, N. M. and Pandis, S. N. (2008). Simulating Secondary Organic Aerosol Formation Using the Volatility Basis-Set Approach in a Chemical Transport Model. *Atmospheric Environment* 42:7439-7451.

Leskinen, A. P., Kulmala, M. and Lehtinen, K. E. J. (2008). Growth of Nucleation Mode Particles: Source Rates of Condensable Vapour in a Smog Chamber. *Atmospheric Environment* 42:7405-7411.

Levitt, N. P., Zhang, R., Xue, H. and Chen, J. (2007). Heterogeneous Chemistry of Organic Acids on Soot Surfaces. *The Journal of Physical Chemistry A* 111:4804-4814.

Li, G., Zhang, R., Fan, J. and Tie, X. (2005). Impacts of Black Carbon Aerosol on Photolysis and Ozone. *J. Geophys. Res.* 110:D23206.

Luo, D., Pierce, J. A., Malkina, I. L. and Carter, W. P. L. (1995). Rate Constants for the Reactions of O(3p) with Selected Monoterpenes. *International Journal of Chemical Kinetics* 28:8.

Magnusson, T. (1989). A Method for Equilibration Chamber Sampling and Gas Chromatographic Analysis of the Soil Atmosphere. *Plant and Soil* 120:39-47.

Markowski, G. R. (1987). Inproving Twomey Algorithm for Inversion of Aerosol Measurement Data. *Aerosol Science and Technology* 7:14.

Matsumaga, A. and Ziemann, P. J. (2009). Gas-Wall Partitioning of Organic Compounds in a Teflon Film Chamber and Potential Effects on Reaction Product and Aerosol Yield Measurements. *Aerosol Science and Technology* In Press.

McMurry, P. H. and Grosjean, D. (1985). Photochemical Formation of Organic Aerosols: Growth Laws and Mechanisms. *Atmospheric Environment (1967)* 19:1445-1451.

McMurry, P. H., Wang, X., Park, K. and Ehara, K. (2002). The Relationship between Mass and Mobility for Atmospheric Particles: A New Technique for Measuring Particle Density. *Aerosol Science and Technology* 36:227 - 238.

Mikhailov, E. F., Vlasenko, S. S., Podgorny, I. A., Ramanathan, V. and Corrigan, C. E. (2006). Optical Properties of Soot - Water Drop Agglomerates: An Experimental Study. *Journal of Geophysical Research* 111:16.

Namieśnik, J., Zabiegała, B., Kot-Wasik, A., Partyka, M. and Wasik, A. (2005). Passive Sampling and/or Extraction Techniques in Environmental Analysis: A Review. *Analytical and Bioanalytical Chemistry* 381:279-301.

Ng, N. L., Kroll, J. H., Keywood, M. D., Bahreini, R., Varutbangkul, V., Flagan, R. C., Seinfeld, J. H., Lee, A. and Goldstein, A. H. (2006). Contribution of First- Versus Second-Generation Products to Secondary Organic Aerosols Formed in the Oxidation of Biogenic Hydrocarbons. *Environmental Science & Technology* 40:2283-2297.

Pankow, J. F. (1994). An Absorption Model of Gas/Particle Partitioning of Organic Compounds in the Atmosphere. *Atmospheric Environment* 28:185-188.

Park, K., Cao, F., Kittelson, D. B. and McMurry, P. H. (2002). Relationship between Particle Mass and Mobility for Diesel Exhaust Particles. *Environmental Science & Technology* 37:577-583.

Pósfai, M., Anderson, J. R., Buseck, P. R. and Sievering, H. (1999). Soot and Sulfate Aerosol Particles in the Remote Marine Troposphere. *J. Geophys. Res.* 104:21685-21693.

Presto, A. A. and Donahue, N. M. (2006). Investigation of A-Pinene + Ozone Secondary Organic Aerosol Formation at Low Total Aerosol Mass. *Environmental Science & Technology* 40:3536-3543.

Presto, A. A., Huff Hartz, K. E. and Donahue, N. M. (2005). Secondary Organic Aerosol Production from Terpene Ozonolysis. 2. Effect of Nox Concentration. *Environmental Science & Technology* 39:7046-7054.

Ramanathan, V., Crutzen, P. J., Kiehl, J. T. and Rosenfeld, D. (2001). Aerosols, Climate, and the Hydrological Cycle. *Science* 294:2119-2124.

Robinson, A. L., Donahue, N. M. and Rogge, W. F. (2006). Photochemical Oxidation and Changes in Molecular Composition of Organic Aerosol in the Regional Context. *J. Geophys. Res.* 111:D03302.

Robinson, A. L., Donahue, N. M., Shrivastava, M. K., Weitkamp, E. A., Sage, A. M., Grieshop, A. P., Lane, T. E., Pierce, J. R. and Pandis, S. N. (2007). Rethinking Organic Aerosols: Semivolatile Emissions and Photochemical Aging. *Science* 315:1259-1262.

Rudich, Y., Donahue, N. M. and Mentel, T. F. (2007). Aging of Organic Aerosol: Bridging the Gap between Laboratory and Field Studies. *Annual Review of Physical Chemistry* 58:31.

Saathoff, H., Naumann, K. H., Schnaiter, M., Schöck, W., Möhler, O., Schurath, U., Weingartner, E., Gysel, M. and Baltensperger, U. (2003). Coating of Soot and (Nh4)2so4 Particles by Ozonolysis Products of [Alpha]-Pinene. *Journal of Aerosol Science* 34:1297-1321.

Sakurai, H., Park, K., McMurry, P. H., Zarling, D. D., Kittelson, D. B. and Ziemann, P. J. (2003). Size-Dependent Mixing Characteristics of Volatile and Nonvolatile Components in Diesel Exhaust Aerosols. *Environmental Science & Technology* 37:5487-5495.

Santoro, R. J., Semerjian, H. G. and Dobbins, R. A. (1983). Soot Particle Measurements in Diffusion Flames. *Combustion and Flame* 51:203-218.

Schnaiter, M., Linke, C., Möhler, O., Naumann, K. H., Saathoff, H., Wagner, R., Schurath, U. and Wehner, B. (2005). Absorption Amplification of Black Carbon Internally Mixed with Secondary Organic Aerosol. *J. Geophys. Res.* 110:D19204.

Schwartz, J. (2004a). Air Pollution and Children's Health. *Pediatrics* 113:1037-1043.

Schwartz, J. (2004b). Is the Association of Airborne Particles with Daily Deaths Confounded by Gaseous Air Pollutants? An Approach to Control by Matching. *Environmental Health Perspectives* 112.

Seinfeld, J. H. and Pandis, S. N. (1998). *Atmospheric Chemistry and Physics: From Air Pollution to Climate Change*. John Wiley & Sons.

Sheehan, P. E. and Bowman, F. M. (2001). Estimated Effects of Temperature on Secondary Organic Aerosol Concentrations. *Environmental Science & Technology* 35:2129-2135.

Stanier, C. O., Donahue, N. and Pandis, S. N. (2008). Parameterization of Secondary Organic Aerosol Mass Fractions from Smog Chamber Data. *Atmospheric Environment* 42:2276-2299.

Tanaka, P. L., Riemer, D. D., Chang, S., Yarwood, G., McDonald-Buller, E. C., Apel, E. C., Orlando, J. J., Silva, P. J., Jimenez, J. L., Canagaratna, M. R., Neece, J. D., Mullins, C. B. and Allen, D. T. (2003). Direct Evidence for Chlorine-Enhanced Urban Ozone Formation in Houston, Texas. *Atmospheric Environment* 37:1393-1400.

Tang, I. N. and Munkelwitz, H. R. (1994). Water Activities, Densities, and Refractive Indices of Aqueous Sulfates and Sodium Nitrate Droplets of Atmospheric Importance. *J. Geophys. Res.* 99:18801-18808.

Twomey, S. (1991). Aerosols, Clouds and Radiation. *Atmospheric Environment. Part A. General Topics* 25:2435-2442.

Weingartner, E., Burtscher, H. and Baltensperger, U. (1997). Hygroscopic Properties of Carbon and Diesel Soot Particles. *Atmospheric Environment* 31:2311-2327.

Wikol, M., Hartmann, B., Brendle, J., Crane, M., Beuscher, U., Brake, J. and Shickel, T. (2008). Expanded Polytetrafluoroethylene Membranes and Their Applications, in *Filtration and Purification in the Biopharmaceutical Industry: Second Edition*, M. W. Jornits and T. H. Meltzer, eds., Informa Healthcare, Newark, Delaware, USA, 23.

Xie, J. and Marlow, W. H. (1997). Water Vapor Pressure over Complex Particles, I: Sulfuric Acid Solution Effect. *Aerosol Science and Technology* 27:591 - 603.

Zhang, D. and Zhang, R. (2005). Laboratory Investigation of Heterogeneous Interaction of Sulfuric Acid with Soot. *Environmental Science & Technology* 39:5722-5728.

Zhang, R., Khalizov, A. F., Pagels, J., Zhang, D., Xue, H. and McMurry, P. H. (2008). Variability in Morphology, Hygroscopicity, and Optical Properties of Soot Aerosols During Atmospheric Processing. *Proceedings of the National Academy of Sciences* 105:10291-10296.

Zuberi, B., Johnson, K. S., Aleks, G. K., Molina, L. T., Molina, M. J. and Laskin, A. (2005). Hydrophilic Properties of Aged Soot. *Geophys. Res. Lett.* 32:L01807.

APPENDIX I

AACES	Ambient Aerosol Chamber for Evolution Studies
APM	Aerosol Particle Mass Analyzer
ARM	Atmospheric Radiation Measurement
BEACHON	Bio-hydro-atmosphere Interactions of Energy, Aerosols, Carbon, H_2O, Organics & Nitrogen
BVOC	Biogenic Volatile Organic Compound
CCN	Cloud Condensation Nuclei
CLASIC	Cloud Land and Surface Interaction
CPC	Condensations Particle Counter
CRDS	Cavity Ringdown Spectrometer
DI	Deionized
DMA	Differential Mobility Analyzer
e-PTFE	Expanded Polytetrafluoroethylene
H-TDMA	Humidified Tandem Differential Mobility Analyzer
HGF	Hygroscopic Growth Factor (D_p/D_p^*)
IN	Ice Nuclei
MGF	Mass Growth Factor
PDB	Passive Diffusion Bag
PTR-MS	Proton-Transfer Reaction Mass Sepctrometer
RH	Relative Humidity
SHARP	Study of Houston Atmospheric Radical Precursors

SGP	Southern Great Plains
SOA	Secondary Organic Aerosol
SSA	Single Scattering Albedo
UV	Ultraviolet
VOC	Volatile Organic Compound

VITA

Name:	Crystal Chanea Glen
Address:	P.O. Box 5800 MS 1135 Albuquerque, NM 87185
Email Address:	ccreed@sandia.gov

Education:	Ph.D., Atmospheric Sciences, Texas A&M University, 2010 B.S., Meteorology, Texas A&M University, 2004
Honors and Awards:	Sandia National Laboratories / Texas A&M University Excellence in Geosciences Fellowship (2005-2010) Presidential Scholarship, Texarkana College (1998-2000) Outstanding Student Award, College of Geosciences
Professional Service: (Short List)	Undergraduate Student Council (2001-2004) Graduate Student Representative (2004-2010) Graduate Student Council (2005-2010) College of Geosciences Graduate Advisors and Curriculum Committee (2005-2010) American Meteorological Society Atmospheric Chemistry Committee (2007-2010)